UNIVERSITY OF CAPE TOWN
IYUNIVESITHI YASEKAPA • UNIVERSITEIT VAN KAAPSTAD

Medical Biotechnology & Immunotherapy Research Unit
Institute of Infectious Disease & Molecular Medicine
South African Research Chair in Cancer Biotechnology
Department of Integrative Biomedical Sciences
Faculty of Health Sciences
University of Cape Town

# *Generation of recombinant SNAP-tag based antibody fusion proteins for immunotherapy of Acute Myeloid Leukemia (AML)*

**Gomolemo Atlegang Molope**

February 2025

**Supervisor:**
Prof. Dr. Dr. Stefan Barth

**Practical support:**
Bernard Murithi Mirianga

Submitted to the Faculty of Health Sciences, University of Cape Town, in fulfilment of the requirements for the degree of Master of Science (Med) in Medical Biochemistry

## Declaration

1. I declare that the work contained in this dissertation is my own work.

2. I know that Plagiarism is wrong. Plagiarism is to use another's work and pretend that it is one's own.

3. Neither the substance nor any part of this dissertation has been (in the past), is currently being, or is to be submitted for a degree at this University, or any other university other than this Master of Science at the University of Cape Town.

4. I have not allowed and will not allow anyone to copy my work with the intention of passing it off as his or her own work.

5. The Modern Language Association (MLA) referencing style has been applied as the convention for in-text citations and referencing. Each significant contribution to, and quotation in, this thesis from the work(s) of other authors and collaborators has been attributed, cited, and referenced.

6. This dissertation has been submitted to the Turnitin module (or equivalent similarity and originality checking software) and I confirm that my supervisor has seen my report and that any concerns revealed by such have been resolved with my supervisor.

7. I grant the University of Cape Town free license to reproduce the content of this dissertation, in whole or in part, for the purpose of research, but request to recognize and confirm its sensitive content.

**Name:** Gomolemo Atlegang Molope

**Signature:** Signed by candidate

**Date:** 16 February 2025

## Acknowledgements

I give all the praise and thanks to the Lord, for He has carried me through the years of this degree with steadfast love and faithfulness.

To Prof. Dr. Dr. Stefan Barth, I truly appreciate the opportunity to work in the MB&I Research Unit. I will forever be grateful for your support, patience, and exceptional supervision throughout this project. You have instilled in me a strong work ethic, always emphasizing the value of perseverance in my quest for excellence.

I am profoundly grateful for the financial support I received from the National Research Foundation (NRF) and the University of Cape Town (UCT). Your generous investment in my education has made my academic pursuits possible.

I am thankful to each and every member of the MB&I Research Unit for your constant encouragement, selflessness, and happy memories. Your willingness to always help without hesitation cannot be commended enough.

Thank you to the Sturrock Lab, Blackburn Lab, H3D Center, and Flow Cytometry & Sorting Core Facilities. The constant support and generosity of their members with resources and equipment, when needed, will always be appreciated.

I would like to express my heartfelt gratitude to Bernard Mirianga, Tatenda Bvudzijena, Dr. Nkhasi Lekena, Thabo Matshoba, and Emmanuel Fajemisin for their willingness to offer crucial support with the writing or experimental work that contributed to this study's success.

To my parents, I can never thank you enough for everything you have done for me. Your prayers, unconditional love, unwavering support, sacrifices, and guidance have formed the foundation of my success. You are truly a blessing that I will cherish forever.

To my sister, your unceasing encouragement throughout this journey has been incredible. Words cannot express how grateful I am for your constant reassurance and for keeping me sane. You are not just my sister—you are my lifelong friend, and I am truly blessed to have you.

To my niece and nephew, thank you for helping me get through some of my toughest days with your radiant smiles and adorable motivational songs. Thank you for being such an important part of my life. I cannot express in words how much you mean to me.

To my loved ones, I am deeply grateful for your support, guidance, love, and encouragement throughout this journey. I truly appreciate each one of you.

## Dedication

To my grandparents, who always encouraged me to dream fearlessly. Your overwhelming love, teachings, wisdom, prayers, and incredible belief in me have molded me into the woman I am today. Your encouragement has sustained my zeal to continually strive for my greatest potential and my enthusiasm for learning. This journey was certainly not easy, but we once more rejoice and say "*Halala, o sareng šate wa duma*!" for having come thus far.

## List of publications

1. Dogbey, D. M., Andong-Koung-Edzidzi, U. C., **Molope, G. A.**, Singh, J., Bvudzijena, T. L., Naran, K., & Barth, S. (2024). EpCAM-targeting cancer immunotherapies: Evidence from clinical studies and the way forward. *Tumor Discovery*, 4926.

# Table of Contents

## Index of figures

## Index of tables

## List of Abbreviations

| | |
|---|---|
| α | Anti |
| ADC | Antibody-drug conjugate |
| AGT | $O^6$-Alkylguanine-DNA Alkyltransferase |
| AML | Acute Myeloid Leukemia |
| AMP | Ampicillin |
| APC | Antigen presenting cell |
| ara-C | Cytosine arabinoside |
| AURIF | Auristatin F |
| BG | Benzylguanine |
| BG-Alexa | BG-modified SNAP-Surface® Alexa Fluor® 488 |
| BleoR | Bleomycin resistance |
| BSA | Bovine serum albumin |
| bsAb | Bispecific antibody |
| Cat# | Catalogue number |
| CCSN | Cell culture supernatant |
| CD | Communicable disease |
| CD33 | Cluster Differentiation Antigen 33 |
| CD45 | Cluster Differentiation Antigen 45 |
| CDR | Complementarity-determining region |
| CFU | Colony forming units |
| $C_H$ | Constant heavy |
| $C_L$ | Constant light |
| CMV | Cytomegalovirus |
| $CO_2$ | Carbon dioxide |
| CR | Complete remission |
| CV | Column volume |

| | |
|---|---|
| DNA | Deoxyribonucleic acid |
| DNR | Daunorubicin |
| Dol-10 | Dolastatin 10 |
| DTT | Dithiothreitol |
| eGFP | Enhanced green fluorescent protein |
| EKS | Enterokinase site |
| EpCAM | Epithelial cell adhesion molecule |
| FACS | Fluorescence-activated cell sorting |
| FBS | Fetal bovine serum |
| FDA | Food and Drug Administration |
| FP | Fusion protein |
| FR | Framework region |
| HAMA | Human anti-mouse antibody |
| HCl | Hydrochloric acid |
| HEK | Human embryonic kidney |
| His-tag | Histidine affinity tag |
| hmAb | Human monoclonal antibody |
| HRP | Horseradish peroxidase |
| HSCT | Hematopoietic stem cell transplantation |
| Ig | Immunoglobulin |
| IMAC | Immobilized Metal Affinity Chromatography |
| IRES | Internal ribosome entry site |
| kDa | Kilodaltons |
| LB | Luria-Bertani |
| mAb | Monoclonal antibody |
| MB&I | Medical Biotechnology and Immunotherapy Research Unit |
| MRD | Minimal residual disease |

| | |
|---|---|
| MW | Molecular weight |
| NCD | Non-communicable disease |
| NEB | New England Biolabs |
| OS | Overall survival |
| ORF | Open reading frame |
| PAGE | Polyacrylamide gel electrophoresis |
| PBS | Phosphate-buffered saline |
| PFA | Paraformaldehyde |
| PVDF | Polyvinylidene Fluoride |
| RCF | Relative Centrifugal Force |
| RPM | Revolutions per minute |
| RPMI | Roswell Park Memorial Institute |
| scFv | Single-chain variable fragment |
| SDS | Sodium Dodecyl Sulphate |
| SES | Socioeconomic status |
| SOC | Super Optimal Broth with Catabolite repression |
| SOP | Standard operating procedure |
| TAA | Tumour-associated Antigen |
| TAE | Tris-acetate-EDTA |
| TBST | Tris-buffered saline with 0.1% Tween® 20 detergent |
| TSA | Tumour-specific antigens |
| UV | Ultraviolet |
| $V_H$ | Variable heavy |
| $V_L$ | Variable light |
| v/v | Volume per volume (%) |
| WB | Western blot |
| w/v | Weight per volume (%) |

| | |
|---|---|
| XTT | 2,3-bis(2-methoxy-4-nitro-5-sulphophenyl)-5-carboxanilide-2H-tetrazolium, monosodium salt |

## Abstract

Acute Myeloid Leukemia (AML) remains a significant challenge to cure. In Africa, Leukemia is among the ten most prevalent cancers. The lack of an updated registry, medical technologies that provide timely diagnosis, and convenient access to appropriate treatments would result in an alarming increase in incidence and fatality rates in the near future. Patients with AML are often treated with chemotherapy, stem cell transplantation, or targeted therapy in an effort to achieve long-term remission and a longer lifespan. However, treatment provision is not always readily available in economically-constrained settings, as in many African countries. Furthermore, while a variety of therapies have been developed for AML, these often result in severe side effects, highlighting the urgent need for advanced medical interventions. Addressing these challenges necessitates innovative therapeutic approaches, such as recombinant antibody-drug conjugates (ADCs), which may offer targeted treatment options with reduced toxicity compared to traditional therapies.

In this study, we focused on developing target-specific next-generation recombinant ADCs to improve treatment outcomes. Immunotherapy, especially the use of ADCs, has demonstrated significant promise in treating leukemia and several other cancers. Targeting CD33 and CD45, which are both highly expressed in AML, by using novel recombinant ADCs offers a promising therapeutic approach. This proof-of-concept study was conducted to show that protein engineering can be used to locally produce immunotherapeutics with potentially fewer adverse effects for the treatment of AML.

Recombinant ADCs comprised of single-chain fragment variables (scFv) fused to a self-labelling human protein called SNAP-tag were generated. SNAP-tag was used for site-specific conjugation to $O^6$-benzylguanine (BG) derivatives to demonstrate functionality against overexpressed and therapeutically relevant AML antigens CD33 and CD45. The scFv component of each recombinant ADC was designed *in silico* and cloned into mammalian expression vectors for production of recombinant SNAP fusion proteins (FPs). Purification of the SNAP FPs was performed using immobilized metal affinity chromatography (IMAC). SDS-PAGE and Western blot analysis were used to characterise the fusion proteins, facilitated by an N-terminal 10x Histidine (His) tag. The αCD33(scFv)-SNAP-Alexa 488 and αCD45(scFv)-SNAP-Alexa 488 fusion proteins were assessed for cell surface binding on AML cell lines using flow cytometry. The recombinant ADCs; αCD33(scFv)-SNAP-AURIF and αCD45(scFv)-SNAP-AURIF were then utilized in an XTT cell viability assay to evaluate targeted cell killing.

The successful design and functionality of these AML-specific recombinant ADCs were demonstrated in this study. This was illustrated by the SDS-PAGE gels results from the initial

IMAC purification showing full-length protein of αCD33(scFv)-SNAP, and αCD45(scFv)-SNAP-tagged fusion proteins at around 51.8 kDa and 52.5 kDa, respectively. Both αCD33(scFv)-SNAP-Alexa 488 and αCD45(scFv)-SNAP-Alexa 488 showed antigen-dependent binding, which was confirmed by flow cytometry. Furthermore, the cytotoxicity assays demonstrated the dose-dependent killing of target AML cells by both αCD33(scFv)-SNAP-AURIF and αCD45(scFv)-SNAP-AURIF. The comparable binding capacity and cytotoxic potential of these generated immunoconjugates to their specific antigenic targets exhibited their hope for use as therapeutic interventions that will advance the field of immunotherapeutics for AML in the future. With the possibility of also using this form of therapy together with other existing AML therapies, there would be chances of enhanced cancer cell death at lower doses of drugs, thus minimizing dose-dependent adverse effects experienced by patients.

In conclusion, encouraging local production of such innovative treatments that are comparable to those sold and made widely available to patients in fully developed countries, can help lessen the impact of the disparities in access to quality healthcare that exist throughout the world as a result of the notably large differences in socioeconomic status. This will in turn also have an overall positive impact on the African economy as less money will be required to purchase and import AML treatments. Instead, the local production of these immunotherapeutics will promote a cost-saving strategy while ensuring that the need for AML patients' access to essential treatments is still met.

# Chapter 1: Literature Review

## 1.1. Background and global statistics on cancer

According to Malacards, a well-established database for human diseases, there have been just over 20,000 entries thus far [1]. Among these, many continue to pose significant challenges regarding their control and complete elimination. Over the years, it has become clear that one of these diseases is cancer. When not in the resting phase, cells typically depend on a series of growth signals within a tightly regulated cell cycle to ensure tissue stability and proliferation through a self-regulating mechanism, even amidst changes to the internal or external conditions they face [2]. In contrast, cancer is characterized by the uncontrolled growth, proliferation, and spread of cells in the body [3]. A crucial aspect of cancer that is often overlooked is that it is not a single disease manifesting uniformly in every patient; rather, it is a vast and extraordinarily complex group of diseases. Its various manifestations and uniqueness in development, survival functions, and treatment outcomes result from its origin in many of the countless cells found in the body [4][5]. The unpredictability in cancer development categorizes it as a diverse or heterogeneous disease [6][7]. Over time, it has been established that this heterogeneous nature is a major reason for ongoing challenges in diagnostic accuracy and the suitability of treatments for some cancer patients.

In a study based on GLOBOCAN estimates of worldwide incidence and mortality for 36 cancers, it was reported that just over 19 million new cases and 10 million fatalities were recorded globally in 2020 [8]. It is anticipated that the global burden of cancer will rise by approximately 58% by 2040, with individuals from developing countries bearing the brunt [9]. Elderly patients aged 50 years and older constitute a sizable portion of the cases and fatalities reported each year [10]. Although this trend seems to prevail annually, the development of cancer and resultant deaths are certainly not exclusively limited to this age group. To support this assertion, researchers have investigated and found that nearly 400,000 individuals between the ages of 0 and 19 are diagnosed with cancer each year [11]. Despite the incidence of cancer in children being lower than in adults, it also continues to slowly rise each year. It is predicted that between 2020 and 2050, there will likely be 13.7 million new cases of childhood cancer worldwide [12]. Thus, in reality, everyone is faced with the risk of developing cancer due to factors that are either within their control or entirely beyond it.

A partial list of prevalent risk factors that contribute to the development of cancer includes age, smoking, excessive alcohol consumption, unhealthy diets, exposure to carcinogens, and hereditary changes due to germline mutations in one's genome. Although these are some of the familiar risk factors, it cannot be said that everyone who is predisposed to them will

undoubtedly develop cancer [13][14]. Differing combinations of the aforementioned risk factors may present concurrently or consecutively in patients to result in various types of this disease. However, the shared mechanisms of cancers on the genetic fundament predominantly exhibit aberrations to the essential growth and proliferation signaling pathways due to the altered expression of the genes and, consequently, the proteins necessary for these specified pathways [15][16]. Furthermore, the varying degrees of severity in patients with cancer, whether it be the same type or not, is attributable to the outcome of the altered expression of genes, otherwise also referred to as genetic mutations [13]. The accumulation of these mutations provides cancer cells with an assortment of capabilities that are deemed advantageous and allow them to live for an extended period of time as opposed to normal cells. In 2000, Hanahan and Weinberg came together and coined these capabilities the "Hallmarks of Cancer", which include self-sufficiency in growth signals, insensitivity to anti-growth signals, evading apoptosis, limitless replicative potential, sustained angiogenesis, and tissue invasion and metastasis [17]. A couple of years later, they brought to light and expanded on the previously mentioned capabilities, which further demonstrated how cancers persevere in acquiring this survival edge [18]. With the help of the exemplary body of work by Hanahan and Weinberg, researchers continue to study the complexities of cancers and strive to find countless advanced ways to treat them.

## 1.2. Cancer research in Africa and its implications

Over time, researchers have succeeded in showing how several factors, including those contributing to the pathophysiological changes causing the development of cancer. As well as those including its initiation, promotion, and progression, have significantly contributed to the variations in cancer severity, incidence, prevalence, and death within and between all countries worldwide. Needless to say, far greater efforts have gone into finding and understanding these contrasts, mainly in developed countries as opposed to developing countries such as those in Africa. A few leading reasons behind this include:

### 1.2.1. Inequalities in global socioeconomic status

Inequalities in socioeconomic status (SES) act as a tremendous contributor to the disparities observed in the aforementioned measures. The lack of financial resources, an up-to-date cancer registry, advanced medical tools, access to effective treatments, awareness and education of individuals on cancer development and control, all form the rudimental point and rationale for the standard of cancer research in Africa. The insufficient funding and dispensation of resources to African countries has resulted in a ripple effect where: (1) pertinent and elaborate work on several cancers still needs to be conducted, (2) timely testing to determine diagnosis of some cancers is rarely achieved and (3) consistency in the

administration of appropriate treatments and provision of exceptional cancer care is yet to be acquired. From the limited studies based on the African population, it has often been observed that low SES is frequently associated with increased risk of cancer, mistimed diagnosis and treatment, as well as increased mortality [19][20][21][22][23]. Similar sentiments have been accentuated by Omotoso (2023) and Coughlin (2019), who state that since the factors and obstacles that have led to such poor quality of research being undertaken in Africa have long been identified, they now need to be addressed and resolved holistically [24][25]. The delay in doing so will not only further disadvantage African patients with cancer, but it will also lead to a sustained rise in the number of cases and deaths. This consequence is evident in a study conducted by Sharma (2022) using the GLOBOCAN 2020 estimates that revealed that there were approximately 1.1 million new cases and 711,429 deaths due to cancer in Africa in the year 2020 [8][26]. Additionally, this study also predicted that between 2020 and 2040, there will be a further increase to 2.1 million new cases and 1.4 million deaths in Africa.

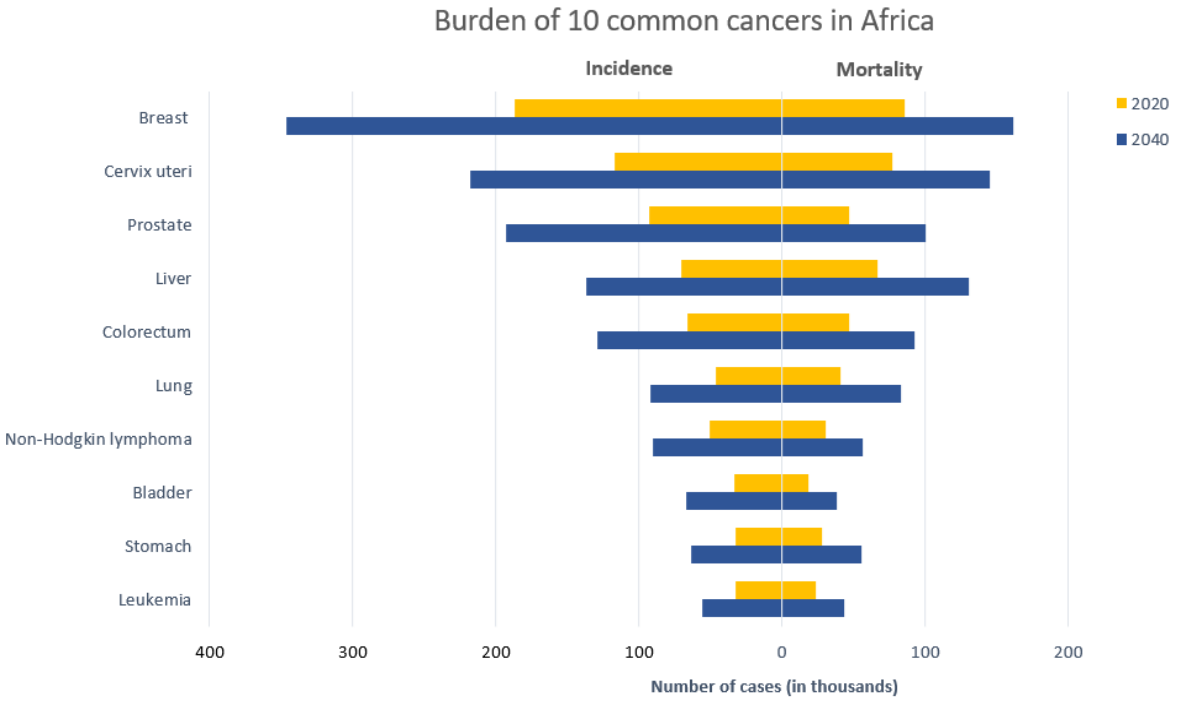


**Figure 1**. **The burden of the ten most common cancers in Africa.** A comparative bidirectional bar chart illustrating the incidence (left) and mortality (right) for the top ten most common cancers in Africa. These cases were reported in thousands for the year 2020 (in yellow) and forecasted for the year 2040 (in blue). Adapted from Sharma *et al.* (2022) [26] and generated using Excel.

### 1.2.2. Underdevelopment in Africa

The quality of cancer research in Africa is also influenced by underdevelopment, which is closely linked to the continent's socioeconomic status (SES). Currently, Africa is considered the most underdeveloped continent, and Wale-Oshinowo (2020) reports that more than 70% of the world's least developed countries are located there [27]. Unlike in developed countries, factors such as incidence, mortality, and prevalence are not thoroughly investigated for certain cancers in African nations. A study conducted by Kayamba (2021) highlights that any published work or information on cancer derived from Africa has focused solely on a very small fraction of the entire continent [28]. This observation calls for increased funding and resources to be allocated to Africa to support comprehensive studies and elevate cancer research to the level conducted in surrounding continents. In line with this work, Ngoma (2019) notes that those in power, responsible for providing such resources, view cancer research in Africa as a “luxury” [29]. Ngoma believes that this perspective has resulted in minimal clinical and epidemiological research being conducted, which are essential for informed decision-making regarding the health of populations. The lack of such research exacerbates the crisis and urgently necessitates a favorable shift in the distribution and acquisition of these vital resources, consequently fostering more informed conclusions about the health of individuals in this population and enhancing their well-being through comprehensive investigations and accurate research findings still needed to be conducted [29]. Therefore, it is evident that there is a pressing need for increased investment in African cancer research to enhance current research output. To achieve this, various approaches can be undertaken; however, the primary recommendation would be to dismantle and rigorously examine the existing cancer research model and its constraints [21][24][30]. Once this is accomplished and necessary reforms are implemented, equity in health practices and norms on a global scale will not only be promoted but will undoubtedly become attainable.

### 1.2.3. The impact of prioritizing communicable diseases

For a notably long time, it has been known that a vast population of Africans have been afflicted with numerous communicable diseases (CDs). The most prominent of these include but are not limited to: respiratory infections, HIV/AIDS, cholera, malaria and tuberculosis [31]. Every year, the number of individuals who succumb to these diseases continues to increase, notwithstanding the ongoing efforts to prevent such occurrences. Although the persistent attempts at controlling and alleviating the burden of CDs is extremely imperative, it has brought about a slightly indubitable diversion from non-communicable diseases (NCDs) in Africa. The immense concentration that has been set on CDs over the years has established a

predicament, perhaps inadvertently so, whereby the rising number of cases and deaths due to NCDs occasionally go unnoticed. Previously, NCDs were not often regarded as the leading causes of mortality. However, with an expectation of further increases in cases and deaths reported, NCDs are now considered the leading cause of death in the foreseeable future [32]. Still, the vast majority of the required efforts to lower these statistics have been devoted to managing CDs rather than NCDs [33]. Evidently, CDs have taken priority in respect to medical research done on this continent; however, this has not halted the escalating burden of cancer in Africa. Hence, the compelling requirement to refocus and comprehensively research NCDs in Africa still remains.

## 1.3. Leukemia: A form of blood cancer

### 1.3.1. Pathogenesis

There are several kinds of cancers known, with the most frequently occurring worldwide being: breast, colon, prostate, lung and bowel [34][35]. These are some cancers that are also well recognized in Africa. Contrarily, blood cancers are a class of diseases that also make quite a significant contribution to cancer statistics through inconspicuous escalations in the number of cases and mortalities (**Figure 1**). For this reason, this group of diseases still needs to be meticulously studied in order to manage them effectively in Africa [36][37][38]. Blood cancers include leukemia, lymphoma, and multiple myeloma. These cancers can be differentiated by their origin, the cells they affect, the formation of a mass, and their treatment courses. Leukemia, the most common of haematological cancers, was named after the Greek words ‘leukos’, which means white, and ‘haima’, which means blood [39]. Conforming to the typical behavior of cancers, leukemia develops from a deviation from the innate process of hematopoiesis, whereby new blood cells and blood cell components are produced throughout one's lifetime to maintain a healthy blood system [40]. The organ responsible for blood formation and regeneration is the spongy bone marrow located in bones such as the ribs, pelvis, thighs and vertebrae. Hematopoietic stem cells (HSCs), which are usually in a quiescent state, are the beginners of hematopoiesis. When active, they initiate what Smith (1990) describes as a "maturational and development program" to produce various lineages of committed and highly functional blood cells and components owing to the pluripotency of HSCs [41][42].

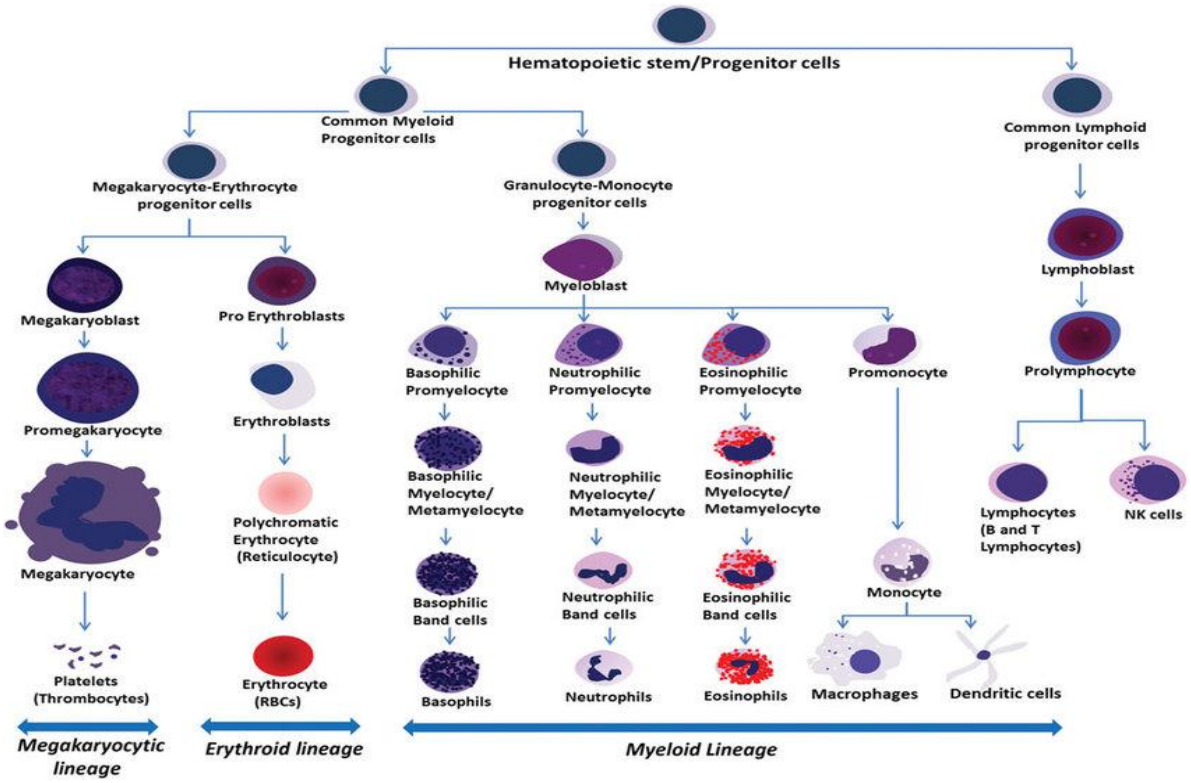


**Figure 2: The blood system's differentiation program from primary pluripotent cells to mature cells.** A depiction of the hierarchical progression of hematopoiesis from immature HSCs to mature and specific blood cells occurring in the bone marrow. Source: Mahalingaiah, Prathap Kumar *et al*. (2018) [43].

### 1.3.2. Leukemia types

Normal blood cells typically live for periods ranging from a few hours to a few weeks, making their continuous replenishment essential [44]. However, to gain a deeper understanding of how leukemia cells deviate from this natural process, it is important to understand the fundamentals of blood cell production. The disruption of hematopoiesis leads to diseases that include, but are not limited to, four main classifications of leukemia: acute lymphoblastic leukemia (ALL), acute myeloid leukemia (AML), chronic lymphoblastic leukemia (CLL), and chronic myeloid leukemia (CML) [39][45]. All these forms of leukemia arise from the production of abnormal white blood cells, known as leukocytes (**Figure 2**) [43][46]. Leukocytes play a crucial role in the human body by participating in innate and humoral immune responses. The body's first line of defense against infections is the innate immune response, which is enhanced by the humoral immune response, that fights infections using antibodies. Leukocytes circulate through the blood and trigger cellular and inflammatory reactions in response to any damage or infections [47]. The leukemias mentioned are caused by disruptions in leukocyte production. This occurs when hematopoietic stem cells (HSCs) divide into lymphoid or myeloid stem cells,

which then further differentiate into granulocytes (neutrophils, basophils, and eosinophils) and agranulocytes (monocytes and lymphocytes). Furthermore, the speed at which these abnormal leukocytes multiply determines whether the condition is acute or chronic. Acute is characterized by a rapid rate of leukocyte proliferation, while chronic indicates a slower rate. Additionally, based on the original stem cell from which the disease develops, the condition is classified as either myeloid or lymphocytic leukemia [45].

### 1.3.3. Standardized classification systems of Leukemia

#### 1.3.3.1. The French-American-British (FAB) classification

AML has been recognized as the most severe and fatal type of leukemia. Consequently, experts developed a system to aid in the diagnosis of the disease. In the 1970s, a group of French, American, and British (FAB) specialists proposed classifying acute leukemia into subtypes based on the type of cells from which it develops and matures [48]. Since the establishment of the FAB classification system, clinicians have succeeded in achieving its initial purpose through the mere visualization of blast morphology using a microscope after staining.

**Table 1**. FAB classification system of Acute Myeloid Leukaemia [49].

| FAB Subtype | Name | Typical Morphology | Characteristics | Immunophenotype | % expression in patients |
|---|---|---|---|---|---|
| **M0** | Acute myeloblastic leukaemia with minimal differentiation | 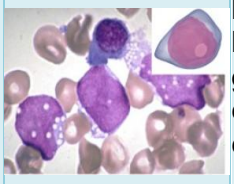 | Rounded nucleus, medium-sized blasts, basophilic non-granular cytoplasm, fine chromatin. | CD33 +<br>CD11b +<br>CD14 +<br>CD15 + | 5% |

| | | | | | |
|---|---|---|---|---|---|
| **M1** | Acute myeloblastic leukaemia without maturation | 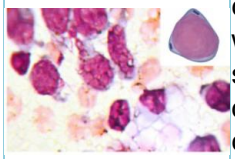 | Rounded nuclei, lightly granulated cytoplasm containing Auer rods, high nucleo-to-cytoplasm ratio within medium-sized blasts, dispersed chromatin. | CD13 +<br>MPO +<br>CD33 +<br>CD34 +/- | 15% |
| **M2** | Acute myeloblastic leukaemia with maturation | 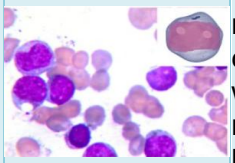 | Prominent Auer rods in cytoplasm, high nucleo-to-cytoplasm ratio within small to medium-sized blasts, rounded nuclei, dispersed chromatin. | MPO +<br>CD13 +<br>CD34 +/-<br>HLA-DR +/- | 25% |
| **M3** | Acute promyelocytic leukaemia | 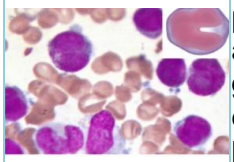 | Monocytic nucleus with an irregular or bilobed deep cleft, proliferation of azurophilic granulation causing little basophilic cytoplasm, sometimes have splinter shaped crystalline | CD13 +<br>CD33 +<br>HLA-DR -<br>CD34 - | 10% |

| | | | | | |
|---|---|---|---|---|---|
| | | | cytoplasmic inclusions. | | |
| **M4** | Acute myelomonocytic leukaemia | 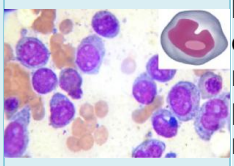 | Lightly granulated cytoplasm, moderate nucleo-to-cytoplasm ratio within large blasts, rounded or kidney-shape nucleus, prominent nucleoli. | CD13 +<br>CD33 +<br>CD15 +<br>CD64 + | 20% |
| **M5** | M5a: Acute monoblastic leukaemia<br><br>M5b: Acute monocytic leukaemia | 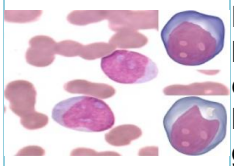 | M5a: Large blasts, rounded nucleus, dispersed chromatin, Auer rods in cytoplasm.<br><br>M5b: Less basophilic cytoplasm with high granulation, sometimes has vacuoles, rounded or kidney -shaped nucleus. | CD14 +<br>CD68 +<br>CD4 +<br>CD64 + | 10% |

| | | | | | |
|---|---|---|---|---|---|
| **M6** | M6a: Erythroid leukaemia with proliferation of mixed blasts<br><br>M6b: Pure erythroid leukaemia | 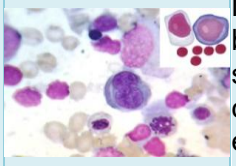 | M6a: erythrocyte morphology is changed with schistocytes.<br><br>M6b: Macrocytes and basophilic stippling constitute erythrocyte. | CD13 +<br>CD33 +<br>CD15 +<br>Glycophorin A +<br>Glycophorin C + | 5% |
| **M7** | Acute megakaryotic leukaemia | 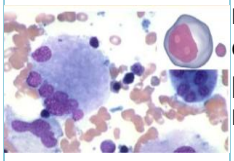 | Non-granular cytoplasm in polymorphic and immature blasts, reticulated chromatin, 1-3 prominent nucleoli. | CD41 +<br>CD33 +<br>CD13 +<br>CD42 + | 5% |

The FAB system has presented repeatability and excellent association in terms of morphology for several years [49][50]. While demonstrating ease of use and practicality, this system was not without its limitations. Specifically, reliance on the analysis of a cell's chromosomal number and structure to identify possible genetic alterations that may be a sign of a particular cancer or hereditary disorder is known as cytogenic data. The absence of this particular data implied that the results obtained from the system were not always precisely associated with the clinical outcomes [51].

#### 1.3.3.2. World Health Organization (WHO) classification

To introduce the slight improvements required in the FAB subcategories, in 2001, the WHO issued their version of acute leukemia classifications. This refined version reposed upon the FAB system by incorporating genetic data together with cytochemical, immunophenotypic,

morphologic and clinical information [52]. In 2022, the 5th edition of the WHO Classification of Hematolymphoid Tumors was released. This edition introduced minor changes in the classification and diagnostic specifications of acute leukemia [53]. These changes aimed to strengthen risk stratification and refine prognosis as a consequence of improved diagnosis and to enhance treatment options as well as their administration.

**Table 2**. WHO classification system of Acute Myeloid Leukaemia [52][54].

| **Classification** | **Description** | |
|---|---|---|
| **WHO2016: AML with recurrent genetic abnormalities**<br><br>**OR**<br><br>**WHO2022: AML defining genetic abnormalities** | Classification of AML into this category is based on the chromosomal mutations that are commonly associated with the disease, such as inversion and translocations mutations**.** | |
| | **WHO2016:**<br><br>▪ AML with t(8;21)(q22;q22.1);RUNX1-RUNX1T1<br>▪ AML with inv(16)(p13.1q22) or t(16;16)(p13.1;q22);CBFB-MYH11<br>▪ APL with PML-RARA<br>▪ AML with t(9;11)(p21.3;q23.3);MLLT3-KMT2A<br>▪ AML with t(6;9)(p23;q34.1);DEK-NUP214<br>▪ AML with inv(3)(q21.3q26.2) or t(3;3)(q21.3;q26.2); GATA2-MECOM<br>▪ AML (megakaryoblastic) with t(1;22)(p13.3;q13.3);RBM15-MKL1<br>▪ Provisional entity: AML with BCR-ABL1 | **WHO2022:**<br><br>▪ AML with RUNX1::RUNX1T1 fusion<br>▪ AML with CBFB::MYH11 fusion<br>▪ Acute promyelocytic leukaemia with PML::RARA fusion<br>▪ AML with KMT2A rearrangement<br>▪ AML with DEK::NUP214 fusion<br>▪ AML with MECOM rearrangement<br>▪ AML with RBM15::MRTFA fusion<br>▪ AML with BCR::ABL1 fusion<br>▪ AML with NUP98 rearrangement |

| | | |
|---|---|---|
| | | ▪ AML with other (rare) defined genetic alterations |
| **AML with myelodysplasia-related changes** | This category comprises AML that started as myelodysplastic syndrome (MDS) and developed into AML as a result of aberrant chromosomes, such as deletions or complete loss of chromosomes, or abnormal blood cell counts. | |
| | **WHO2016:**<br><br>**Complex karyotype (≥ 3 abnormalities)**<br><br>**Unbalanced abnormalities**<br>▪ del(5q) or t(5q)<br>▪ Loss of chromosome 7 or del(7q)<br>▪ Loss of chromosome 13 or del(13q)<br>▪ del(11q)<br>▪ del(12p) or t(12p)<br>▪ isochromosome 17q or t(17p)<br>▪ idic(X)(q13)<br><br>**Balanced abnormalities**<br>▪ t(11;16)(q23.3;p13.3)<br>▪ t(3;21)(q26.2;q22.1)<br>▪ t(1;3)(p36.3;q21.2)<br>▪ t(2;11)(p21;p23.3)<br>▪ t(5;12)(q32;p13.2)<br>▪ t(5;7)(q32;q11.2)<br>▪ t(5;17)(q32;p13.2)<br>▪ t(5;10)(q32;q21)<br>▪ t(3;5)(q25.3;q35.1) | **WHO2022:**<br><br>**Cytogenetic abnormalities**<br><br>**Complex karyotype (≥ 3 abnormalities)**<br>▪ 5q deletion or loss of 5q<br>▪ monosomy 7, 7q deletion, or loss of 7q<br>▪ 11q deletion<br>▪ 12p deletion or loss of 12p<br>▪ Monosomy 13 or 13q deletion<br>▪ 17p deletion or loss of 17p, isochromosome 17q<br>▪ idic(X)(q13)<br><br>**Defining somatic mutations**<br>▪ *ASXL1*<br>▪ *BCOR*<br>▪ *EZH2*<br>▪ *SF3B1*<br>▪ *SRSF2*<br>▪ *STAG2*<br>▪ *U2AF1*<br>▪ *ZRSR2* |

| | |
|---|---|
| **Therapy-related myeloid neoplasm** | Myelodysplastic syndrome (MDS) and AML patients who were exposed to cytotoxic or radiation therapy for an unrelated malignancy or autoimmune disease are included in the subgroup. |
| **AML, not otherwise specified (NOC)** | This group categorises cases that do not meet the requirements for placement in one of the other major groups, as to say that this group was categorized by morphology and did not have any genetic abnormalities.<br><br>This includes:<br>• AML with minimal differentiation<br>• AML without maturation<br>• AML with maturation<br>• Acute myelomonocytic leukemia<br>• Acute monoblastic/monocytic leukemia<br>• Acute erythroid leukemia<br>• Pure erythroid leukemia<br>• Acute megakaryoblastic leukemia<br>• Acute basophilic leukemia<br>• Acute panmyelosis with myelofibrosis |
| **Myeloid sarcoma** | This group includes the AML cases whereby the malignant cells grow into a solid tumour outside of the bone marrow. |
| **Myeloid proliferations related to Down syndrome** | Cases of AML that manifest in individuals with Down syndrome fall under this category. Most cases of AML in people with Down syndrome are acute megakaryoblastic leukemia. |
| **Blastic plasmacytoid** | This group categorises the rare and peculiar cases of AML whereby there is an unusual proliferation of white blood cells known as |

| | |
|---|---|
| **dendritic cell neoplasm** | plasmacytoid dendritic cells which play a pivotal role in immune response. |

### 1.3.4. Epidemiology

Leukemia has accounted for nearly 3% of the global cancer incidence in men and women [55]. Moreover, in 2020, it was ranked the 15$^{th}$ most recurrent cause of incidence and the 11$^{th}$ most common cause of cancer-related deaths worldwide [56]. Of the four recognized types of leukemia, AML is the most common in adults and has consistently exhibited the lowest survival rate as opposed to the other three types [57]. Albeit AML is also present in children, accounting for approximately 15% – 20% of childhood leukemias and almost 33% of adolescent and young adult leukemias [58]. However, AML in adults accounts for approximately 80% of leukemia cases, which is substantially greater than the cases recorded for children [59]. Studies examining and contrasting various aspects of AML in different age groups have shown that age undoubtedly influences treatment, prognosis, overall survival, and other factors [60]. It has been shown that overall survival decreases with an increase in age. This trend was made apparent in a study by Chaudhury (2018), which found that the overall survival rate of AML in children was 60–75% and that it decreased progressively with age to about 5–15% for the elderly [61].

## 1.4. Current AML diagnosis and treatment options

### 1.4.1. Summary of AML diagnostic approaches

The rapidity with which AML begins and progresses generally makes diagnosis complex. Due to the fact that AML is a blood condition, it can be difficult for specialists to confirm a diagnosis based solely on symptoms, which often resemble those of other diseases. Common AML symptoms include frequent infections, easy bruising, fever, bone pain, lethargy, shortness of breath, and irregular bleeding [62]. In most cases, blood tests requested by a doctor for completely unrelated conditions or routine check-ups are usually when AML is discovered in individuals who do not exhibit any symptoms at the time of diagnosis [63]. Only after an individual's blood tests reveal an increased concentration of immature white blood cells, a decreased concentration of red blood cells and platelets does a doctor proceed to utilise other testing approaches to confirm the diagnosis of AML. These further assessments can be seen in **Figure 3** below.

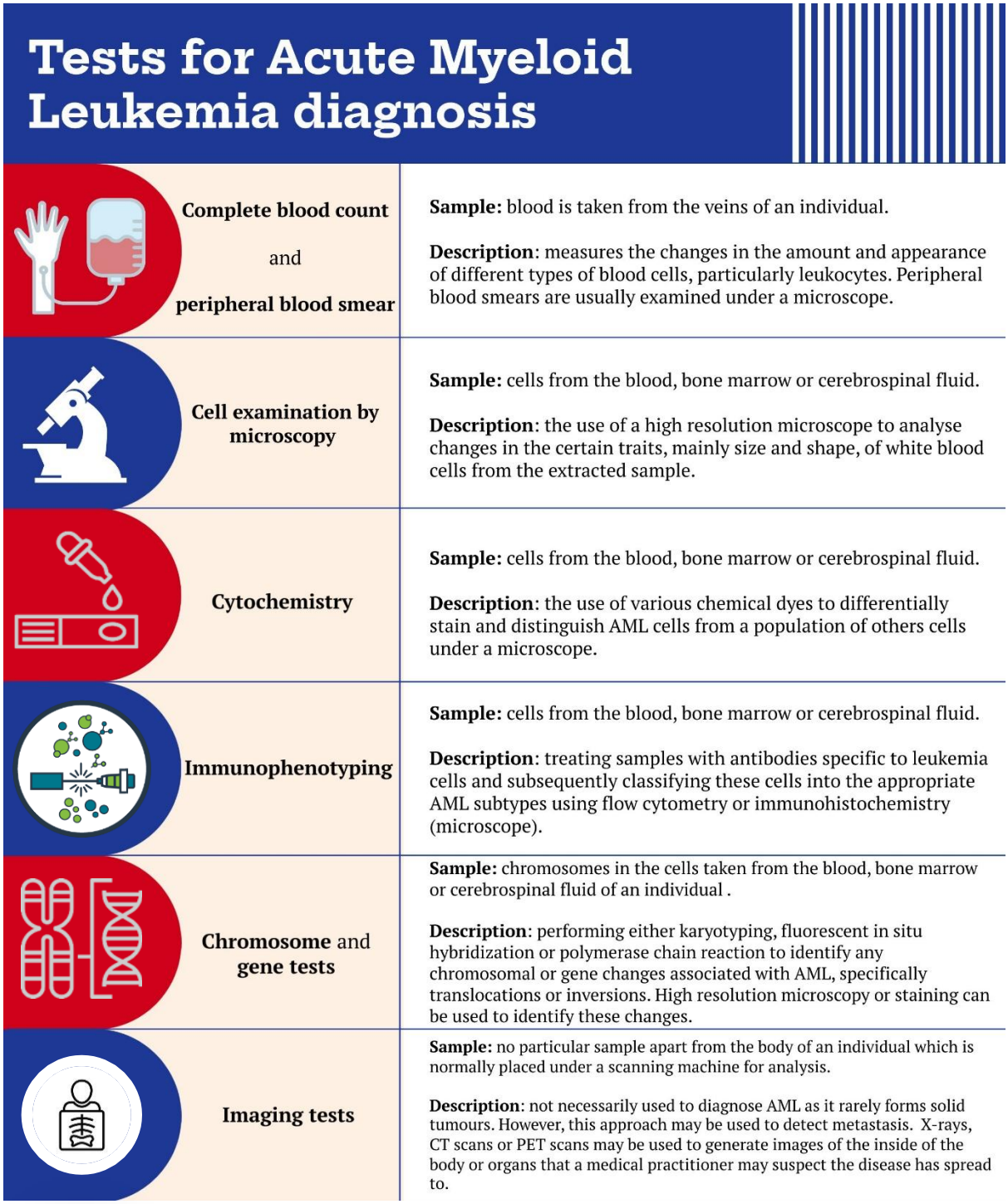


**Figure 3: The various tests which can be performed by doctors to diagnose a patient with AML.** A figure demonstrating the different strategies that diagnosis of AML can be achieved. Several samples such as the blood, bone marrow or cerebrospinal fluid can be assessed using various machines or stains to reach this diagnosis [65]. Image generated using Piktochart.

Apart from the common tests mentioned in **Figure 3**, doctors have also used other methods like magnet resonance imaging (MRI), lumbar puncture, and ultrasound. These methods are not usually opted for as they are not quite economical, largely in the context of Africa.

### 1.4.2. Conventional AML therapies and prevailing challenges

#### 1.4.2.1. Chemotherapy

Chemotherapy is composed of substances that kill cells or cause cytotoxic reactions, which strive to either totally eradicate tumors or significantly reduce their burden [65]. The use of chemotherapy to treat cancer dates to the 1930s, and Bosch (2008) describes it as the enduring success of Paul Ehrlich, the German scientist whose fascination for alkylating agents played a remarkable role in the "transition from experimental pharmacology to pharmacological therapeutics" thus giving rise to chemotherapy [66]. For blood-related diseases, chemotherapy was produced as early as 1948, whereby aminopterin and amethopterin, which are folate antagonists, were used to achieve leukemia remission in children [67]. From this initial point on, chemotherapeutic treatment of AML has evolved and is now done in three phases.

The first phase, known as remission induction, aims to quickly kill and eliminate as many leukemia cells as possible using two or more intensive drugs. One of the drug combinations utilized in this phase, introduced in the 1970s and still relevant today, is the '7+3 regimen.' This regimen involves continuous intravenous administration of cytosine arabinoside (ara-C) for 7 days and short infusions of an anthracycline called daunorubicin (DNR) on the first 3 days [68]. This regimen was developed from a study by Yates (1973) and colleagues, which sought to examine the impact of extending the administration of ara-C and DNR from 5 days and 2 days to 7 days and 3 days, respectively. It was found that just over 60% of the patients, all of whom were younger than 60 years, achieved complete remission. For patients older than 60, the increased duration did not appear to be as beneficial. Currently, doctors tend to administer less intensive treatments to older leukemic patients, particularly lower doses of ara-C and DNR for fewer days, to maximize favorable outcomes. To avoid triggering harmful side effects, doctors may also prescribe other approved low-intensity medications for elderly patients, such as Decitabine or Azacitidine [68].

The second phase of chemotherapy is referred to as consolidation or post-remission therapy. It involves administering additional treatments to prevent a possible relapse. There are several options for consolidation therapy, including further administration of ara-C alone at a higher dose or opting for stem cell transplantation. A doctor selects the most suitable consolidation treatment based on the patient's age and which option has the least chance of causing a relapse.

The final phase is called ‘maintenance’ and is generally not essential. The purpose of the maintenance phase is to further prevent the return or development of leukemia for the longest possible duration by providing patients with treatments such as oral chemotherapeutic drugs [69]. While the method of administering chemotherapy to patients is well-structured and has shown favorable outcomes over many years, it unfortunately does not work as effectively for everyone. Some patients experience short-term side effects like nausea, diarrhea, hair loss, and infections. Others may face long-term side effects, including organ dysfunction, fatigue, and neuropathy [70]. Additionally, some patients may still harbor a small number of leukemic cells in their body, despite undergoing chemotherapy; this condition is known as minimal residual disease (MRD). When active, these remaining cells have a high likelihood of causing relapse. Moreover, chemotherapy has a significant limitation in that, while it effectively eliminates cancer cells, it also destroys a portion of healthy, rapidly proliferating cells. Consequently, researchers have made efforts to develop improved treatments that aim to mitigate these negative effects.

#### 1.4.2.2. Hematopoietic stem cell transplantation

In an attempt to rule out the limitation related to the loss of healthy proliferating cells together with cancer cells following intensive chemotherapy, doctors perform hematopoietic stem cells transplantation (HSCT). The two main types of HSCT that patients are strongly advised to undergo are either: (1) allogeneic HSCT or (2) autologous HSCT. An allogeneic HSCT is the procedure where healthy stem cells are harvested from the blood or bone marrow of a donor via apheresis or a needle and syringe, respectively. The most suitable donor for this procedure can either be related to the patient or not an identical twin. Alternatively, they can be an unrelated individual sharing genetic similarities with the patient. These stem cells are frozen and stored during the time that a patient receives chemotherapy. Only once the patient has completed treatment do the donor's stem cells get infused into the patient's blood. An autologous HSCT is a process whereby healthy stem cells are taken from a patient's own blood or bone marrow. These stem cells are frozen and stored during chemotherapy. Similarly, the patient's own healthy stem cells are introduced back into their blood following chemotherapy treatment. With the aid of their stem cells, the bone marrow heals and is then able to produce healthy cells for blood production [71].

Both types of HSCT have their pros and cons; however, in most cases, patients are encouraged to undergo an autologous HSCT as opposed to an allogenic HSCT. Often times an allogenic HSCT causes graft-versus-host disease (GvHD) which occurs when an immune response in a patient is elicited by the donor transplanted stem cells. Transplanted bone marrow or blood from a donor is perceived by the patient's body as ‘alien’ and as a result, the

donor's body experiences detrimental effects from the donation [72]. On the other hand, the immune system cells obtained from donors may be more potent than those from the patient. Thus, they will work to prevent AML relapse. Conversely, leukemic cells could unintentionally be obtained when healthy patient cells are extracted via apheresis in preparation for an autologous HSCT. When these cells are reinfused, the cancer typically develops again as a result of this [73].

As with chemotherapy, both HSCT types hold shared limitations that have prompted researchers to look into producing and providing more desirable and advanced treatments. Firstly, even though HSCT is highly recommended after chemotherapy, not all patients can meet the expense of such a procedure. Secondly, it is difficult to perform HSCT in areas that lack the resources required for their success, for instance, most African countries. Lastly, these approaches tend to be associated with early mortality due to GvHD, infections, and toxicity [74]. Evidently, novel and ingenious treatments still need to be created in order to accommodate AML patients who receive conventional treatments and still suffer from unfavorable side effects.

#### 1.4.2.3. Targeted therapy

Targeted therapy refers to a treatment approach that attacks proteins essential for cancer cell survival. As mentioned earlier, the sustenance of cancer cells is due to the accumulation of mutations in the genes that typically control normal and healthy cell growth. As more was learned about how these genetic abnormalities originated and produced proteins that supported cancer development, scientists seized the opportunity to create treatments specifically targeting these mutated genes and proteins. It was discovered that a key distinction between the drugs used in targeted therapy and chemotherapy is that the former do not contain cytotoxic agents. This means that these drugs only affect the cancer cells they are designed to target and destroy, sparing healthy cells. Consequently, targeted therapy often results in fewer side effects unrelated to cytotoxicity.

The first targeted therapy approved for cancer treatment was in 1977 [76]. Since then, numerous other targeted therapies have been developed as small molecules or monoclonal antibodies (this form is discussed in 1.4.2.4). The small size of these drug molecules allows them to penetrate cancer cells, target internal proteins, and ultimately destroy the cells. Small molecules designed to treat AML help combat the disease by preventing angiogenesis-promoting signals and suppressing new blood vessel formation. Additionally, apoptosis can be triggered by small molecule inhibitors binding to specific proteins commonly linked to cancer development**.**

**Table 3.** A descriptive table of common FDA approved targeted drugs used for the treatment of AML [77].

| | **HEDGEHOG PATHWAY INHIBITOR** | **IDH INHIBITORS** | **BCL-2 INHIBITORS** | **FLT3 INHIBITORS** |
|---|---|---|---|---|
| **YEAR OR APPROVAL:** | 2012 (Vismodegib) | 2017 (Enasidenib) | 2016 (Venetoclax) | 2017 (Rydapt) |
| **ROLE:** | Hedgehog proteins (namely: PTCH, SMO and Gli), These proteins are responsible for the growth, survival and specialisation of cells. Most importantly, they play a role in chemical signalling that is essential for embryonic development. | IDH1 and IDH2 proteins which are responsible for producing enzymes that allow the cells to produce energy. These enzymes also keep the cellular redox state constant and prevent oxidative state. IDH1 expression occurs in the cytoplasm and IDH2 expression occurs in the mitochondria. | BCL-2 proteins are responsible for controlling cell death and ensuring that it occurs at the correct rate. This is achieved by using anti-apoptotic and pro-apoptotic proteins. BCL-2 is expressed on the outer membrane of mitochondria. | FLT3 protein is responsible for the proliferation and growth of the cells, which include blood cells in the body. This protein is expressed on hematopoietic stem cells and granulocyte/macrophage progenitor. |
| **REASON FOR TARGETING:** | Preventing abnormal and dysregulated activation of the Hh pathway which has been | A mutation in any one of the IDH genes prevents the blood cells from maturing and | The BCL-2 gene is able to transfer from the chromosome on which it is | A mutation in the Flt3 gene results in increased production of |

| | | | | |
|---|---|---|---|---|
| | known to result in tumorigenesis and other developmental disorders. | from developing normally. | naturally found (chromosome 18) to another chromosome. This causes increased amounts of BCL2 to be produced and consequently prevents apoptosis from occurring. | immature white blood cells. |
| **MECHANISM OF ACTION:** | The elevation of GLI transcriptional activity in cancer cells exposed to SHH ligands is inhibited by SMO blocked by a small molecule. When induction does not occur, SHH signalling is limited and the capacity to support tumour growth and cancer stem cell sustenance is stopped. | IDH inhibitors block mutant IDH proteins and promote the differentiation of leukaemia cells into normal cells. | BCL-2 inhibitors function by activating core intrinsic regulators of apoptosis, specifically BAK and BAX proteins. This leads to mitochondrial membrane permeabilizatio n and eventual cell apoptosis. | FLT3 inhibitors competitively block ATP from binding at the ATP-binding site of intracellular tyrosine kinase domain (TKD). Therefore preventing autophosphoryl ation and then inducing cell cycle arrest and differentiation. |

| | | | | |
|---|---|---|---|---|
| **FREQUENCY OF MUTATION:** | Has not been thoroughly assessed and recorded yet. | Of adult AML patients, 6–16% have IDH1 mutations and 8–19% have IDH2 mutations. | 95% of patients with relapsed acute myeloid leukaemia and 84% of patients at diagnosis often have BCL-2 overexpression. | 25% in adults and 10% in children. |
| **SIDE EFFECTS:** | Anaemia, muscle and bone pain, sores in the mouth. | Nausea, increased bilirubin predisposing to jaundice and loss appetite. | Low level of white and red blood cells, bleeding and pneumonia. | Fever, headache, vomiting and respiratory infections. |

The effectiveness of targeted therapy compared to chemotherapy for the treatment of AML has been remarkable to the extent that there have recently been more new targeted therapies in development and others undergoing clinical trials [77]. Although it has been established that targeted therapies are powerful and achieve their goal with reduced damage to healthy cells, they still show adverse effects and challenges as seen in **Table 3**. Moreover, some patients develop resistance due to changes in the protein being targeted, ultimately disrupting the necessary interaction with the drug once administered. In addition, another challenge is that the structure and function of a few targets are complex, and it can, therefore, be challenging to produce targeted therapies for them.

#### 1.4.2.4. Immunotherapy

Immunotherapy refers to a cancer treatment in which a patient's immune system is stimulated and strengthened to fight off cancer with the aid of specific substances that are made naturally by the body or in a laboratory [78]. This form of therapy is believed to have been pioneered by the American bone surgeon and cancer researcher called William Coley [79]. In 1891, W. Coley injected a mixture of live and inactivated *Streptococcus pyogenes* and *Serratia marcescens* in an inoperable cancer patient. This resulted in erysipelas and stimulated the immune system to attack the tumor and eventually lead to tumor regression [80]. For a while after this, he expanded on his research and findings and continued to treat numerous sarcoma patients using this method. This work has provided the groundwork for successive researchers

to produce immunotherapies for various other cancers. There are two types of immunotherapy, which can be categorized either as active or passive. Active immunotherapy can be defined as immunization that evokes an immune response through antigens which potentially act as immunological stimulants [81]. Immune checkpoint inhibitors, immunomodulators, oncolytic viruses, cancer viruses that are DNA- or peptide-based, and whole cell vaccines are all considered active immunotherapy. Contrarily, passive immunotherapy can be defined as the process of administering either cytokines or tumor-specific monoclonal antibodies (mAbs), which may be attached to toxins for the killing of cancer cells. It can also be defined as the administration of augmented immune cells through adoptive transfer [82].

Currently, there are over five approved immunotherapy options for leukemia [77][83]. Two of these are immunomodulators named Interferon alfa-2a and Interferon alfa-2b, which are cytokines that target the IFNAR1/2 pathway. The mechanism of action of these treatments is not well understood. However, the pathway they target is known to play a major role in facilitating a key cellular response that is anti-viral and prevents proliferation. The use of these immunomodulators was approved for patients with hairy cell leukemia. Two other immunotherapies that were approved less than a decade ago are Brexucabtagene autoleucel and Tisagenlecleucel. Both these drugs were classified as adoptive cell transfer therapies that utilize CAR-T cells to target CD19 in older patients and young adults or children with ALL, respectively. These drugs work similarly in that once they have bound to CD19, a signal that prompts CAR T-cell expansion and activation is transmitted. Resultantly, the CAR-T cells release chemokines and cytokines, which work together to destroy tumors. All remaining produced and approved immunotherapies use monoclonal antibodies to treat various antigens that are highly and abnormally expressed in leukemias. For instance, a CD52 targeting naked monoclonal antibody called Alemtuzumab was produced to treat CLL. Likewise, drugs such as Rituximab, Ofatumumab, and Obinutuzumab, which are also aimed at treating CLL, were designed to target overexpressed CD20. Clinicians often administer any one of these drugs with another form of therapy to ensure effectiveness.

As an alternative, researchers have discovered additional surface proteins that are overexpressed in the same kind of leukaemia, which can be targeted simultaneously to improve the efficacy of the treatment. By doing this, they have been able to design numerous monoclonal antibodies, such as those for CLL, which can be given simultaneously to maximize treatment. However, some patients have experienced adverse effects due to being given different treatments at the same time. As a way to combat this disadvantage, bispecific antibodies (BsAb) have been created. A BsAb refers to an antibody that consists of two binding sites that allow it to attach to a cell either at two distinct antigens or at differing epitopes, which

may be found on the same antigen [84]. Blinatumomab, which was approved it 2014, is a BsAb for children and adults with ALL and minimal residual disease (MRD). It is composed of a pair of the variable regions of two different antibodies that target CD19 and CD3. The dual functionality of this BsAb and the many others that have been produced has led to their unlimited application with respect to diagnosis and treatment [85].

Similar to BsAbs, another form of immunotherapy that has shown practicality in more than one way is an antibody-drug conjugate (ADC). ADCs are fast becoming a compelling medical implement to fight cancer as they are composed of a mAb which is conjugated to a cytotoxic drug via a stable chemical linker [83]. In 2000, the first ADC called Gemtuzumab ozogomicin (GO) was approved to treat CD33-positive AML in adults. Approximately 85-90% of adults and pediatrics express the CD33 antigen, which is targeted by GO. A decade later, the manufacturing company of GO voluntarily withdrew the drug from the market due to fatal adverse side effects that a portion of patients experienced in the long run. These side effects included infections, hemorrhage and respiratory distress syndrome [86]. Soon after this discovery, researchers conducted further studies on GO, which mostly concluded that a decrease in the initial FDA-approved dosage administered to patients would instead be more beneficial. These studies included three clinical trials with over 500 CD33-positive patients. The administration of GO in these trials was given either in combination with chemotherapy in one study or as a monotherapy in the remaining two studies. In the combinatorial therapy trial, it was seen that the event-free survival was higher in the patient group receiving both forms of treatment versus the group that received chemotherapy alone. In one trial study where GO was administered as a monotherapy, the median overall survival of the treatment group was 1.3 months more than the control group. Furthermore, in the second monotherapy trial, 26 out of 57 patients achieved complete remission lasting approximately 11.6 months after receiving the first course of GO [87]. In spite of these intriguing findings which demonstrated an overall favorable risk-to-benefit profile, researchers still aim to further improve this medical intervention as the information about it continues to broaden.

## 1.5. Developing AML specific medical interventions

As discussed in section 1.4.2, many different blood cancer treatments are available. However, more targeted immunotherapies specifically for AML still need to be created, as the ones currently on the market are not widely available to patients in Africa and are not affordable.

### 1.5.1. Identifying suitable antigens to target for AML treatment

#### 1.5.1.1. Therapeutically relevant AML antigens

Every cell in the body expresses macromolecules which can be referred to as 'identification markers' and are traditionally called antigens. In the beginning, perfecting the design and targeting ability of mAb-based treatments posed a minor challenge because antigen expression is not always unique to cell types. To be precise, healthy cells largely express normal antigens, whereas cancer cells predominantly express mutated antigens and some normal antigens too [88]. The expression of antigens on cancers can be classed into two groups, either the tumor-specific antigens (TSAs) or tumor-associated antigens (TAAs). Both of these types arise due to various mutations, however, TSAs occur endogenously and present exclusively on tumor cells. Contrastingly, TAAs can be found on tumor cells and on some healthy cells too [89]; they have shown higher levels of expression on tumors compared to TSAs [90]. The expression of TAAs on healthy cells has hindered the capacity of the mAb treatment to specifically attack the cancer cells, which should ideally be the only cells expressing the mutated antigens [91]. With the knowledge of this barrier, researchers have based their selection of targeted antigens on a few factors with the most dominant being 'overexpression'. Antigen overexpression refers to a phenomenon whereby antigens on cancer cells are expressed at a much greater level relative to healthy cells [92], thus making it more feasible to target a greater number of cancer cells as opposed to healthy cells.

**Table 4.** A non-exhaustive table of antigens that studies have shown to be overexpressed in AML [93][94].

| Target | Function | Level of expression |
|---|---|---|
| **CLL-1** | A transmembrane glycoprotein that plays a role in immune response modulation by recognition of molecular patterns linked to either pathogens or damage. | 85 - 92% on leukemic stem cells and blast cells. |
| **CD7** | A glycoprotein which is expressed on the surface of T-cells and natural killer cells. This protein is essential for lymphoid development, particularly T-cell and B-cell interaction and differentiation. | Approximately 90% of lymphoblastic T-cell leukaemia and lymphoma.<br><br>Approximately 30% of AML cases. |

| | | |
|---|---|---|
| **NKG2DL** | An activator receptor which plays a role in both types of immunities by recognizing abnormal cells and cellular stress. | 75 – 80% |
| **CD33** | A transmembrane receptor which is commonly found on myeloid cells. This protein constitutes two tyrosine residues, and when phosphorylated it has an inhibitory effect. | 85 – 90% |
| **CD123** | An extracellular marker which contributes to the production and function of hematopoietic cells. As well as the differentiation of these HPCs into myeloid and lymphoid cells | 45 – 95% |
| **WT-1** | An intracellular suppressor protein which functions in the modulation of growth, death and differentiation of cells | 70 – 90% |
| **CD45** | A protein tyrosine phosphatase that functions as a major modulator of cell signaling in hematopoietic cells, including leukemic cells, and is essential for cell activation, proliferation, and differentiation. | >20% |

The following antigens have been identified as therapeutically relevant and will be the primary focus in this particular study:

#### 1.5.1.2. Cluster of differentiation 33 (CD33)

CD33 is the smallest member of the sialic acid-binding immunoglobulin-related lectin family. The gene encoding this 67 kDa transmembrane glycoprotein can be found on chromosome 19 [95]. CD33 is expressed when HSCs commit to myelomonocytic differentiation and appears on the cell surface of mature and immature myeloid progenitors, monocytes, a few granulocytes and macrophages [96][97]. This protein is composed of an extracellular variable-set immunoglobulin-like domain that mediates sialic acid binding. Additionally, CD33 also

contains a C2-set immunoglobulin-like domain in the extracellular region, a transmembrane domain and an intracellular cytoplasmic tail that has two conserved immune tyrosine-based inhibitory motifs (ITIM) [98]. Although the structure of this protein has been determined, its exact physiological function is yet to be discovered. Phosphorylation of the cytoplasmic ITIM causes a response that attracts Src homology protein tyrosine phosphatases 1 and 2 (SHP-1 and SHP-2), which assist in reducing the activation of cells expressing this antigen. Due to this, CD33 is considered an inhibitory receptor [99]. Cell signaling, adhesion, and proliferation are all impacted by CD33 in healthy cells. When this antigen is produced in excess by cancer cells, as in the case of AML, these processes occur not just abnormally but also quite rapidly [100]. Moreover, studies continue to make it increasingly clear that CD33 suppresses tyrosine kinase-driven signaling pathways, hence affecting immunological and inflammatory responses [101]. CD33 antigen expressed on bone marrow blasts of AML patients is slightly over three times more frequent than on CD33-positive healthy cells [102]. Furthermore, studies have shown that 85–90% of recorded AML cases, both adult and pediatric, are often CD33-positive [103]. Although further research is necessary to fully grasp the role of CD33 in AML development, its differential expression in AML has essentially made it a very appealing target for therapy [97].

#### 1.5.1.3. Cluster of differentiation 45 (CD45)

CD45 is a 180-240 kDa glycoprotein also known as leukocyte common antigen or protein tyrosine phosphatase receptor type C. The expression of CD45 occurs on nearly all hematopoietic cells, except for mature erythrocytes and plasma cells [104]. T-cells, in particular, display the highest levels of CD45, accounting for up to 10% of the proteins on their surface [105]. In cases of leukemia, this protein is reported to be expressed in over 80% of ALL cells and an even greater proportion of AML cells [106]. The gene that encodes this protein is located on chromosome 1 [107] and consists of an extracellular domain, a short transmembrane domain, and two intracellular domains [108]. The extracellular domain can vary in length due to alternative splicing but mainly includes three membrane-proximal fibronectin type II repeats, a cysteine-rich region, and a variable N-terminal region [109]. While the major effects of this variability caused by splicing are yet to be fully understood, recent investigations have highlighted its role in cellular signaling [110]. The level of activation and differentiation of hematopoietic cells influences the cell surface expression of specific CD45 isoforms. The intracellular region contains two phosphatase domains: one that participates in intrinsic kinase activity and another that is typically inactive; however, both are essential for optimal phosphate activity [108]. Generally, the dephosphorylation of the C-terminal negative regulatory phosphotyrosine site of CD45 constitutively primes src-kinase molecules, which

positively regulates T cell receptor signaling. Conversely, CD45 has also been shown to exert a counteracting effect by dephosphorylating constituents of the T cell receptor complex and negatively influencing the autocatalytic tyrosine phosphorylation site of src-kinase enzymes [111]. Ultimately, the various CD45 isoforms have slightly different capabilities to achieve the same result: promoting T cell activation through T cell receptor costimulation by scr-kinase enzymes for enhanced functions such as proliferation, differentiation, and cytokine production.

### 1.5.2. Establishing an appropriate immune response

For an adaptive immune response to be triggered in the body, it is essential that antigens are present. Antigens exist either as toxins, bacteria, fungi, parasites or viruses [112]. Some are produced internally, while others are exogenous and can enter through the nose, mouth and wounds in the skin. As a means to protect itself, the body recognizes these antigens as 'foreign' or 'non-self' and subsequently prompts the adaptive immune system. When antigens are detected in the body, there are two types of immune responses that may occur, which are both directed by lymphocytes. One of these responses is cell-mediated and it eliminates unwanted cells decorated with the target antigen through antigen presenting cells (APCs) which internalize and then break down the antigen. APCs set forth the broken down fragments of the antigen to activated T cells which either kill cells that display this antigen or recruit other immune cells to remove these unwanted cells. The second response, which relies greatly on B-cells, is antibody-mediated and is initiated by the binding of paratopes or antigen-binding sites on antibodies to unique binding sites or epitopes on target antigens [113].

### 1.5.3. Antibody production for AML treatment

#### 1.5.3.1. The natural development of antibodies

Normally, both B- and T-lymphocytes are inactive and can be found circulating within the blood and lymphatic system. In the event that antigens enter the body, circulation of the idle B-cells becomes terminated and this is swiftly followed by the binding of these cells onto the foreign antigens. Upon this encounter, B-cells become active with the help of T-cells and then proliferate and differentiate into plasma cells and memory cells [114]. Plasma cells are fully differentiated and enlarged and are responsible for producing and secreting the antibodies that bind specifically to the antigen that prompted their production. Alternatively, memory cells are differentiated, smaller and are in charge of memorizing the encountered antigen in order to rapidly identify and attack it when re-exposed to it in the future [115]. The basic structure of the secreted antibodies is Y-shaped, and constitutes of four polypeptide chains, namely: two identical inner heavy chains and two identical outer light chains. On each chain a variable (V) region and constant (C) region can be found at the amino and carboxyl terminal ends, respectively [116]. To be exact, the light chains are comprised of one variable domain ($V_L$) and

one constant domain ($C_L$), whereas the heavy chains are made up of one variable domain ($V_H$) and 3 or 4 constant domains ($C_H1$ - $C_H4$). At a location known as the "hinge," disulfide bonds hold the two identical heavy chains together. Disulfide linkages also bind the heavy chains to the light chains.

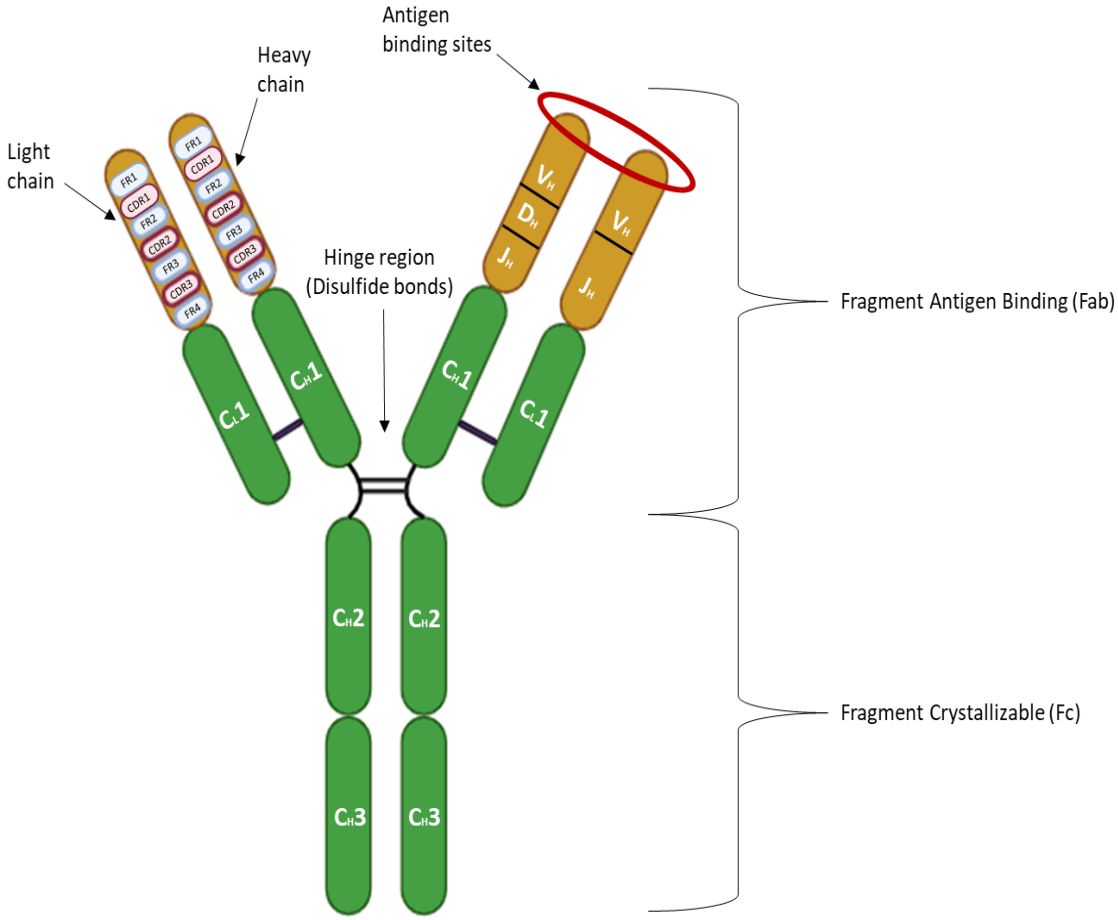


**Figure 4: Typical structure of a IgG antibody**. A diagram illustrating the structure and specific regions of an antibody. The constant regions of both the light ($C_L1$) and the heavy chains ($C_H1$, $C_H2$ and $C_H3$) are depicted in green. The variable regions are depicted in yellow, demonstrating the FR and CDR regions on the left and V(D)J gene segments present on both the light and heavy chains on the right. Linkage of the chains occurs by disulfide bonds. The antigen binding site also known as the paratope can be found in the area circled in red. The arms of the Y-shaped antibody are referred to as the fragment antigen binding region (Fab) and the tail is called the fragment crystallizable region (Fc). This image was generated using Biorender and adapted from Giovanni (2013) [120].

### 1.5.3.2. Antibody isotypes and functions

The variable domains on the heavy and light chains work together to achieve antigen binding and specificity, and are together referred to as the antigen-binding fragment (Fab). The function of the tail end Y-shaped antibody, which is also termed the crystallizable region (Fc), is dependent on the heavy chain present. The differences in size and composition of the heavy chains puts forth the diversity that antibodies exhibit structurally and functionally. IgA, IgD, IgE, IgG and IgM are the five types of mammalian immunoglobulin heavy chains that can be found. The monomeric IgD and IgE each only make up less than 1% of immunoglobulin in serum. The function of IgD still remains unclear, however it is known to react with certain bacterial proteins. Contrary, IgE functions in hypersensitivity, responses to allergies and defenses against parasitic infections. IgM, a pentameric immunoglobulin, is the third most expressed in serum at about 10%. These antibodies act as the first responders to any foreign substances, defend against infections and partake in immunoregulation. The monomeric, but usually dimeric, form of IgA plays a crucial role in protecting mucosal surfaces from pathogens and makes up about 10-20% of immunoglobulins in the serum. The last isotype of immunoglobulins which is often also referred to as the main antibody due to its increased circulation is IgG. This monomeric antibody makes up approximately 70-85% of total serum immunoglobulins [117][118]. Unlike other immunoglobulin types, IgG can be further divided into IgG1, IgG2, IgG3 and IgG4, which all result in differing effects once bound to their respective effector cells. However, the main functions of the IgG subtypes can be summarized as: (1) neutralization and opsonisation of pathogens, (2) phagocytosis, (3) activation of the complement system responsible for the removal of unwanted cells and finally (4) placental transfer from a mother to a fetus whilst their humoral response is developing [119].

### 1.5.3.3. Achieving specificity for antibody-based therapeutics

To produce effective antibody-based therapeutics, scientists focus on ensuring that antibody designs are highly complementary to the surfaces of targeted antigens. This is facilitated by available technologies that enable the manipulation of protein structures. An individual's immune system can produce a diverse range of antibodies, achieving specificity through a process known as 'VDJ recombination. Each $V_H$ and $V_L$ chain can be divided into four interchangeable conserved framework regions (FR) and three polymorphic complementarity-determining regions (CDR) (**Figure 4**). The third CDR on these variable chains contains the VDJ recombination junction [120]. VDJ recombination involves the unique repositioning and joining of specific variable (V), diversity (D), and joining (J) gene segments by a recombinase complex, generating different antibodies that bind uniquely to encountered antigens. So far, it has been reported that the $V_L$ chain can be derived from a pairing of any one of 30 V gene

segments and 4 J gene segments, resulting in approximately 120 different types of antibodies. Similarly, the $V_H$ chain can be generated from a combination of any one from each of the 46 V gene segments, 27 D gene segments, and 6 J gene segments, thereby producing over 7,000 types of antibodies [121]. Given that the previously mentioned V region genes can additionally attach to any of the 9 C region genes on each chain, it is estimated that the human antibody repertoire exceeds one billion [122].

### 1.5.4. Strategies to produce antibodies

Some of the research done over the years which has made astounding contributions to the production of antibodies in large quantities for commercialization traces back to 1970, where Askonas and colleagues reported the isolation of a single plasma cell clone that produced a homogenous antibody reproduced through serial spleen cell passaging into irradiated syngeneic mice [123]. About half a decade later, Milstein and Köhler advanced on the former work by immunizing and then extracting B-lymphocytes from the spleen of mice. These B-lymphocytes were then fused to an immortal myeloma cell line resulting in hybridomas [124]. The process of cell fusion is often performed by centrifugation and the addition of a polymer called Polyethylene glycol, which aids in ensuring that the process of merging two or more desired cells occurs smoothly. Another method involves the fusion of cells by the application of an electric field and is termed electrofusion [125]. The resultant hybridomas from Milstein and Köhler's work proved to be highly convenient as they could be propagated indefinitely to produce monoclonal antibodies and thus eliminate the need to perform serial passaging. This was made possible as the hybridomas had gained immortality and selective resistance through the fusion of B-lymphocytes and myeloma cells. As the earliest form of antibody-based therapeutics at that time, these murine-derived monoclonal antibodies managed to achieve the desired effect; however, due to their species of origin they later exhibited issues related to hypersensitivity reactions, increased immunogenicity and fast clearance from a patient's immune system by human anti-mouse antibodies (HAMAs) as they were recognized as foreign when administered to humans [126][127].

Scientists have used different techniques to circumvent the aforementioned side effects, especially those related to immunogenicity. The first of these is known as chimerization and it involves replacing the constant regions of a murine antibody with the constant regions of a human antibody thus making it approximately 30% murine and 70% human. The combination between these two regions was found to slightly reduce the chances of it being recognized and removed from the body [128][129]. Quite a few chimeric antibodies have been approved by the FDA [130][131][132], and although they undoubtedly had a higher efficacy than murine mAbs, these chimeric mAbs also could not completely evade elimination when provided to

patients because the murine portion, albeit small, could still be identified by HAMAs [133]. In another effort to further improve these antibody-based treatments, CDR grafting was employed to produce humanized mAbs. Gregory P. Winter developed this technique in 1986, which made it possible to introduce mutant murine CDR sequences into a human framework that is most similar to them and modify the structure's amino acids to improve stability [134]. Beyond the reason that humanized mAbs induced minimal immunogenicity contrary to murine and chimeric mAbs as they only contained roughly 5 - 10% of murine content. These humanized mAbs also promoted the performance of human effector functions through the human crystallisable region and exhibited an extended serum half-life. Despite the significant evolution from murine mAbs to humanized mAbs over a period of ten years, there still remained a need to ensure that they comprised zero murine components for optimal potency.

Recent advancements in antibody therapeutics have led to the development of fully human monoclonal antibodies (hmAbs), which can be produced via phage display, transgenic mice, or single B cell antibody technology [127]. Phage display is a method for generating hmAbs that starts with displaying polymerase chain reaction (PCR) generated antibody fragments on the pili of filamentous bacteriophages. A combinatorial library of over a million antibody fragments attached to bacteriophages undergoes multiple rounds of biopanning and eventual screening to identify immuno-positive phage clones or antigen-specific antibody fragments. After screening, full-length hmAbs are created by modifying the DNA from selected bacteriophages. The second method, comparable to the work of Milstein and Köhler, involves immunizing trans-chromosomic mice, enabling gene editing in their embryonic stem cells, specifically replacing mouse antibody genes with human antibody genes. With these genes inserted, the mice can produce fully hmAbs in larger quantities [135]. The final method involves using various techniques to isolate and sort single B cells from a population of peripheral blood mononuclear cells or specific tissue cells from an infected donor. Reverse transcription - polymerase chain reaction is then employed to clone and express the variable heavy and light chains of each immunoglobulin from the isolated single B cells in mammalian cell lines for hmAb generation [127][133].

## 1.6. A novel approach for AML immunotherapy

### 1.6.1. Protein engineered antibody fragments

Although antibody-based immunotherapies have shown great success, especially fully hmAb, these treatments also regrettably exhibit some issues pertaining to high production costs, limited tumour penetration and minimal potency in just a few instances. To overcome these challenges, researchers have begun to explore the production of immunotherapies comprising of antibody fragments rather than full mAbs by maximising the use of bioengineering tools and

techniques that produce these antibody fragments through enzymatic digestion of full mAb [136]. **Figure 5** demonstrates the several Ab fragments that have been generated thus far [137], and their reduction in size compared to full mAbs have shown highly enhanced permeability into tumours [138]. Additionally, the size of Ab fragments offers better binding specificity and affinity, even on antigenic targets, which could be considered to be concealed. The most notable advantage of this form of Abs is their low cost of production which consequently encourages high yield production [139]. Quite a few Ab fragment-based immunotherapies have been approved by the FDA and European Medicines Agency [137][140].

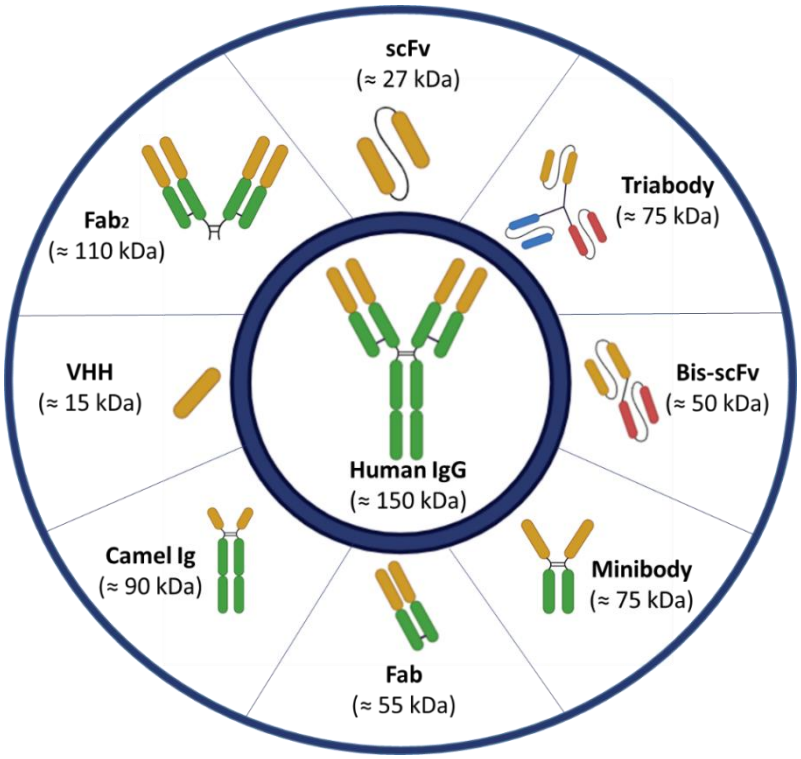


**Figure 5: A schematic diagram illustrating several variants of antibody fragments [137].** Using protein engineering, numerous antibody fragments with different sizes have been generated from the fully human IgG which is 150 kDa. The scFv is composed of is of the variable heavy ($V_H$) and variable light ($V_L$) chains joined by a short flexible peptide linker. A triabody has 3 warheads comprised of three scFv molecules joined by a polypetide linker. A bispecific (bis) – scFv is made of two different antigen binding sites connected by a flexible linker and binds two varying antigens simultaneously. Two scFvs connected by the human IgG $C_H3$ region form the basis of a minibody. A Fab is made of $V_H$ and $V_L$ chains joined to $C_H1$ and $C_L1$by a disulphide bond. This Ab fragment lacks the essential C region that plays a major role in antigen binding and specificity. A camel Ig comprises of two 'variable heavy domain on heavy chain' (VHH) fragments connected to the Fc region of an Ig. A Fab2 is made up of two Fab fragments joined together by disulphide bonds. This image was adapted from Zeng *et al.* (2012) [137] and generated using Biorender and Powerpoint.

### 1.6.2. Using SNAP-tag to advance ADCs

Regardless of the withdrawal and eventual re-approval of GO (1.4.2.4), this ADC has demonstrated, to some extent, what researchers aimed to achieve regarding the specificity and fundamental purpose of this therapy, leading to the production of over a dozen additional ADCs for the treatment of other cancers [141]. However, ADCs also present a significant drawback related to the unknown stoichiometric conjugation between the antibody and effector molecule, which affects payload delivery and treatment efficacy [142]. The reason for this issue revolves around two primary antibody-to-toxin conjugation methods: binding to lysine side chains of a mAb or reactive sulfhydryl groups from reduced disulfide bonds [143]. Due to the abundance of lysine and cysteine side chains on a mAb, numerous conjugation reactions inadvertently occur, resulting in a variety of ADC products with differing drug properties [144]. Further investigation of this diverse population of ADCs revealed that enhanced therapeutic potency could be achieved by precisely controlling the number of drugs attached to an antibody [145]. Consequently, several conjugation methods have been developed, enabling site-specific conjugation between an antibody and a drug, thereby ensuring reliable synthesis through protein engineering and uniformity in the ADCs produced.

One site-specific conjugation strategy which has been developed and is being implemented due to its innovative nature and production feasibility is SNAP-tag. This protein emerged from an engineered mutant of a human DNA repair enzyme known as $O^6$-alkylguanine-DNA alkyltransferase (AGT). In its natural state AGT is responsible for the restoration of damaged DNA by the removal of a substrate's alkyl group located at position 6 of a mutagenic guanine base to an active cysteine acceptor site ($^{145}$Cys) within the protein [146]. Similar to AGT, SNAP-tag functions by quickly and irreversibly transferring the benzyl group from an $O^6$-benzylguanine (BG) derivative to an active cysteine residue specifically through nucleophilic substitution and thus releases a free guanine from the BG derivative (**Figure 6**) [147]. The refinements executed through engineering to create SNAP-tag resulted in a mutant protein with reduced size (182 amino acids and ~19.4 kDa), decreased binding to DNA, increased specificity and reactivity, and improved folding under oxidative conditions [146][148]. Although SNAP-tag is relatively much smaller than other proteins, this ingenious enzyme offers unique fusion to almost any protein of interest, for example an antibody fragment, in order to facilitate precise & highly efficient autocatalytic labelling under physiological conditions of BG-modified substrates with a consistent 1:1 stoichiometry [148].

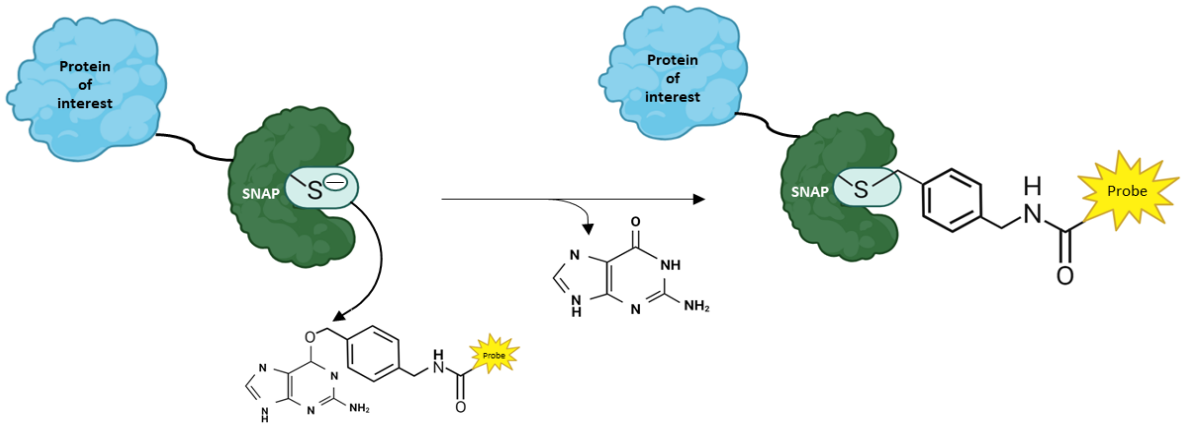


**Figure 6: Site-specific protein labelling with a $O^6$ - benzylguanine (BG) probe by means of SNAP-tag.** This schematic illustrates the manner in which a protein of interest recombinantly fused to SNAP-tag (also referred to as SNAP-tag fusion protein) is conjugated to an $O^6$-BG modified substrates such as a fluorophore or a toxin. BG causes the SNAP-tag to undergo a nucleophilic substitution reaction involving a cysteine present on SNAP-tag. Consequently, a stable and irreversible covalent link between the two molecules is created. This image was adapted from Deyer *et al.* (2023) [149] and modified using Biorender.

The use of SNAP-tag is a promising tool for clinical purposes because of its minimised risk of immunogenicity and convenience by virtue of the reaction's simplicity under physiological conditions. In addition, the ability of this protein tag to accomplish selective and site-specific conjugation with a variety of readily available substrates modified with BG makes it more propitious [146][148][150]. The great vastness presented by the functionality of SNAP-tag has allowed for its use in *in vivo* and *in vitro* imaging, protein isolation and purification, ascertaining protein function and interactions as well as producing recombinant ADCs [143][151].

### 1.6.3. Selection of appropriate effector molecules

The efficacy of an immunoconjugate highly depends on the type and delivery of the chemical warhead conjugated to the antibody targeting a specific tumour antigen. Effector molecules that constitute immunoconjugates are radioisotopes, toxins, or fluorophores. In the particular case of ADCs, mAbs or antibody fragments are chemically bound to biologically active cytotoxic drugs which can be classed either as microtubule inhibitors or DNA damaging agents. Cytotoxic drugs which have gained great attraction from how they were discovered to their effectiveness are Auristatins. These antineoplastic molecules were synthesized from marine-derived Dolastatin 10 (Dol-10), which is a pentapeptide that obstructs the growth of tumour cells by potently suppressing tubulin-dependent GTP hydrolysis and microtubule assembly, eventually inducing cell cycle arrest and apoptosis. Furthermore, they have the ability to trigger an immunological response against malignant cells, cause immunogenic cell death, and increase intratumoral vascular damage [152][153]. An analogue of Dol-10 which is commonly

used for cancer immunotherapy and was generated by making modifications to its backbone scaffold is Monomethyl auristatin F (MMAF/ AURIF). Another analogue of Dol-10 called Monomethyl auristatin E (MMAE) has a lower half maximal inhibitory concentration and is more membrane permeable than MMAF. However, due to the increased hydrophilicity and reduced aggregation propensity of MMAF, it exhibits less systemic toxicity than MMAE and allows it to be conjugated using non-cleavable linkers without losing its cytotoxic properties. Numerous studies and clinical trials done on MMAF and MMAE have ultimately revealed their great potency even over existing chemotherapeutic drugs. Studies have also shown their vigorous activity against multi-drug resistant tumours [154]. These analogues are currently employed in almost one third of ADCs undergoing clinical trials and account for approximately 35% of FDA approved ADCs on the market [155].

In previous studies, researchers have demonstrated leveraging the key characteristics of auristatins which have essentially aided in overcoming some of the obstacles faced when producing ADCs. To accomplish this, Woitok and colleagues (2016) were able to demonstrate the economic production of recombinant ADCs by producing SNAP-tagged scFvs coupled to BG-auristatin F [156]. Overall findings from these studies revealed that the conjugation of BG-auristatin F to scFv-SNAP fusion proteins did not hinder the targeting and binding capacity of the scFvs to the tumor antigens. Moreover, the use of unconjugated scFv-SNAP fusion proteins and non-binding SNAP controls displayed no impact on the viability of the target cells. This verified the specificity and the absence of off-target cytotoxicity of these conjugated scFv-SNAP fusion protein ADCs. Moreover, the circulation of these conjugated scFv-SNAP fusion proteins, with over 50% retention in activity after 48 hours, further validated their stability and supported their use in cancer patients [156].

### 1.6.4. scFv-SNAP tag fusion proteins: proposed mechanism of action

Having GO as the leading antibody-based treatment for AML at present, research efforts could be directed at exploring slightly alternative forms such as those brought forth by Woitok et al (2016) [156]. By choosing and fine-tuning the appropriate components to produce incredibly efficient and developed ADCs for AML, while maintaining a similar mode of action to that of GO would lead in significant progress in the relentless pursuit of producing immunotherapeutics for AML. Just as GO is administered intravenously to prevent destruction by gastric acids and proteolytic enzymes, delivery of the scFv-SNAP tag ADC would be achieved in a similar manner. Once the drug is in circulation, the paratope of the antibody fragment would target and bind to the antigen epitope on the surface of the targeted cancer cell [157]. Binding between the antibody fragment and antigen usually occurs through hydrogen bonds and van Der Waals forces, additionally the affinity and specificity of this bond

can be strengthened by genetic engineering of the CDR regions [158]. Once bound, a signal to initiate internalisation of the scFv-SNAP tag ADC by receptor-mediated endocytosis is transmitted [159]. Following this, the surface antigen-antibody complex or cargo is internalised and enveloped into endocytic vesicles which later merge to form an early endosome. At this stage the cargo is caused to undergo any one of three intracellular routes. The first of these routes is known as cell surface receptor recycling whereby cargo in the endosome can either be kept in the mature endosome or recycled directly back to the plasma membrane. Alternatively, the antigen and the ligand or scFv-SNAP tag ADC separate, prompting only the antigen to be recycled back to the cell surface [160]. The second route, known as retrograde transport, involves the cargo being transported from the mature endosome to the trans-Golgi network for repackaging and translocation into the cytosol or secretion into the extracellular space. The final route entails the endosome developing into multivesicular bodies. This maturation process also forms intraluminal vesicles (ILVs) made during the fluid phase of the developing multivesicular bodies (**Figure 7**). These ILVs internalise the necessary cargo and deliver it to the lumen of lysosomes for degradation by inducing an acidic environment or proteolysis which eventually lead to cell death [161].

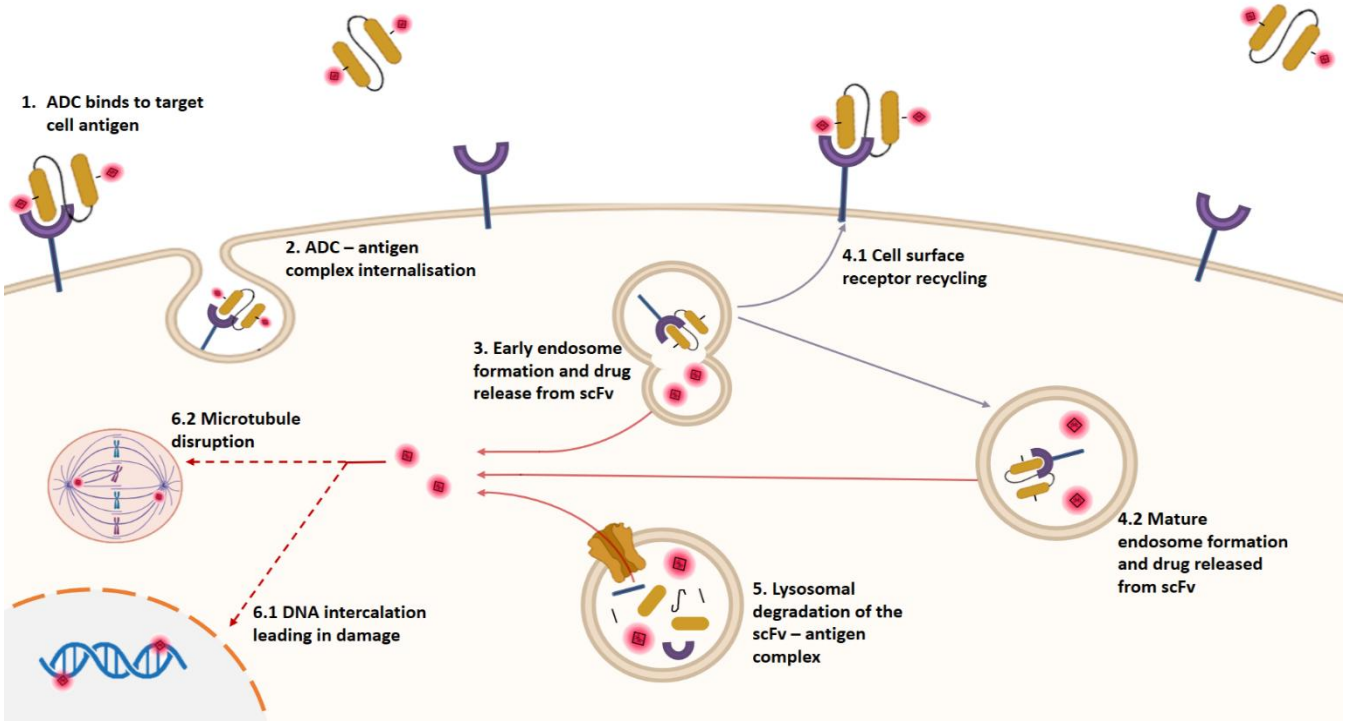


**Figure 7: The general mechanism of action of an antibody-drug conjugate (ADC).** A schematic diagram demonstrating the how an ADC such as Gemtuzumab ozogamicin is able to promote cancer cell killing. (1) The ADC composed of an antibody (fragment) and a toxin moves in the bloodstream until it identifies and attaches to its antigen target. (2) This attachment leads to a signal which prompts receptor-mediated endocytosis leading to enhanced uptake of the ADC-antigen complex and internalisation of the toxin. (3) Once properly internalised, the complex is enveloped into an early endosome whereby it can either be (4.1) recycled back to the surface of the cancer cell or (4.2) remain in a maturing endosome allowing for its intracellular route to be established. Once the maturation of the late endosome has occurred, the cargo may be subjected to retrograde transport or (5) enzymatic degradation in the lysosome. Once the toxin detaches from the antibody (fragment), it is channelled in the cytosol and eventually to the nucleus for (6.1) attachment to DNA resulting in DNA damage or (6.2) microtubule disruption [86][162]. The red dashed and solid arrows depict the intracellular movement of the toxic payload. The blue arrows depict the intracellular movement of the antibody – antigen complex. This image was generated using Biorender and modified on Powerpoint.

The development and provision of appropriate AML treatments continues to be a top priority. According to available research, new therapies—more specifically, ADCs—can be created by striking the right balance between the key characteristics that define this form of therapy. Furthermore, the production of such treatments raises the prospect of managing and mitigating the number of AML-related cases and fatalities.

### 1.7. Study rationale

Due to the aggressive nature of AML, it is imperative that the development of this disease be well understood to achieve prompt diagnosis, provide the most fitting treatments, supportive care and improve prognosis. Malignant transformation and rapid proliferation typify AML and thus demand for swift medical action to be taken. In the case of any disease, it is only more

convenient for a patient and a medical practitioner to have access and be in possession of the resources required for good healthcare.

The trajectory of leukemia across the world has differed markedly over the past decades. AML survival rates have significantly increased in high-income countries as a result of being well equipped to combat this illness. Patients in resource poor countries, on the other hand, have not been able to benefit from the same advantages as their counterparts. In the African context, tremendous dependence on morphological classification of cells for diagnostic inference has proven to be a limiting and inconclusive approach as it lacks sensitivity or the ability to detect and classify cells during the early stage of AML. Needless to say that unavailability of the latest methods for accurate diagnosis and precise identification of AML subtypes has had a significant impact on therapeutic and prognostic outcomes.

Expectedly, a stumbling block in advancing diagnostic technologies has adversely influenced the timely provision of therapeutics. The effect of this persisting predicament, particularly in Africa, has not only affected the likely outcome of AML in individual patients, but it has also led researchers to envisage a drastic rise in cases and mortalities over the next few years. Substantial efforts need to be made, especially on the preventive aspect, to veer from the projected increases. Addressing the primary concerns around the majority of patients succumbing before receiving therapy and developing more targeted and efficacious treatments for the few who can afford those currently on the market but experience severe side effects could be a good start.

Having analyzed various studies that also explored the development of innovative treatments for cancers, it was observed that drugs that directly target and attack cancer cells have gained traction due to their selectivity and strengthened ability to spare non-target cells from toxicity. Similarly, the basic purpose of this study is to focus on improved ADCs as they have redefined cancer treatment quite hugely in recent years. Early ADCs that contain a monoclonal antibody, linker, and cytotoxic payload are known to have limitations. Thus alternative and modern forms were generated in this case using computational and wet bench techniques aiming to alleviate some of these drawbacks. The monoclonal Ab was replaced with a scFv antibody fragment to increase permeability, quicken clearance and decrease immunogenicity. Furthermore, the scFv was coupled to a self-labelling SNAP-tag protein for later conjugation to a BG-modified fluorophore or toxin.

### 1.8. Aims and objectives

This study explored the use of SNAP-tag technology to produce CD33- and CD45-targeting ADCs and evaluated their specificity, binding and cytotoxic effects on AML cell lines. The study workflow to accomplish this aim is outlined in **Figure 8** below.

The specific objectives of this study included:

1. In silico designing and molecular cloning of the specific antibody fragments (pCB-CD33(scFv)-SNAP and pCB-CD45(scFv)-SNAP) into a mammalian plasmid to generate recombinant plasmids.
2. αCD33(scFv)-SNAP and αCD45(scFv)-SNAP fusion protein expression and cultivation from HEK293T cells, purification by immobilised affinity chromatography and characterization by SDS-PAGE and Western blot.
3. Assessing the specificity of binding of the recombinant SNAP fusion proteins conjugated to a BG-modified fluorophore on AML cell lines by flow cytometry.
4. Analysis of the cell killing ability of the recombinant SNAP fusion proteins conjugated to a BG-modified toxin on AML cell lines by cell viability assays.

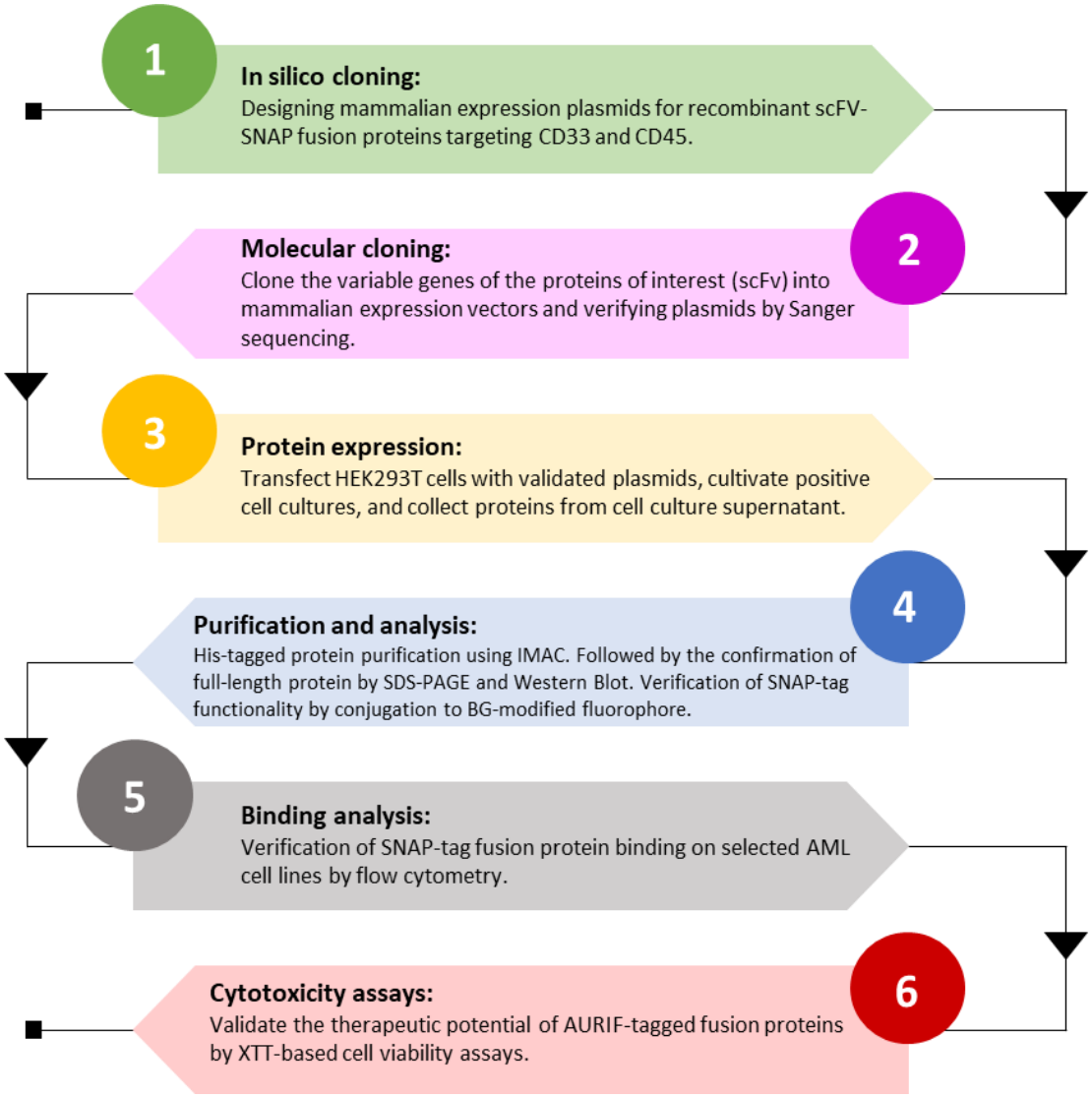


**Figure 8: Diagrammatic representation of the objectives contributing to the study work flow.** Abbreviations: single –chain variable fragment (scFv); cluster of differentiation (CD); Human embryonic kidney (HEK); Histidine (His); immobilised metal affinity chromatography (IMAC); sodium dodecyl sulphate polyacrylamide gel electrophoresis (SDS-PAGE), benzylguanine (BG); Acute myeloid leukaemia (AML); methoxynitrosulfophenyl-tetrazolium carboxanilide (XTT).

# Chapter 2: Methods

This chapter outlines the procedures and techniques used to achieve the aim of this study, which is to produce SNAP-tag-based antibody fusion proteins (FPs) for the immunotherapy of AML. With the background and rationale for this study provided in Chapter 1, these procedures meticulously plan and guide the development of these immunotherapeutics to address the crisis surrounding the treatment of AML in Africa, carefully considering the accessibility of resources and their cost-effective production over time.

All the materials and equipment listed in this chapter were utilized in accordance with the Medical Biotechnology and Immunotherapy (MB&I) Research Unit methods, protocols, and standard operating procedures (SOPs), which were obtained from a private server. These SOPs were compiled and modified where necessary based on other original publications that strived to achieve similar experimental outcomes. The MB&I SOPs, former students' dissertations, and other blood cancer treatment research all form the groundwork and logical sequence of the investigations and objectives carried out.

## 2.1. *In silico* design of mammalian expression vectors

### 2.1.1. Sourcing patents to obtain pertinent sequences for designing recombinant antibodies

To design and eventually produce the mammalian expression vectors of interest, namely pCB-αCD33(scFv)-SNAP and pCB-αCD45(scFv)-SNAP, computational methods were used. The initial *in silico* design of both vectors was conducted by MB&I members Bernard Mirianga (PhD) (data not published) and Tatenda Bvudzijena (MSc) [163], whose work also aimed to produce recombinant scFv-SNAP FPs for the diagnosis and treatment of AML. First, the variable region ($V_H$ and $V_L$) gene sequences comprising each scFv were identified and obtained from publicly accessible and credible patent files, journals, and antibody databases.

### 2.1.2. Verification of accurate acquisition of sequences from patents

Using a software tool developed by Gene Infinity LLC (San Diego, USA) called the Gene Infinity Back Translation Tool (http://www.geneinfinity.org/sms/sms_backtranslation.html), the V-gene amino acid sequences from the most suitable sources were converted into their corresponding nucleotide sequences. The obtained nucleotide sequences were analysed and compared to previously published homologous immunoglobulin germline variable region gene sequences using IgBLAST (https://www.ncbi.nlm.nih.gov/igblast/). Since the variable portions of homologous immunoglobulins are the smallest yet most functional units involved in antigen binding, it was crucial to conduct these comparisons with a focus on these regions. The

variable heavy ($V_H$) and variable light ($V_L$) chains contain the antigen-binding sites that enable the antibody fragments to attach to targeted antigens with great affinity and specificity. Therefore, it was essential to perform these comparisons with precision and care. Following the recognition of these chains and the clear identification of the FR and CDR regions within them, optimization of the codons represented by these nucleotide sequences was conducted using the IDT™ Codon Optimization Tool (© 2022 Integrated DNA Technologies, USA; https://eu.idtdna.com/pages/tools/codon-optimization-tool). Because this tool facilitates recombination based on multiple factors without changing the amino acid sequence [164], codon optimization is essential to the process and can lead to increased yields of recombinant gene expression in various host organisms. The Expasy Translate Tool (Lausanne, Switzerland; https://web.expasy.org/translate/) was then used to convert nucleotide sequences back into amino acid sequences. Subsequently, EMBL-EBI Clustal Omega (https://www.ebi.ac.uk/), a multiple sequence alignment tool, was utilized to align the resultant amino acid sequences with the parental amino acid sequences for quality control and to ascertain whether the corresponding sequences had changed after optimization. Modifications were made to enhance stability, reduce immunogenicity, and minimize nuclease degradation in cases where unusual and repeated codons were identified [165].

### 2.1.3. Assembling the scFv antibodies based on the optimized sequences

By joining the $V_H$ and $V_L$ sequences through a short, flexible peptide linker, the scFv format was achieved. Each scFv was flanked with *SfiI* and *NotI* restriction sites for potential insertion into a pCB-based mammalian plasmid using SnapGene® software version 5.0.8 (GSL Biotech LLC, USA). The pCB mammalian expression plasmid utilized in this experiment is called pCB-αEPCAM-SNAP (8032 bp), also referred to as the parental plasmid. This plasmid was previously produced and made readily available for mammalian expression under suitable conditions by the MB&I unit (as seen in **Figure 9**). Additionally, **Table 5** lists all the essential characteristics of this plasmid and its role in supporting effective cloning, harvesting, purification, and functionality, which were all assessed in subsequent experiments. The integrity of each scFv open reading frame (ORF) was confirmed through sequence alignment, and their sequences were obtained from GenScript Biotech Corporation (New Jersey, USA) and supplied within a pUC57 commercial vector. The *SfiI* and *NotI* restriction sites flanking the scFvs also facilitated the excision of the antibody fragments from the pUC57 commercial vectors into the pCB-SNAP backbone vectors during molecular cloning.

**Table 5**: Every crucial feature of the mammalian expression vectors (pCB-α(scFv)-SNAP).

| Component | Function |
|---|---|
| Igκ (Kappa) leader | Fusion proteins are guided into the secretory route and ultimately into the cell culture supernatant by a signalling peptide [166]. |
| T7 promoter | Permits in vitro transcription through the insert's positioning and sequencing [167]. |
| N-terminal polyhistidine tag (10 Histidine-tag) | This tag facilitates detection in western blot analysis and aids in protein purification by fusing with the target protein and simplifying affinity chromatography purification [168]. |
| Enterokinase (EKS) cleavage site | By encoding a highly selective and active cleavage site for fusion proteins with a DDDDK recognition sequence, it facilitates the removal of the polyhistidine tag and isolation [169]. |
| Single-chain fragment variable (scFv) | Encodes the unique antigen-binding recombinant antibody fragment [170]. |
| SNAP-tag | A self-labelling protein that can be utilized to label, through a covalent bond, a protein of interest [171]. |
| Chimeric intron | Helps to enhance mRNA processing and increase the levels of protein-coding genes' expression [172]. |
| Internal ribosome entry site (IRES) | Enables the translation of several genes from a single mRNA transcript [173]. |
| eGFP reporter gene | A reporter gene that makes it possible to see and identify DNA that has been effectively transfected and eventually translated into proteins [174]. |
| bGH poly(A) signal | Facilitates both the efficient termination and polyadenylation of mRNA [175]. |
| F1 origin | Plays a role in promoting single-stranded DNA replication and phage packaging [176]. |
| SV40 promoter | Is made up of the enhancer promoter and the SV40 replication origin, which help large T antigen-expressing cell lines express and replicate at high levels [177]. |
| SV40 poly(A) signal | Cleavage and polyadenylation events that result in steady-state mRNA are made possible by Simian Virus 40 late polyadenylation [178]. |

| | |
|---|---|
| Bleomycin resistance (BleoR) | Confers Bleomycin (antitumor antibiotic) resistance for selection of transfected mammalian cells [179]. |
| M13 rev | Aids in polymerase chain reaction (PCR) techniques as a single-stranded oligonucleotide with 5'-hydroxyl and 3'-hydroxyl ends (5'-CAG GAA ACA GCT ATG ACC-3') with a variety of four fluorescent markers [180]. |
| lac promoter | Controls how lac operon genes that are involved in the metabolism and uptake of lactose by bacteria are transcriptionally regulated [181]. |
| lac operator | A DNA region that controls the production of genes downstream in the lac operon by binding to the Lac repressor protein [182]. |
| EM7 promoter | A bacterial promoter that permits Escherichia coli (E. coli) to continuously produce the antibiotic resistance gene [183] |
| Ampicillin resistance gene ($AMP^R$) | The gene that confers E. coli resistance to the antibiotic ampicillin and is utilized to select efficiently transformed bacteria [184]. |
| Cytomegalovirus (CMV) promoter | The CMV promoter is often utilized in mammalian cells to generate higher amounts of recombinant protein [185]. |

## 2.2. Molecular cloning of mammalian expression vectors

### 2.2.1. Transformation of competent bacterial cells with plasmid DNA

GenScript Biotech Corporation manufactured pUC57 plasmids containing αCD33(scFv) and αCD45(scFv). The MB&I-derived pCB parental plasmid was introduced and propagated exponentially through heat shock transformation using chemically competent NEB® DH5α *E. coli* cells (Cat#: C2987I, New England Biolabs, USA). DH5α cells have the following genotype, defined by the bolded mutations: fhuA2Δ(argF-lacZ)U169 phoA glnV44 **Φ80Δ(lacZ)M15** gyrA96 **recA1** relA1 **endA1** thi-1 hsdR17. Following the manufacturer's instructions, transformation was initiated by thawing the DH5α cells on ice for 10 minutes. After dilution with nuclease-free water to a final concentration of 100 ng/µL, the plasmid DNA was mixed with 50 µL of DH5α cells and incubated on ice for 30 minutes. Through heat shock treatment for 60 seconds at 42°C using an Eppendorf Thermomixer Comfort heating block (Sigma-Aldrich, USA), the cellular membrane of the *E. coli* cells was disrupted, after which the cells were immediately cooled on ice for 5 minutes. Subsequently, 950 µL of Super Optimal Broth with Catabolite Repression (SOC, Cat#: B9020S) was added to the cells and incubated on a shaker

(at 250 RPM) for 1 hour at 37°C. Once removed from the shaker, the entire mixture was inoculated in 50 mL of Luria Bertani (LB) supplemented with 100 ng/nL of ampicillin (AMP) antibiotic and incubated for 16 hours (overnight) in a shaking incubator. After incubation, glycerol stocks composed of each incubated culture mixed with 50% glycerol in a 1:1 ratio were stored at -80°C for long-term preservation in case of future use.

### 2.2.2. Isolation of plasmid DNA

Plasmid DNA was extracted from bacterial cultures using either the NucleoBond® Xtra Midi extraction (Cat#: 740410.50, Macherey-Nagel, Germany), which is a silica-based method that enables nucleic acid separation through alkaline cell lysis and anion exchange resin [186]. An alternative technique for extracting plasmid DNA from bacterial cells was the phenol-chloroform extraction method, which allows for separation using immiscible liquids and differing solubilities [187]. Essentially, both plasmid isolation techniques aim to achieve identical outcomes; however, the chosen method was based on the availability of reagents at the time.

#### 2.2.2.1. NucleoBond® extraction method

Midi-scale plasmid extraction using the NucleoBond® kit began with some adjustments to the manufacturer's recommendations. First, bacterial cells from the overnight cultures were harvested by centrifugation for 15 minutes at 4255 RCF at 4°C (Allegra X-22R, Beckman Coulter). The supernatant was discarded, and the bacterial cells were resuspended in 4 mL of Buffer S1 (containing RNase). To ensure a homogeneous mixture, 4 mL of Buffer S2 (lysis buffer) was then added and mixed gently by inversion. The suspension was incubated for 5 minutes at room temperature. After incubation, 4 mL of pre-cooled Buffer S3 (neutralization buffer) was added to the lysate and mixed by inversion until an off-white precipitate formed. The mixture was then centrifuged at 4255 RCF for 20 minutes at 4°C after being incubated on ice for five minutes. In parallel to the centrifugation, 2.5 mL of Buffer N2 (equilibration buffer) was added to a NucleoBond® Xtra Midi Column with a NucleoBond® Xtra Column Filter for equilibration. Once the buffer fully drained from the column, a sheet of NucleoBond Folded Filter was placed inside the column and equilibrated with a few drops of Buffer N2. The centrifuged lysate was transferred onto the wet filter for clear separation between the cellular debris and the DNA intended to bind to the column. Buffer N2 was utilized to remove any residual lysate from the column. Next, a repeated wash with 10 mL of Buffer N3 (wash buffer) was applied directly to the column. The DNA plasmid bound to the column was eluted using 5 mL of Buffer N5 (elution buffer). Room-temperature isopropanol was then added directly to the elution for precipitation and centrifuged at 4255 RCF for 30 minutes at 4°C. After discarding

the supernatant, another centrifugation at 5000 RCF for 10 minutes at room temperature was conducted, with 2 mL of 70% ethanol added to the pellet. The supernatant was discarded, and the pellet was either dried on the bench at room temperature or using a SpeedVac Vacuum (Thermo Fisher Scientific, USA). Finally, the pellet was reconstituted in 35 µL of nuclease-free water preheated to 50°C for 10 minutes to speed up dissolution. A spectrophotometer (Denovix NanoDrop™ ND-2000, ThermoFisher Scientific) was used to measure the DNA concentration after the plasmid DNA was successfully extracted.

#### 2.2.2.2. Phenol-chloroform extraction method

The overnight cultures were retrieved, and bacterial cells were harvested by centrifugation at 4000 RCF for 10 minutes at 4°C. The supernatant was discarded, and the pellet containing the bacterial cells was resuspended in 1 mL of Lysis Solution I (**Table A1**). After adding 2 mL of Denaturation Solution II (**Table A1**) and placing the mixture on ice for 5 minutes, 1.5 mL of Solution III (**Table A1**) was added. Solution III facilitated the renaturation of circular DNA by restoring the appropriate pH for the precipitation of protein and genomic DNA. The solution was then centrifuged at 15000 RCF for 10 minutes at 4°C to facilitate the separation of plasmid DNA from cell debris and denatured DNA. The supernatant was collected, mixed by inversion with 1 mg/mL RNase A, and then incubated for 30 minutes at 42°C to remove RNA impurities. To precipitate the plasmid DNA, cold 30% (v/v) isopropanol was added and incubated at room temperature for 10 minutes. Subsequently, 300 mM sodium acetate and 700 µL of phenol: chloroform (1:1 v/v) were added and briefly vortexed to separate the proteins from the DNA. Centrifugation at 15000 RCF for 10 minutes was performed to achieve DNA isolation by phase density. Following this, 300 µL of chloroform: isoamyl alcohol (24:1; v/v) was added, and the mixture was centrifuged for 10 minutes at 15000 RCF, resulting in a clear separation of the solution into its component phases. Using a pipette, the DNA in the top aqueous phase was carefully isolated. The isolated DNA was precipitated with 100% ethanol at -20°C for 30 minutes, and afterwards centrifuged at 15000 RCF for 30 minutes to form a pellet. The pellet was rinsed with 70% cold ethanol and then dried at room temperature. Once dried, the plasmid pellet was resuspended in 35 µL of nuclease-free water preheated to 50°C for 10 minutes. A spectrophotometer (Denovix NanoDrop™ ND-2000, Thermo Fisher Scientific) was used to measure the DNA concentration after the successful extraction of the plasmid DNA.

### 2.2.3. Restriction digestion

New England Biolabs (NEB, USA) restriction enzymes were used to enzymatically cleave the desired genes from their respective plasmids, specifically αCD33(scFv) and αCD45(scFv) (without the pUC57 backbone) as well as the pCB-SNAP backbone (without αEpCAM(scFv)

gene). The manufacturer's recommendations were followed when performing restriction digestion with the supplied materials to produce two sticky ends of DNA fragments that were suitable for succeeding ligation. The reaction mixtures for this experiment comprised mainly of 1 µg of DNA, rCutSmart buffer (NEB, MA), *SfiI* (Cat#: R0123S, NEB, MA), *NotI* (Cat#: R0189S, NEB, MA) and nuclease-free water topped up to the recommended volume as seen in **Table A2**. Various reactions, including an undigested control, single digest, and double digest, were performed to ensure the proper digestion of each plasmid. Reaction conditions when using *SfiI* and *NotI* required incubation at 50°C for 4 hours and 37°C for up to 16 hours, respectively. After every plasmid was digested, the enzymes were deactivated at 65°C for 10 minutes in order to prevent any non-specific activity or target DNA degradation.

### 2.2.4. Agarose gel electrophoresis

The restriction-digested DNA fragments were separated based on their molecular weight into those that were essential and non-essential for downstream experiments, particularly ligation. Agarose powder was dissolved in boiling 1x Tris-acetate-EDTA (TAE) buffer (**Table A3**) to cast a 1.2% weight per volume (w/v) agarose gel. A 1:10000 dilution factor of SYBR Safe DNA Gel Stain (Cat#: S33102, Invitrogen, South Africa) was added to the agarose solution as it cooled to room temperature to allow for visualization and tracking of the DNA. Once the agarose solution was cooled, it was poured into a gel tray with a gel comb set in place to create the wells needed for sample loading. To impart color and enable visualization of migration on the gel, 2 µL of 6X Purple Gel Loading Dye (Thermo Fisher Scientific, USA) was added to the DNA samples. 5 µL of Quick-Load 1 kb DNA ladder (NEB, MA) was used as a reference for molecular weight. Electrophoresis was run in a flat sub-cell GT wide mini buffer tank (Bio-Rad, South Africa) and provided with electrical energy at 100 V for 60 minutes through a PowerPac™ HC power supply (Bio-Rad, South Africa). The Molecular Imager® Gel Doc™ XR+ Imaging System (Bio-Rad, South Africa) at 509 nm and Image Lab v6.1.0 software were used to visualize the gel after electrophoresis was complete.

### 2.2.5. Recovery of restriction digested DNA

Gel extraction and purification of the restriction digestion fragments of interest were conducted using the QIAquick® Gel Extraction Kit (Cat#: 28704, Qiagen, Germany) with minor modifications to the manufacturer's instructions. First, a sterile sharp scalpel was utilized to excise the desired fragments, specifically the two scFv fragments and the pCB-SNAP backbone, from the agarose gel. After recovery, each gel slice was weighed in a microcentrifuge tube. To dissolve the gel, three volumes of buffer QG were added to one volume of gel, and the mixture was incubated at 50°C for 10 minutes. Then, one gel volume of

isopropanol was mixed with the dissolved gel sample. A QIAquick spin column, placed in a 2 mL collection tube, was used to bind the DNA once the sample was loaded onto it. The tube was centrifuged until the entire sample passed through the column, and the flow-through was discarded. The QIAquick spin column was subsequently washed with 750 µL of Buffer PE and centrifuged at 15000 RCF for 1 minute. After transferring the QIAquick spin column to a new microcentrifuge tube, 50 µL of pre-warmed nuclease-free water was added to its filter, and the tube was incubated at 50°C for 5 minutes. Following the incubation, DNA was eluted by centrifugation at 15000 RCF for 1 minute.

### 2.2.6. DNA ligation of recovered DNA

The T4 DNA Ligase kit (NEB, MA) was utilized following the manufacturer's instructions to integrate the extracted DNA (scFv inserts) into the backbone vector (pCB-SNAP) to develop the desired vectors. First, the appropriate vector-to-insert ratio needed for each ligation reaction was determined using NEBioCalculator® version 1.15.5 (https://nebiocalculator.neb.com/). To enhance the success rate of ligation, two reactions were prepared at ratios of 1:1 and 1:5. Controls, consisting of the parental vector alone and lacking the inserts, were included to identify vector self-ligation. Each ligation reaction included T4 DNA ligase enzyme, T4 DNA buffer, DNA insert (scFv), backbone vector (pCB-SNAP), and nuclease-free water (**Table A4**). The mixtures were incubated overnight at 16°C, and the ligation enzymes were inactivated for 10 minutes at 65°C following incubation. Applying the methodology in subsection 2.2.1, 100 ng of the ligation product was transformed into 50 µL of DH5α competent cells for recombinant plasmid propagation. Subsequently, the transformed cells were plated on agar plates supplemented with 100 mg/mL ampicillin and incubated overnight at 37°C to distinguish correctly ligated recombinant plasmids from partially digested ones. Transformation efficiencies (**Table A5**) were assessed to ensure the acquisition of at least one clone with the properly ligated plasmid. A minimum number of individual clones was selected for restriction mapping based on a comparison of the colony-forming units (CFUs) on the control agar plate to those on the experimental agar plates. The individual colonies that were ultimately chosen were then cultured at 37°C, 180 RPM overnight in 10 mL of LB media supplemented with ampicillin.

### 2.2.7. Mini preparation of recombinant plasmid DNA

The overnight LB cultures of selected colonies were collected, and DNA extraction from these cultures was performed using the Zyppy™ Miniprep Kit (Cat#: D4019, Zymo Research, USA). With a few minor adjustments to the manufacturer's instructions, the extraction process began by transferring the cultures to 1.5 mL microcentrifuge tubes for centrifugation at maximum

speed for 30 seconds. This centrifugation was repeated as needed, and the pellet formed was resuspended in nuclease-free water. Then, 100 µL of 7X Lysis Buffer was added to the resuspended pellet and mixed by inversion until the solution appeared light blue, indicating complete lysis. Next, 350 µL of cold Neutralization Buffer was added and mixed until a yellow precipitate formed. The solution was centrifuged at 13000 RCF for 4 minutes, and the supernatant was loaded into a Zymo-Spin IIN column placed in a collection tube. Centrifugation was repeated for 30 seconds, and the flow-through was discarded. Following this, 200 µL of Endo-Wash Buffer was added to the column and centrifuged for 30 seconds. Afterward, 400 µL of Zyppy Wash Buffer was added to the column and centrifuged for another 30 seconds. The column was then transferred to a clean 1.5 mL microcentrifuge tube, and 35 µL of nuclease-free water, pre-heated to 50°C, was added to the column matrix. The column was allowed to stand for 2 minutes at room temperature before centrifugation for 1 minute, facilitating the elution of plasmid DNA. The concentration of the eluted DNA was measured using a spectrophotometer (Denovix NanoDrop™ ND-2000, Thermo Fisher Scientific).

### 2.2.8. Confirmation of recombinant plasmid DNA

#### 2.2.8.1. Restriction mapping

Restriction mapping was performed to confirm successfully cloned recombinant plasmids and to distinguish them from parental plasmid controls. Similar to the techniques described in subsections 2.2.3 and 2.2.4, the recombinant plasmids were enzymatically cleaved and subjected to agarose gel electrophoresis to verify the accuracy of ligation based on molecular weight and the cleavage patterns of each cloned recombinant plasmid at unique restriction sites. The manufacturer's recommendations were strictly followed when performing the restriction mapping with the provided materials. The reaction mixtures for this experiment primarily consisted of 1 µg of DNA, rCutSmart buffer, *BamHI* (Cat#: R0136S, NEB, MA), *SpeI-HF* (Cat#: R3133S, NEB, MA), and nuclease-free water topped up to the recommended volume as shown in **Table A6**. The reactions included undigested, single digested, and double digested samples of the parental plasmid (pCB-αEpCAM(scFv)-SNAP) and scFv clones (pCB-αCD33(scFv)-SNAP and pCB-αC45(scFv)-SNAP). The reaction conditions for the aforementioned restriction enzymes required incubation at 37°C for up to 16 hours. After digestion, the enzymes were inactivated at 65°C for 10 minutes to prevent any non-specific activity or degradation of the target DNA.

#### 2.2.8.2. DNA sequencing analysis

Following the restriction mapping screening (in 2.2.8.1), the cloning and plasmid composition of the recombinant clones were further confirmed using Sanger sequencing. Bulk samples of

the recombinant plasmids were prepared and purified using the NucleoBond® extraction kit, as described in subsection 2.2.2.1. A set of forward and reverse primers was designed and procured from Inqaba Biotechnical Industries (Pretoria, South Africa) to amplify the ORFs of each recombinant clone from the T7 promoter to the SNAP-tag. SnapGene® software was used to align the sequencing results with the *in silico* designed ORF files as a reference (section 2.1). Mammalian expression was conducted after validating the successful cloning through sequencing and restriction mapping.

## 2.3. Cell culture for recombinant SNAP FP expression

### 2.3.1. Mammalian expression of recombinant SNAP FPs in HEK293T cells

Human embryonic kidney T-cells (HEK293T; ATCC: CRL-3216, USA) were selected as the most suitable mammalian expression system for producing recombinant SNAP FPs. Cell culture was performed in a sterile biosafety cabinet located within a Biosafety Level 2 facility. To maintain HEK293T cells, Roswell Park Memorial Institute **(**RPMI) 1640 Medium with GlutaMAX (Cat#: 61870036, Gibco, USA) was utilized. Additionally, 10% fetal bovine serum (FBS) (Cat#: A5256701, Gibco, USA) and 100 µl/ml penicillin-streptomycin (Cat#: 15140122, Gibco, USA) were added to further supplement the RPMI medium. The cells were incubated at 37°C with 95% humidity and 5% $CO_2$. Regular visualization for growth and confluency was conducted using the ZOE™ Fluorescent Cell Imager (Bio-Rad, USA). Physical aspiration was performed every four days to replenish the nutrient-rich medium, and cell passaging was conducted once 90% confluency was reached.

### 2.3.2. Transfection in eukaryotic expression system

The sequenced recombinant plasmids were artificially introduced into a eukaryotic expression system using a chemical-based technique. To begin, HEK293T cells were subcultured or seeded into 35 mm round cell culture dishes (Cat#: CLS430165, Sigma-Aldrich, USA) until they reached approximately 70% confluency. The cells were monitored and cultured in RPMI 1640 medium with GlutaMAX (Gibco, USA), which was supplemented as described in subsection 2.3.1. Two days after seeding, transfection master mixes were prepared using the chemical XtremeGENE HP DNA Transfection Reagent Quick Protocol (Cat#: XTGHP-RO, Sigma-Aldrich, USA) with minor modifications to the manufacturer's instructions. Two transfection mixtures were prepared at different ratios to maximize the likelihood of successful nucleic acid delivery. One reaction contained 188 µL of unsupplemented RPMI media, 9 µL of transfection reagent, and 3 µg of DNA (1:3 v/v), while the other contained 185 µL of unsupplemented RPMI media, 10 µL of transfection reagent, and 5 µg of DNA (1:2 v/v). Both reactions were added to their respective seeded cells dropwise after being set aside in the

biosafety cabinet for 10 minutes. A negative control consisting of cells without transfected DNA was also included. The cells were incubated at 37°C with 95% humidity and 5% $CO_2$. The medium was replaced 72 hours after transfection, and the expressed enhanced green fluorescent protein (eGFP) was examined using the ZOE™ Fluorescent Cell Imager (Bio-Rad, USA).

### 2.3.3. Transfection efficiency of clones in HEK293T cells

Quantitative and qualitative measures were employed to assess transfection efficiency. The transfection efficiency was calculated after each successful transfection. As a result, at least two biological repeats and two technical repeats were carried out overall. The quantitative approach utilized the ZOE™ Fluorescence Cell Imager (Bio-Rad, USA) to visually monitor the enhancement of eGFP expression in positively transfected HEK293T cells. Transfection efficiencies were calculated as the percentage of eGFP-positive cells in the total cell population within the cell culture dish. For qualitative analysis, flow cytometry was conducted 96 hours post-transfection. 1 mL of transfected cells and non-transfected controls were transferred from their 35 mm cell dishes to fluorescence-activated cell sorting (FACS) tubes. Phosphate-buffered saline (PBS, **Table A7**) was used to wash the cells, which were then centrifuged at 4°C at 2161 RPM. LIVE/DEAD Fixable Dead Cell Stain (Cat#: L34959, ThermoFisher Scientific, USA) was subsequently added to evaluate cell viability prior to permeabilization and fixation necessary for intracellular antibody labeling, or before formaldehyde fixation, which is required for the elimination of biohazardous substances [188]. The tubes were placed on ice and covered with foil due to the light sensitivity of the LIVE/DEAD stain. After washing with PBS, the cells were centrifuged once more at 4°C at 2161 RPM before being resuspended in FACS buffer. A 2-4% Paraformaldehyde (PFA) solution was used to fix the cells, ensuring stable light scattering during analysis with the BD LSRFortessa™ Cell Analyzer (BD Biosciences, USA). FlowJo software (version 10.9.0; BD Biosciences, USA) was utilized to analyze the raw data obtained from the flow cytometer.

### 2.3.4. Recombinant SNAP FP selection and harvesting

To ensure the consistent and continuous growth of positively transfected cells, all subcultures remaining after aliquoting cells for flow cytometry (section 2.3.3.) and transferred to T25 cell culture flasks (SPL Life Sciences, USA). To selectively enrich the eGFP-expressing population, the cells were treated with Zeocin Selection Reagent (Cat#: R25001, ThermoFisher Scientific, USA), starting at a concentration of 100 mg/mL and gradually increasing to 300 mg/mL over a period of 8 weeks. Once the cells reached approximately 90% confluency and fluorescence, assessed using the ZOE™ Fluorescence Cell Imager (Bio-Rad,

USA), they were transferred to T75 cell culture flasks and finally to T175 cell culture flasks (SPL Life Sciences, USA) in preparation for protein harvesting. The cells were maintained at a confluency greater than 80% in supplemented RPMI 1640. The recombinant SNAP FP-containing cell culture supernatant (CCSN) was harvested every 3 days through centrifugation at 4°C at 4500 x g for 8 minutes. This harvesting process was repeated until at least one liter of CCSN was obtained for downstream experiments.

## 2.4. Protein purification and characterization

### 2.4.1. Protein purification by immobilized metal affinity chromatography (IMAC)

The extraction and clarification of the proteins of interest were performed using immobilized metal affinity chromatography (IMAC). This purification process facilitated the separation of proteins by employing a matrix loaded with chelating agents that immobilize metal ions such as Cu2+, Ni2+, and Zn2+, promoting their differential affinity interactions with protein-exposed metal-coordinating ligands like histidine or cysteine [189]. The ÄKTA Avant System (GE Healthcare, USA) was utilized in this experiment to purify the collected mammalian CCSN. The constituents of the buffers (**Table A8**) were dissolved in ultrapure water, adjusted to a pH of 8.0, and degassed in an all-glass vacuum filtration system. The equilibration buffer was applied at 5 column volumes (CV) at a rate of 5 mL/min to ensure optimal binding between the metal ions and proteins. Next, a 4X incubation buffer was added to CCSN in a ratio of 1:3. Cellular debris and air bubbles that could potentially clog the column during a purification run were removed by filtration using a Nalgene™ vacuum filtration system (Cat#: 300-4000, Sigma-Aldrich, South Africa) containing a 0.45 µm Durapore® membrane filter (Cat#: HVLP04700, Millipore, USA) prior to loading the sample. The protein sample was loaded at a rate of 1 mL/min onto a 5 mL HisTrap Excel column (Cat#: 17524802, Cytiva, USA) pre-charged with Ni2+ Sepharose for specific affinity interactions with the negatively charged polyhistidine tag incorporated in the DNA plasmid encoding each recombinant SNAP FP (see section 2.1.). The wash buffer was subsequently applied for 20 CV at a rate of 5 mL/min. Elution of the recombinant SNAP FPs was performed first using a gradient from 0 to 75 mM imidazole for 5 CV at a rate of 1 mL/min, followed by a step elution at 250 mM imidazole for 10 CV at 1 mL/min. Eluted proteins were collected in 96 deep-well fraction collectors placed in a cassette (Cat#: P-DW-20-C-S, faCellitate, Germany). The absorbance profile at UV = 280 nm and the protein elution profile pattern of each purification run were assessed on chromatograms generated by UNICORN™ 7 control software (Cytiva, USA). Additionally, the chromatograms provided a range of eluted fractions containing the highest concentration of recombinant proteins for use in subsequent experiments.

### 2.4.2. Protein characterisation

#### 2.4.2.1. Sodium dodecyl sulphate polyacrylamide gel electrophoresis (SDS-PAGE)

For the visualization and detection of purified recombinant SNAP FPs following IMAC, sodium dodecyl sulphate polyacrylamide gel electrophoresis (SDS-PAGE) was used**.** SDS-PAGE is an analytical method employed to separate proteins by electrophoresis based on their molecular weight. The following reagents were mixed to cast a 10% SDS gel: Acrylamide (Cat #: A3574-5X100ML), Tris-HCl buffer (**Table A9**), 10% SDS (**Table A9**), 10% APS (**Table A9**), and TEMED (Cat#: 1107320100 Sigma-Aldrich, South Africa). Protein samples were first mixed with 5 µL of loading dye prepared in a 1:9 ratio of β-mercaptoethanol to 4x Laemmli sample buffer (Cat#: 1610710 and BBRD1610747, respectively, Bio-Rad, USA). Subsequently, they were denatured at 95°C for 10 minutes on the Eppendorf Thermomixer Comfort heating block (Sigma-Aldrich, USA). The samples were loaded and run against a colour pre-stained protein standard broad range marker (Cat#: P7719S, NEB, USA) used to determine the molecular weight of the recombinant SNAP FPs. Electrophoresis was performed at 150 V for 90 minutes in a Mini-PROTEAN Tetra cell (Bio-Rad, USA) filled with 1X Running buffer (**Table A9**). Once completed, the SDS-PAGE gel was stained with AcquaStain (Cat#: AS001006, Bulldog Bio, UK) for visualization of the protein bands and migration by electrophoresis. A Gel Doc XR+ system was used to acquire images of the stained gels. The theoretical molecular weight of the recombinant SNAP FPs was ascertained using the Expasy translate tool (https://web.expasy.org/translate/).

#### 2.4.2.2. Analysis and concentration of protein eluates

For analysis and confirmation of the presence of full-length recombinant SNAP FPs, a number of eluate fractions selected from the range provided on the chromatogram (section 2.4.1.) were run on a 10% SDS-PAGE gel prepared as detailed in section 2.4.2.1. A mix of 5 µL loading dye and 15 µL of individual fractions was denatured at 95°C for 10 minutes prior to commencing electrophoresis. Each fraction that displayed a protein band at the correct molecular weight after staining the gel with AcquaStain was pooled and concentrated using a 30 kDa Amicon® Ultra-15 Centrifugal Filter Unit (Cat#: UFC9030, Sigma-Aldrich, USA) to eliminate contaminating proteins and obtain the highest quantity of purified scFv-SNAP FPs. Centrifugation at 4500 RCF for 20-30 minutes at 4°C was performed to concentrate the proteins, and this process was repeated until all selected fractions were concentrated down to approximately 500 µL. Any residual reagents from the purification buffers that could potentially interfere with the enzymatic activity of the SNAP-tag were removed by adding 5 mL of 1X PBS into the Amicon column and centrifuged at 4500 RCF at 4°C. The remaining protein in the

Amicon filter was divided into 50 µL aliquots. The concentration of the aliquots was recorded using Denovix NanoDrop™ ND-2000 (ThermoFisher Scientific, USA).

#### 2.4.2.3. Densitometry

Quantification was performed by densitometry to determine the concentration of purified full-length recombinant SNAP FPs. A 1 mg/mL stock solution of Bovine Serum Albumin (BSA) (Cat#: 10711454001, Merck, USA) was made. A two-fold dilution with 1X PBS of the stock solution was done to make the following BSA protein standards: 16 µg, 8 µg, 4 µg, 2 µg and 1 µg. 10 µg of purified recombinant protein to be run alongside the BSA protein standards was prepared. All samples were mixed with loading dye and made up to a final volume of 25 µL as seen in **Table A10**. Protein samples were then heated on the Eppendorf Thermomixer Comfort heating block (Sigma-Aldrich, USA) at 95°C for 10 minutes before being run on a 10% SDS-PAGE prepared and stained as outlined in 2.4.2.1. Images of the gel were captured using the Gel Doc XR+ (Gel Doc™ XR System). ImageJ software v.1.53e (https://imagej.net/) was used to quantify the total amount and percentage purity by comparison of optical densities of the SNAP FPs bands to the associated BSA standards of known concentrations. To measure the optical colour intensity of the protein and BSA standards, a standard curve was created using Microsoft Excel software. The calculation of the protein concentration was based on the alignment to the trend line. To determine the percentage purity of the protein sample, these results were compared to the concentration obtained using the DenovixTM Spectrophotometer.

#### 2.4.2.4. Western blot (WB) analysis

The expression and presence of full-length recombinant proteins were further verified using WB techniques. To achieve this, the N-terminal polyhistidine-tag (section 2.1.) was targeted using a specific anti-polyhistidine antibody. To begin, two identical 10% SDS-PAGE gels were prepared, one which would be utilized for WB and the other was to be stained using AcquaStain as described in section 2.4.2.1. The stained gel served to compare the protein bands and ensure accurate duplication between the denaturing polyacrylamide gel and the WB. 10 µg of purified protein was run on these gels at 150 V for 90 minutes. In the interim, an Immuno-Blot® Polyvinylidene Fluoride (PVDF) membrane (Cat#: 3010040001, Thermo Fisher Scientific, USA) was first activated with methanol, rinsed with nuclease-free water and then soaked in 1X Transfer buffer (**Table A11**) in preparation for WB. Following electrophoresis, the protein was transferred from one gel to the activated PVDF membrane by sandwiching both the transfer membrane and the gel between layers of WB filter paper soaked in 1X Transfer buffer. Electrotransfer was conducted using the Trans-Blot® Turbo™ transfer system (Bio-

Rad, South Africa) at 2.0 A, 25 V for 20 minutes. Once completed, the transfer sandwich was carefully dissembled and the PVDF membrane was blocked with fat-free milk for 60 minutes at room temperature. Subsequently, the PVDF membrane was incubated at 4°C overnight with a 1:10000 dilution of anti-polyhistidine horseradish peroxidase (HRP) mouse monoclonal antibody (Catalogue number: A7058-1VL, Sigma-Aldrich, USA) in fat-free milk. The next day, the PVDF membrane was washed thrice at 5-minute intervals with Tris-buffered saline–Tween® 20 (TBST) (Cat#: 1047183, ThermoFisher Scientific, USA). Thereafter, the PVDF membrane was incubated for 1 minute with 2 mL 1-Step Ultra TMB-Blotting Solution (ThermoFisher Scientific, USA) to detect the HRP-bound proteins and immediately rinsed with ultrapure water to halt further reaction of the blotting solution.

### 2.4.3. Conjugation of recombinant SNAP FPs with BG-modified derivatives

To verify the functionality of the enzymatic SNAP-tag located at the C-terminus of the recombinant SNAP FPs, conjugation with benzylguanine (BG) derivatives was performed. The experiment began by using an online conversion tool (https://www.bioline.com/media/calculator/01_04.html) that converted mass concentration to molar concentration for the recombinant SNAP FPs. This conversion matched the units of recombinant proteins with the recommended units for BG-modified derivatives, facilitating conjugation. Reagents, including SNAP-Surface® Alexa Fluor® 488 (NEB, USA), Dithiothreitol (DTT, Sigma-Aldrich, South Africa), and 1x PBS buffer, were mixed with the SNAP FPs at established molarities (**Table A12**) and made up to a volume of 20 µL. A loading dye was added to the reaction mixture, which was then incubated at 37°C in the dark for 60 minutes. Subsequently, the fluorescently labeled sample was resolved on a 10% SDS-PAGE gel in the dark and visualized using a blue light-emitting Dark Reader Transilluminator (Clare Chemical Research, USA) to detect the fluorescent signal. Finally, the gel was stained with AcquaStain and visualized according to the methodology outlined in section 2.4.2.1.

## 2.5. In vitro functionality assays

### 2.5.1. Tumour cell culture

To assess the binding efficacy of the SNAP FPs and their cytotoxic effect as ADCs against AML tumor cells, in vitro studies were performed. The cell lines THP-1 (ATCC: TIB-202), HL60 (ATCC: CCL-240), and HEK29T (ATCC: CRL-1573) were selected based on either high or low expression of the target antigens CD33 and CD45. RPMI 1640 Medium with GlutaMAX (Cat#: 61870036, Gibco, USA) was used to culture the cells mentioned above. The culture medium was supplemented with 10% FBS (Cat#: A5256701, Gibco, USA) and 100 µl/ml penicillin-streptomycin (Cat#: 15140122, Gibco, USA). The cells were incubated at 37°C, 95% humidity,

and 5% $CO_2$. After reaching 90% confluency, tumor cells were passaged, and the culture medium was changed every three days. Since THP-1 and HL60 are suspension cells, the medium change involved drawing out a specific volume of the previous medium while retaining a small amount, depending on the confluency of the cells. The same volume of removed medium was replaced by adding fresh supplemented RPMI culture medium to the small volume of remaining cells.

### 2.5.2. Binding analysis

The binding potential of the recombinant proteins to antigen-positive AML cell lines was assessed by flow cytometry. In addition, this approach distinguished between the different cell types based on the antigens present on their surface.

#### 2.5.2.1. Fluorescently labelled antibody titration

To begin, each recombinant SNAP FP was first conjugated to Alexa Fluor® 488 and incubated as described in section 2.4.3. Flow cytometry is considered a sensitive technique that can often detect background signals such as spectral overlap, cell auto fluorescence, and erroneous fluorescent detection due to the use of increased antibody concentrations causing unwanted binding. Thus, to prevent this, the fluorescently labelled protein was subjected to titration after incubation to obtain the ideal antibody concentration whereby background signal from the negative population of cells is minimized whilst still producing the strongest signal from the positive population of cells [190]. Several serial dilutions of the fluorescently labelled recombinant proteins were prepared beginning at a concentration of 250 µg/mL as shown in **Table A13**. Titration was carried out in 8 microcentrifuge tubes readied for dilution with 50 µL of 1X PBS. The entire volume of the conjugated recombinant SNAP FP was added into the first microcentrifuge tube and briefly vortexed before drawing 50 µL of the diluted protein and adding it into the next tube. This process was repeated until the eighth tube was reached and the final 50 µL of drawn diluted protein was discarded. The titrated microcentrifuge tubes were placed on ice under dark conditions until they needed to be used for staining. This sensitive experiment included two biological replicates and at least four technical repeats.

#### 2.5.2.2. Cell surface antigen staining

For each AML cell line, approximately 5 x $10^5$ cells in RPMI-1640 medium (Gibco, USA), supplemented with 10% FBS (Gibco, USA) and 100 µl/ml penicillin-streptomycin (Gibco, USA), were aliquoted and evenly distributed into 8 FACS tubes. The cells were then centrifuged at 932 RCF for 5 minutes at 4°C. The supernatant was discarded, and the cells were washed with 2 mL of 1X PBS before being resuspended in 50 µL of a 1:1000 dilution of LIVE/DEAD™

Fixable Violet Dead Cell Stain (Cat#: L34963, ThermoFisher Scientific, South Africa) and incubated in the dark for 20 minutes. Using 2 mL of FACS buffer (**Table A14**), the cells were washed twice and centrifuged at 932 RCF for 5 minutes at 4°C. Subsequently, the cells were resuspended in the remaining volume and treated on ice for 60 minutes with 50 µL of recombinant SNAP FP labelled with Alexa Fluor 488. Following incubation, the cells were washed twice with 1 mL of FACS buffer and immediately fixed by resuspending the cell pellet in 300 µL of 1% (v/v) PFA solution. The resuspended cells were incubated for 10 minutes at room temperature in the dark. After another wash with 2 mL of 1X PBS, the cells were resuspended in 200 µL of 1X PBS and stored at 4°C in the dark until data collection using the BD LSRFortessa™ Cell Analyzer (BD Biosciences, USA).

#### 2.5.2.3. Data acquisition and analysis

FACSDiva™ software (v8.0.1) (BD Biosciences, USA) was used to acquire data on the BD LSRFortessa™ Cell Analyzer (BD Biosciences, USA), equipped with fluorescein isothiocyanate (FITC)/Alexa488 and Brilliant Violet 421/Pacific Blue laser lines. For each sample, approximately 2 x $10^5$ events were acquired. Data analysis was performed using FlowJo software version 10.9.0 (Biosciences, USA), which displayed the specific gating strategy applied to each pseudocolour plot generated. Additionally, each pseudocolour plot showed the percentage of binding by the SNAP FPs to the selected cell lines. To compare the distribution of antigens among the target cell lines, bar graphs were created using the frequency (%) and median fluorescence intensity (MFI) values produced by FlowJo software. To determine if there were any significant variations in the distribution of antigens among the antigen-positive and antigen-negative cell lines used, the statistical Student's t-test was performed.

### 2.5.3. Cytotoxicity assay

#### 2.5.3.1. Analysis of the SNAP FPs conjugated to BG-AURIF

In order to prepare AML cell lines for ADC treatment, the SNAP FPs were conjugated to BG-AURIF in a 1:2 ratio (**Table A15**). Once the necessary reagents had been added, the conjugated mixture was incubated at 37°C, for 3 hours on an Eppendorf Thermomixer Comfort heating block (Sigma-Aldrich, USA). Following incubation, efficient conjugation was verified on a 10% SDS gel run at 150 V for 90 minutes as described in section 2.4.2.1.

#### 2.5.3.2. Spectrophotometric reading of treated cells

To assess the delivery and efficacy of the recombinant ADCs (recombinant SNAP FPs conjugated to cytotoxic BG-AURIF) in AML cell lines, the XTT Cell Proliferation Kit II

(Catalogue number: X12223, Roche, Switzerland) was used. HL60 and HEK293T cell lines were used in this experiment. To start, 5 x $10^3$ cells were seeded in a 96-well plate using RPMI 1640 medium with GlutaMAX (Gibco, USA), supplemented as described in subsection 2.3.1. The cells were incubated for 24 hours at 37°C, with 95% humidity and 5% $CO_2$ before treatment with the recombinant ADCs. After incubation, the cells were treated with serially diluted recombinant ADCs starting at a concentration of 1000 nM, with the volume adjusted to a total of 125 µL. Before adding the recombinant ADC to the AML cells, each dilution was prepared on a separate 96-well plate to minimize dilution errors. Following treatment, the cells were maintained in this cytotoxic environment for an additional 48 hours at 37°C with 5% $CO_2$. For analysis of the treatment effects, XTT (2,3-bis(2-methoxy-4-nitro-5-sulphophenyl)-5-carboxanilide-2H-tetrazolium, monosodium salt) and N-methyl dibenzopyrazine methyl sulfate were mixed in the dark at a ratio of 50:1. Once the mixture was added to metabolically active cells, the tetrazolium salt XTT was converted into orange formazan compounds. The water-soluble formazan dye absorbs light at 450 nm, facilitating the measurement of metabolic activity and cell viability. After adding 51 µL of XTT to each well, the cells were incubated at 37°C for 4 hours to allow the conversion of the tetrazolium salt XTT reagent into orange formazan crystals. Measurements were taken using an iMark™ Absorbance Reader Spectrophotometer (Bio-Rad, USA) at absorbance readings of optical density 450 nm (measurement filter) and optical density 650 nm (reference filter). GraphPad Prism version 5 (GraphPad Software, La Jolla, USA) was employed to analyze the obtained data. The controls used to normalize absorbance measurements were untreated (0% killing) and Zeocin-treated (100 µg/ml) cells. Furthermore, the software was used to determine the 50% inhibitory concentration ($IC_{50}$) value of each recombinant ADC against the selected cell lines. To enhance the accuracy of these experiments, biological quadruplicates and technical triplicates were included. Each cell viability (%) measurement was presented as the mean ± standard deviation, with vertical error bars indicating significant variations among the technical repeats.

# Chapter 3: Results

## 3.1. *In silico* design of αCD33(scFv)-SNAP and αCD45(scFv)-SNAP mammalian expression vectors

The acquisition of sequences used to form αCD33(scFv) and αCD45(scFv) was previously performed by Bernard Mirianga (PhD) and Tatenda Bvudzijena (MSc). To construct the amino acid chains of each scFv vector, the following patents were referred to: CD33 (US11136390B2) [191] and CD45 (US11034752B2) [192], respectively. The sequences obtained from these patents were converted into their corresponding nucleotides using the Gene Infinity Back Translation Tool. The generated nucleotide sequences were then aligned and analyzed parallel to their homologous immunoglobulin germline variable region sequences using IgBlast. The results demonstrated the presence of the correct CDR and FR regions, as well as a high degree of similarity between the sequences compared (data not shown). Following this, codon optimization in preparation for translating the nucleotide sequences back to amino acid sequences was achieved using Expasy, and alignment was conducted using EMBL-EBI Clustal Omega to further confirm homology. After completing optimization, the $V_H$ and $V_L$ chains containing the CDR and FR regions were prepared for linkage via a flexible peptide linker. The carboxyl terminus of one variable chain and the amino terminus of another variable chain were joined to produce scFvs by a connecting linker made up of hydrophilic amino acids, such as glycine and serine $(Gly_4Ser)_3$. These scFvs were then flanked with *SfiI* and *NotI* restriction sites to facilitate their insertion into the pCB-SNAP backbone plasmid, utilizing SnapGene®, as shown in **Figure 9A** below.

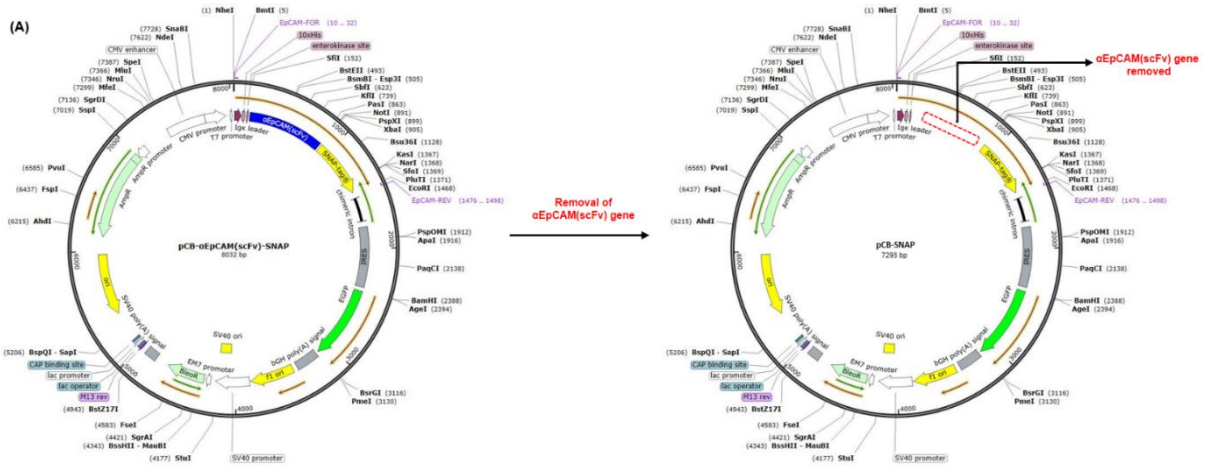

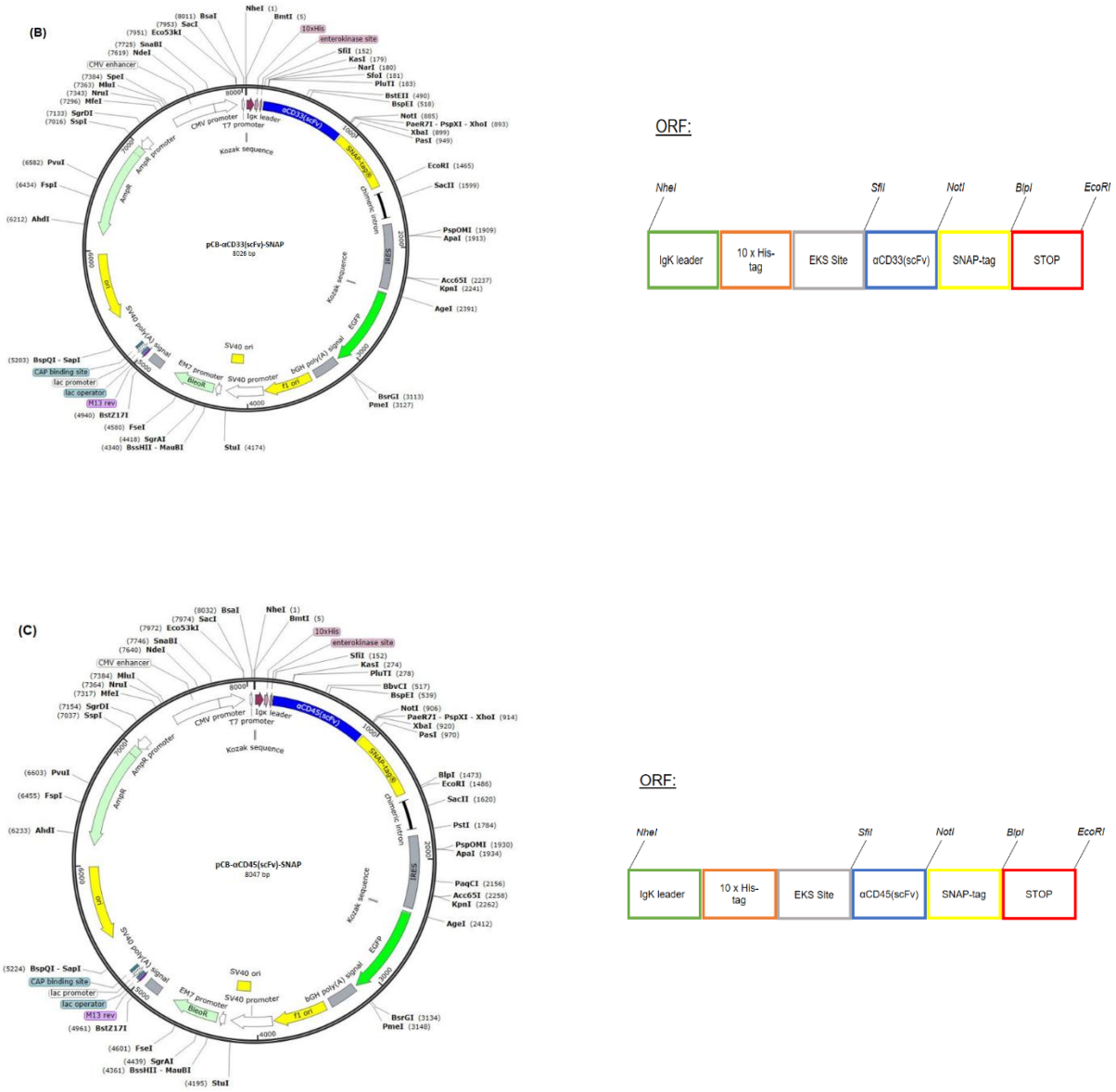


**Figure 9. The *in silico* design of pCB-αCD33(scFv)-SNAP and pCB-αCD45(scFv)-SNAP**. A schematic illustration of the process by which the desired plasmid vectors were produced using SnapGene. (A) The αEpCAM gene from the parental plasmid vector (pCB-αEpCAM-SNAP) was excised at the *SfiI* and *NotI* restriction sites, thus resulting in the pCB-SNAP vector. (B) The mammalian plasmid map of pCB-αCD33(scFv)-SNAP created following the insertion of αCD33(scFv) into the pCB-SNAP backbone vector. (C) The mammalian plasmid map of pCB-αCD45(scFv)-SNAP created following the insertion of αCD45(scFv) into the pCB-SNAP backbone vector. The ORF of each plasmid is demonstrated beside it. The ORFs highlight the features which are most essential for best productivity in downstream experiments. These include: IgK leader, His-tag (10x), EKS, scFv, SNAP-tag, Stop codon and *SfiI/NotI* restriction sites.

## 3.2. Molecular cloning of the mammalian expression vectors

Molecular cloning of pCB-αCD33(scFv)-SNAP was previously and successfully conducted by Bernard Mirianga (PhD) using the methods outlined in sections 2.2.1 to 2.2.8. However, to confirm the success of these experiments, molecular cloning was repeated for this plasmid (already provided in the mammalian expression vector pCB-SNAP backbone), along with that of pCB-αCD45(scFv)-SNAP using the aforementioned methods.

### 3.2.1. Transformation, isolation and purification of the plasmids from *E. coli* cells

The ORFs of the relevant antibody fragments were synthesized by GenScript Biotech Corporation and powdered into 4 µg plasmid pellets. These plasmids (pUC57-αCD33(scFv) and pUC57-αCD45(scFv)) were resuspended in nuclease-free water to a concentration of 100 ng/µL prior to DNA transformation in *DH5α E. coli* cells, as detailed in section 2.2.1. Additionally, pCB-αEpCAM-SNAP (provided by the MB&I unit) was transformed into *DH5α E. coli* cells, amplified, and isolated using the appropriate technique described in section 2.2.2. The concentrations and purity (260/280 and 260/230 ratios) of each isolated plasmid were measured using a spectrophotometer. Absorbance values of approximately 1000 ng/µL, 1.8 - 2.0, and 2.0 - 2.2 were recorded, respectively (**Table A16**). These values enabled progress to subsequent studies, confirming the isolation of high-quality DNA.

### 3.2.2. Restriction digestion of the plasmids

Using the restriction endonucleases *SfiI* and *NotI* (outlined in section 2.2.3), the appropriate sequences (αCD33(scFv), αCD45(scFv), and pCB-SNAP) were successfully cleaved, creating the sticky ends required for subsequent ligation. The expected DNA sizes of these digested fragments were obtained from a SnapGene® simulated agarose gel and are detailed in **Table 6**. Physical separation and isolation of the relevant digested fragments were performed by electrophoresis on a 1.2% (w/v) agarose gel as described in section 2.2.4. After electrophoresis, the agarose gel was observed under UV light, and the DNA band sizes shown in **Figure 10** were determined using a DNA molecular weight marker and were verified against the expected sizes provided in **Table 6**. The highlighted backbone and insert DNA bands were excised from the gel (see section 2.2.5) and purified in preparation for ligation.

**Table 6.** Expected DNA sizes obtained from a SnapGene® agarose gel electrophoresis simulation with samples digested using *SfiI* and *NotI* restriction enzymes.

| Vector | Insert (bp) | Backbone (bp) | Total (bp) |
|---|---|---|---|
| pCB-αEpCAM(scFv)-SNAP | 739 | 7293 | 8032 |
| pCB-αCD33(scFv)-SNAP | 733 | 7293 | 8026 |
| | | | |
| **Vector** | **Insert (bp)** | **Backbone (bp)** | **Total (bp)** |
| pCB-αEpCAM(scFv)-SNAP | 739 | 7293 | 8032 |
| pUC57-αCD45(scFv) | 754 | 2710 | 3464 |

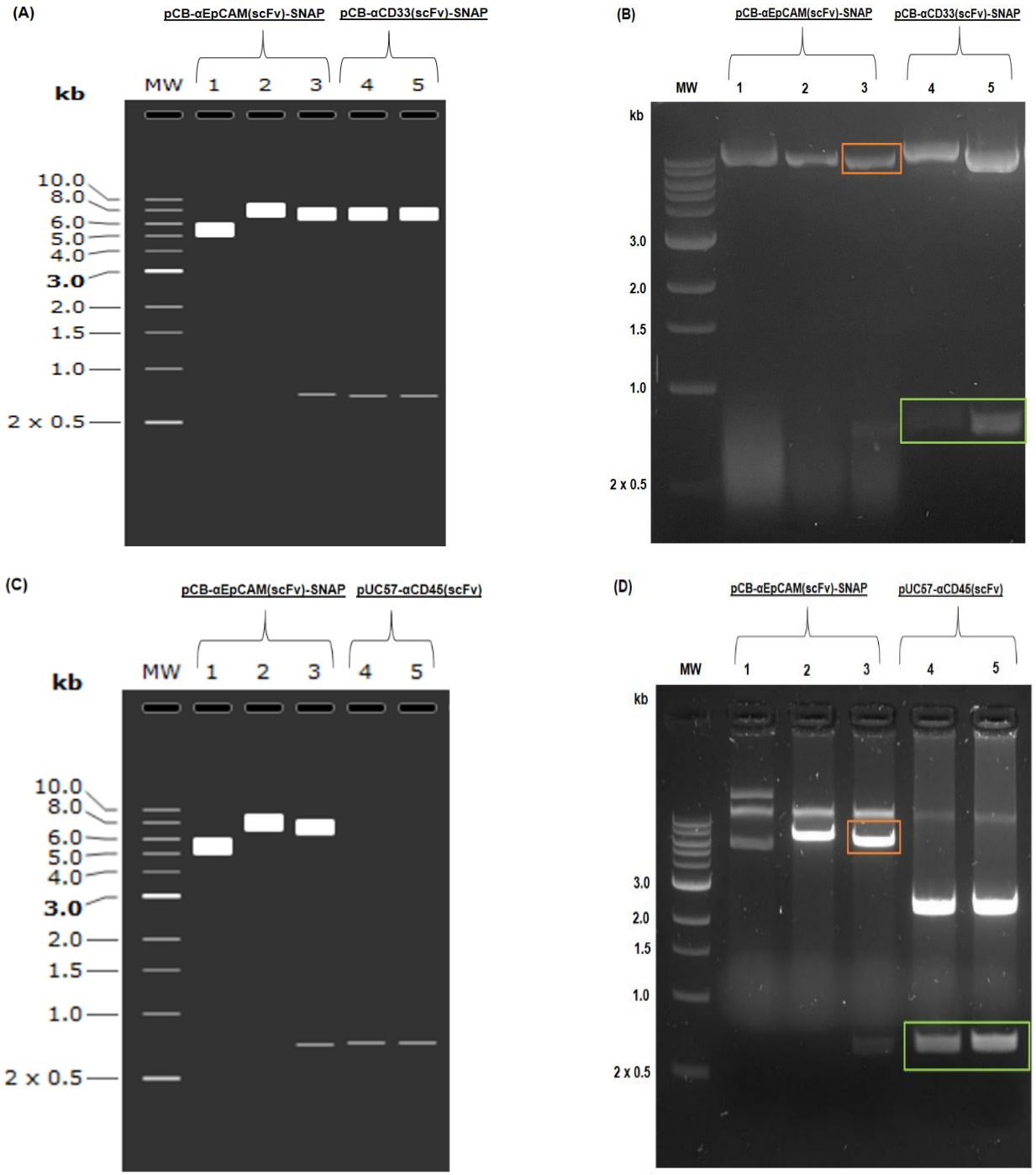


**Figure 10. Restriction digestion analysis by agarose gel electrophoresis. (A, C)** SnapGene® generated agarose gel electrophoresis simulations used as reference to determine the expected DNA sizes following restriction digestion of plasmid samples with *SfiI* and *NotI*. Lanes 1, 2 and 3 represent the parental plasmid with no enzyme (undigested), *SfiI* only (single digest) and both *SfiI* and *NotI* (double digest), respectively. Lanes 4 and 5 represent either pCB-αCD33(scFv)-SNAP or pUC57-αCD45(scFv) digested with both endonuclease enzymes. **(B, D)** 1.2% agarose gels showing the results of plasmid sample digestion using *SfiI* and *NotI*, with each lane representation remaining identical to the simulation. The bands highlighted in orange and green display the pCB-SNAP and scFv inserts, respectively, which are essential for subsequent ligation.

### 3.2.3. DNA ligation and transformation

Following the excision and purification of the appropriate DNA bands, DNA ligation was performed for the effective fusion of the parental backbone vector and inserts. Using T4 DNA ligase, two different reactions of vector to insert were prepared at ratios of 1:1 and 1:5 as described in section 2.2.6. Bacterial transformation of the ligated products was then done in *DH5α* competent *E. coli* cells. Once transformed, the bacterial cells were plated onto ampicillin-supplemented agar plates. The growth and isolation of colonies with positively transformed plasmids, seen in **Figure 11**, were enabled by the ampicillin gene, which imparted antibiotic resistance to the plasmids.

(A) pCB-αCD33(scFv)-SNAP bacterial transformation

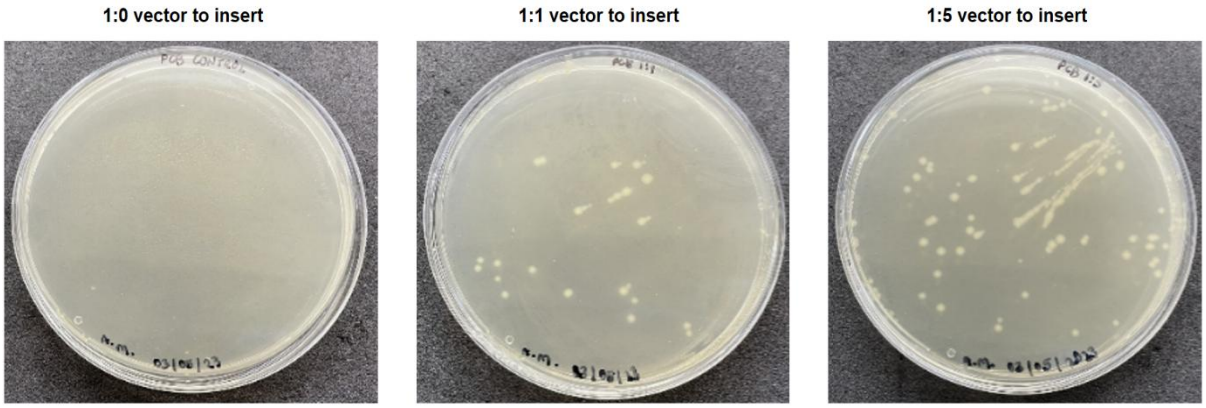


(B) pCB-CD45(scFv)-SNAP bacterial transformation


**Figure 11. Bacterial growth of *E. coli* cells transformed with recombinant plasmid DNA.** (A) Bacterial transformation of pCB-αCD33(scFv)-SNAP and (B) Bacterial transformation of pCB-αCD45(scFv)-SNAP. Using LB agar, *E. coli* cells transformed with different ratios of parental backbone vector to scFv inserts were used to increase efficacy of transformation of the plasmid DNA. (Left: control plate; middle: 1:1 pCB-SNAP vector to scFv insert; 1:5 pCB-SNAP to scFv insert).

Transformation efficiencies for the different ligation ratios were tabulated (see **Table A5**). Colony formation was not observed on the control plates that contained bacterial cells transformed with ligase and backbone vector without an insert. With a clear and favourable difference in CFUs between the control and experimental agar plates, only two of the experimental plates containing the highest colony growth for each plasmid were chosen for further analysis. With the intent to raise the likelihood of selecting colonies with suitably ligated plasmids, at least five colonies were isolated from each experimental plate. Selected colonies were cultivated in LB media supplemented with 100 mg/mL Ampicillin. As described in sections 2.2.6. to 2.2.7., the culture was kept overnight in a shaking incubator to allow for DNA amplification in preparation for the studies that followed.

### 3.2.4. Confirmation of molecular cloning

#### 3.2.4.1. Restriction mapping of recombinant plasmids

Through restriction mapping, it was verified that the insert fragments (αCD33(scFv) and αCD45(scFv)) had been properly ligated into the pCB-SNAP backbone vector. After the chosen colonies were grown and purified (refer to section 2.2.7.), it was anticipated that correctly ligated plasmids had been retained. A set of restriction endonucleases was employed to distinguish ligated plasmids from the backbone plasmid control by cleaving distinct or different sites of each plasmid. *BamHI* and *SpeI* restriction endonucleases were used in this experiment. The digested reactions were subjected to electrophoresis run on a 1.2% agarose gel (see section 2.2.8.1.). An agarose gel simulation, generated on SnapGene®, was referred to for the determination of the expected band sizes resulting from digestion with *BamHI* and *SpeI*. Comparisons between the simulation and the 1.2% gel (seen in **Figure 12**) revealed differential cleavage patterns between the ligated plasmids and backbone plasmid, precisely within the scFv sites, thus confirming successful cloning and functionality for downstream experiments.

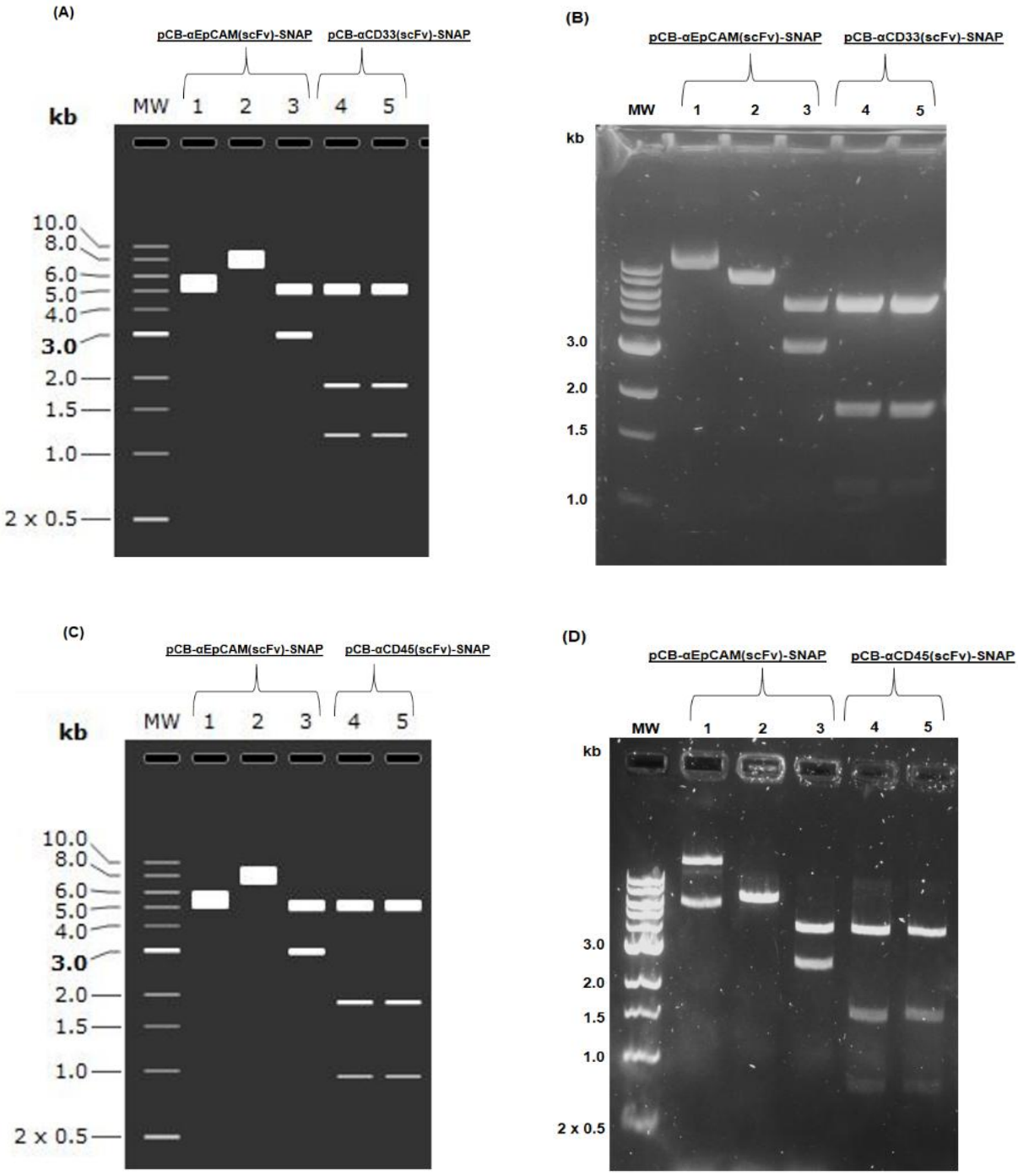


**Figure 12. Restriction mapping analysis by agarose gel electrophoresis. (A, C)** SnapGene® generated agarose gel electrophoresis simulations used as reference to determine the expected DNA sizes following restriction mapping of plasmid samples with *BamHI* and *SpeI*. Lanes 1, 2 and 3 represent the parental plasmid with no enzyme (undigested), *BamHI* only (single digest) and both *BamHI* and *SpeI* (double digest), respectively. Lanes 4 and 5 represent either pCB-αCD33(scFv)-SNAP or pCB-αCD45(scFv)-SNAP digested with both endonuclease enzymes. **(B, D)** 1.2% agarose gels showing the results of plasmid sample mapping using *BamHI* and *SpeI*, with each lane representation remaining identical to the simulation.

#### 3.2.4.2. Sanger sequencing of recombinant plasmids

The colonies showing promising results for restriction mapping were sent to Inqaba Biotechnical Industries for Sanger sequencing as an additional measure to validate the molecular cloning process and the successful production of ligated plasmids (see section 2.2.8.2). To conduct sequencing, several primers designed by Inqaba and the MB&I Research Unit were aligned to the ligated plasmid sequences to ensure that all key genes were included. After analyzing the resultant sequences using SnapGene® software (version 3.1.1, GSL Biotech, Chicago), it was found that the clones were almost identical to their *in silico* ORF sequences, as seen in **Figure A1**. This analysis validated the correct cloning and viability of the desired plasmids.

## 3.3. Mammalian expression of recombinant FPs

### 3.3.1. Transfection and maintenance of recombinant FPs

Following confirmation of effective molecular cloning, pCB-αCD33(scFv)-SNAP and pCB-αCD45(scFv)-SNAP plasmid DNA were transfected into HEK293T cells at two different ratios as detailed in section 2.3.2. The enhanced green fluorescent protein (eGFP) of positively transfected cells was monitored every 24 hours for 4 days using a ZOE™ Fluorescence Cell Imager (BioRad, USA) as seen in **Figure 13**. Antibiotic selection with Zeocin achieved increased expression of the positively transfected cells. Enrichment of eGFP positive cells was enabled by the bleomycin gene incorporated in the plasmids. Initial selection was conducted with 100 µg/mL of Zeocin over a course of 4 weeks. This was followed by a 1-week interval with no Zeocin, allowing for recovery and growth of cells. Antibiotic selection was repeated at a slightly increased concentration of 150 ug/mL for approximately 2 weeks, which resulted in enhanced expression and expansion of cells. These cells were maintained by culturing with RPMI-1640 culture medium (supplemented with 10% FBS and 1% penicillin-streptomycin). The nutrient-rich medium was replaced every 4 days to allow the continual expansion of eGFP-positive cells. Target FPs were obtained by collecting cell culture supernatant of the highly eGFP expressing cells beginning approximately one week after Zeocin selection had been completed.

(A) αCD33(scFv)-SNAP cell culture

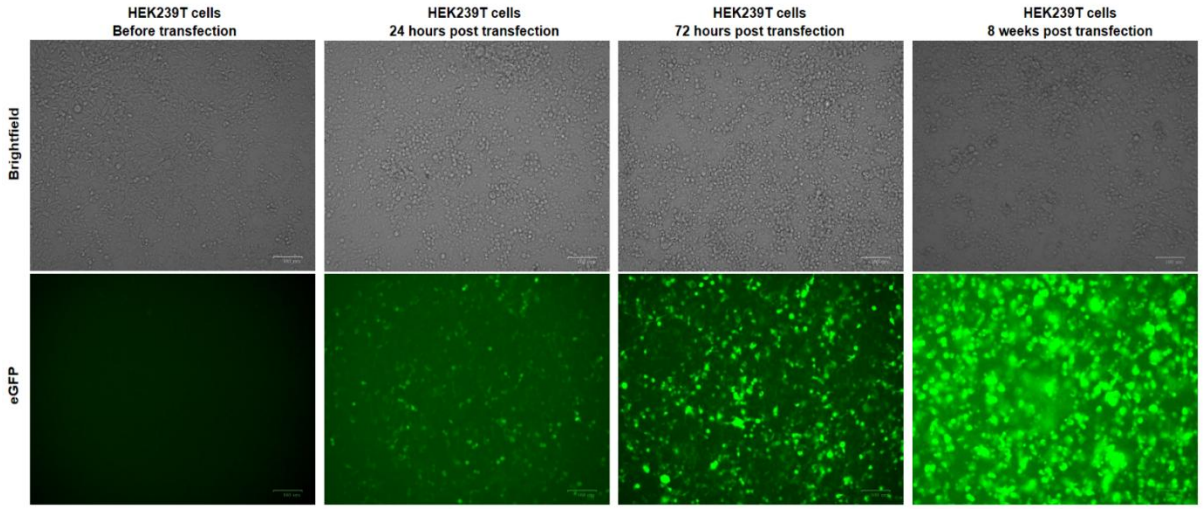


(B) αCD45(scFv)-SNAP cell culture

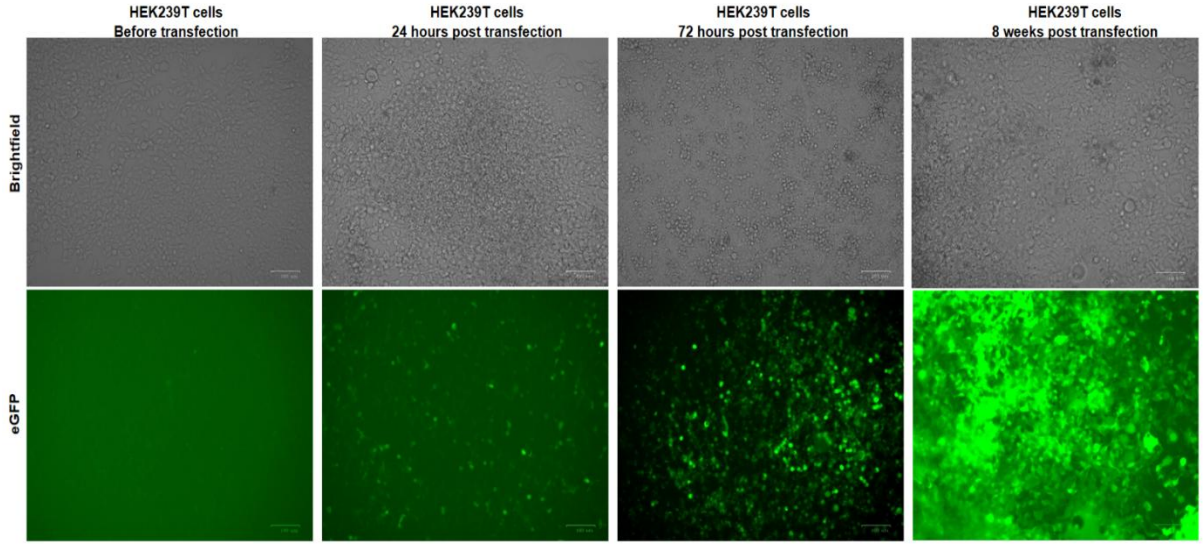


**Figure 13. Visualization of recombinant plasmid uptake into HEK293T cells.** (A) pCB-αCD33(scFv)-SNAP transfection into HEK293T cells and (B) pCB-αCD45(scFv)-SNAP transfection into HEK293T cells. Using the ZOE™ Fluorescent Cell Imager, each image showed distinct phases of each recombinant plasmid's transfection and cell culture in brightfield (top panel) and the green fluorescent channel (bottom panel). Stages captured: Before transfection (1$^{st}$ column), 24 hours post transfection (2$^{nd}$ column), 72 hours post transfection (3$^{rd}$ column) and 8 weeks post transfection (4$^{th}$ column).

### 3.3.2. Transfection efficiency by flow cytometry

Flow cytometry was used to determine the transfection efficiency of the recombinant plasmids in HEK293T cells. 96 hours post-transfection, 1 mL of transfected cells was obtained, stained according to section 2.3.3, and analysed using a BD LSRFortessa™ Cell Analyzer (BD Biosciences, USA). FlowJo software (version 10.9.0; BD Biosciences, USA) was then used to establish the percentage of cells effectively transfected compared to non-transfected cells, which is displayed in **Figure A2**.

## 3.4. Purification and characterisation of recombinant proteins

### 3.4.1. IMAC purification of recombinant FPs

Upon collection of sufficient mammalian CCSN (> 1 L), His-tag mediated IMAC was performed to achieve isolation and enrichment of each recombinant FP. As detailed in section 2.4.1., the ÄKTA Avant system (GE Healthcare) facilitated purification by selectively capturing the target proteins through high affinity interactions between the 10 x His-tag residues of each recombinant FP and $Ni^{2+}$ metal ions immobilised within the resin of the IMAC column. By adding a low concentration of imidazole during the washing step, nonspecific binding of bulk impurities and contaminating proteins containing shorter polyhistidine tags was prevented, thus the purification process was further improved. Elution and collection of the recombinant SNAP FP were achieved by elevating the concentration of imidazole by a substantial amount relative to the wash step. Increased concentration effected gentle displacement of the recombinant SNAP FP through competitive binding between the imidazole, which has a higher affinity for the $Ni^{2+}$ charged column, and the 10 X His-tag of each protein. The chromatograms produced for each IMAC run showed the resulting absorbance peaks against the elution volume (mL) (**Figure 14**). These chromatograms were consulted to determine which particular eluted fractions contained the target proteins.

(A) αCD33(scFv)-SNAP IMAC purification

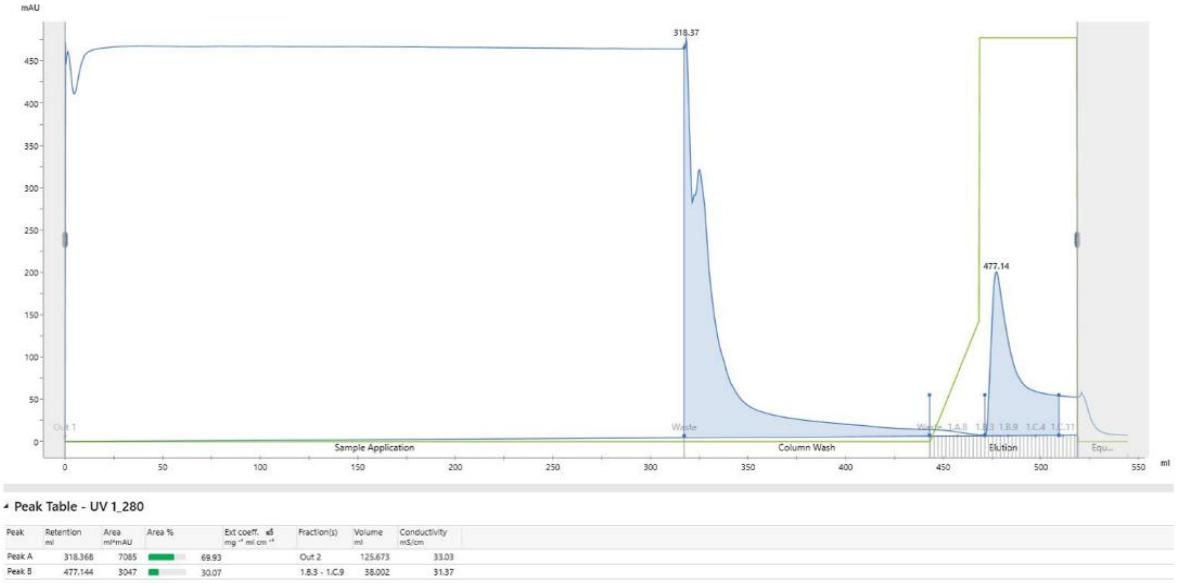


(B) αCD45(scFv)-SNAP IMAC purification

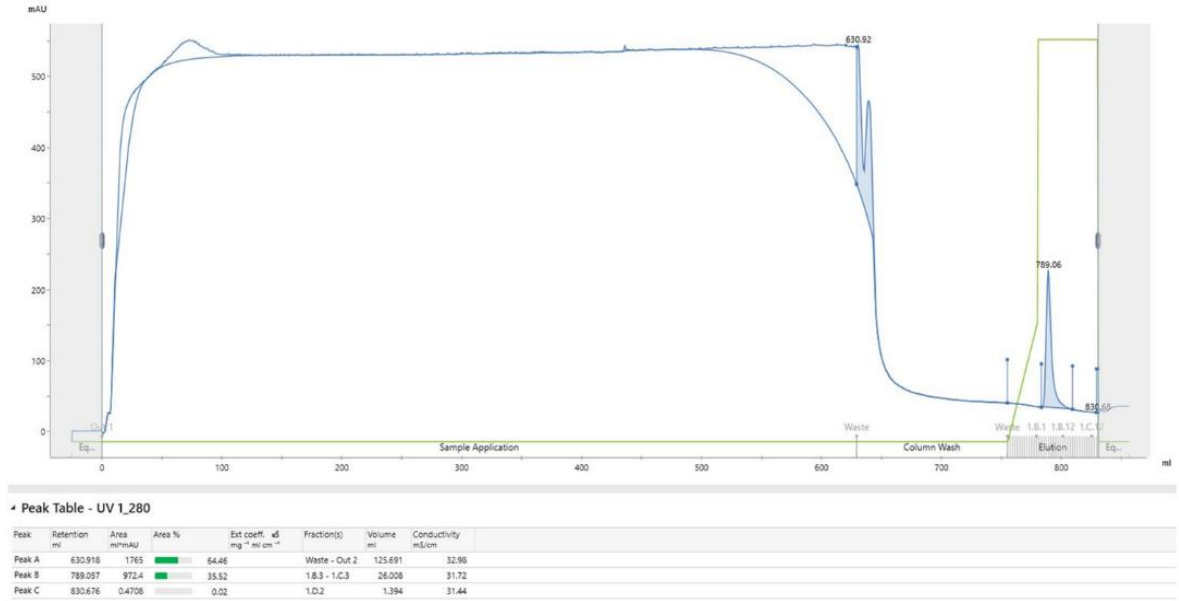


**Figure 14. IMAC purification chromatograms of the recombinant SNAP FPs.** (A) αCD33(scFv)-SNAP and (B) αCD45(scFv)-SNAP. The absorbance profiles of IMAC purified and eluted mammalian-expressed SNAP FPs at UV=280 nm were shown in the chromatograms with the elution buffer percentage (y-axis) against volume (x-axis) over the different phases of each purification run. The absorbance profile and imidazole concentration on each chromatogram are depicted by the narrow blue and green lines, respectively. The elution peak of each SNAP FP is presented beneath the narrow green line. (Phases of purification: 1$^{st}$: Sample application, 2$^{nd}$: Column wash and 3$^{rd}$: Elution).

### 3.4.2. IMAC fraction analysis using SDS-PAGE

The range of protein fraction eluates corresponding to the elution peak identified from each chromatogram (see **Figure 14**) was screened on a 10% SDS-PAGE gel to validate the presence and precise size of the recombinant SNAP FPs. The theoretical molecular weights of αCD33(scFv)-SNAP and αCD45(scFv)-SNAP were calculated to be 51.8 kDa and 52.5 kDa, respectively, using a protein molecular weight calculator (https://web.expasy.org/compute_pi/). After electrophoresis, it was observed that all selected fractions run on the agarose gel displayed a protein band close to the 52 kDa mark of the molecular weight ladder (see **Figure 15**), indicating effective IMAC purification. To avoid using multiple individual fractions in subsequent experiments, the relevant fractions were pooled by centrifugation through a 30 kDa Amicon® filter column to concentrate the proteins for simpler use in downstream experiments.

(A) αCD33(scFv)-SNAP IMAC eluted fractions

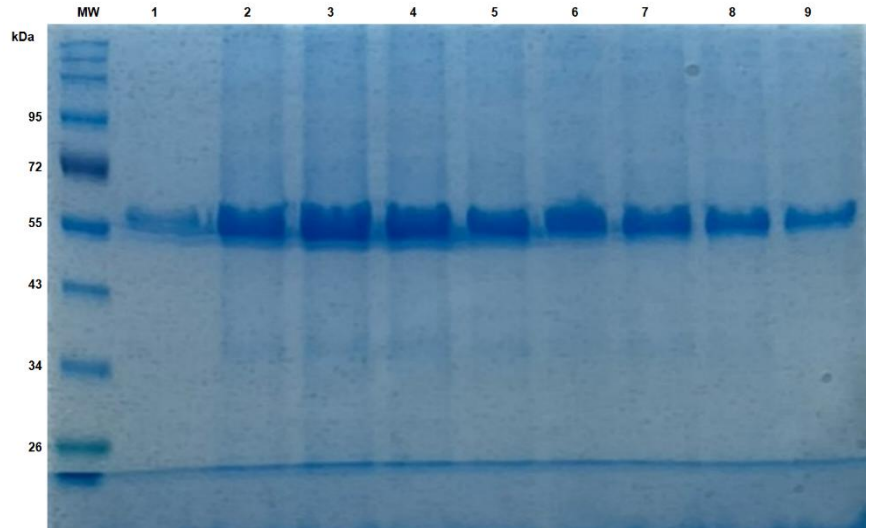


(B) αCD45(scFv)-SNAP IMAC eluted fractions

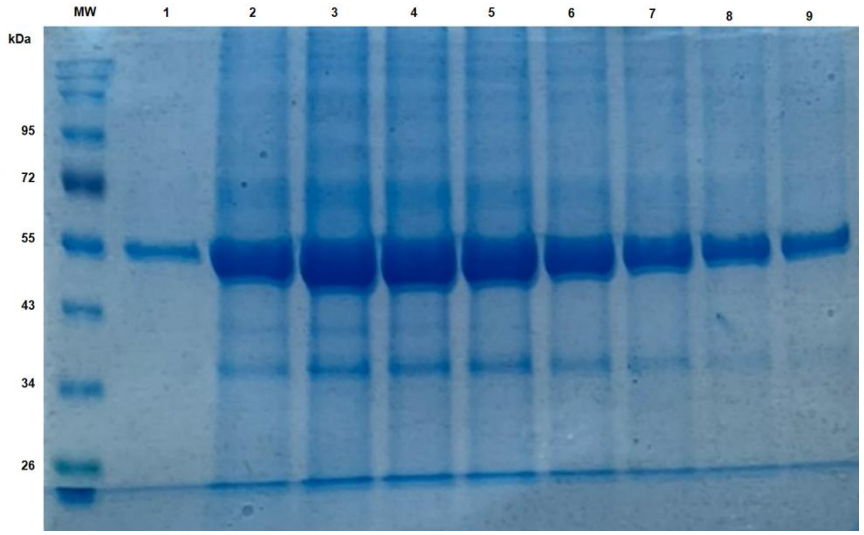


**Figure 15. Analysis of protein fraction elutes by SDS-PAGE prior to concentration.** (A) αCD33(scFv)-SNAP and (B) αCD45(scFv)-SNAP. 10% SDS-PAGE gels were run following IMAC purification to identify the eluates containing SNAP FP with the least amount of contaminants. A pre-stained protein standard was used as a reference to determine the molecular weight (MW) of each SNAP FPs' eluted fraction. The SNAP FP eluates were represented by bands of ~ 52 kDa from lanes 1 to 9. Narrow bands between 34 kDa and 43 kDa represented minor proteolytic degradation.

### 3.4.3. Concentrated protein analysis by densitometry

After concentrating the protein fraction eluates, a densitometric approach was used to determine the purity (as a percentage) and total protein yield of each recombinant SNAP FP from the CCSN purified (section 3.4.1). The quantity of total protein following concentration was immediately quantified using the Denovix NanoDrop™ ND-2000 (Thermo Fisher Scientific, USA). An additional quantification step was performed to measure the total amount of recombinant SNAP FPs while excluding any impurities. This step was taken due to the possibility that the concentrated proteins may have contained extra contaminants during fraction pooling, which could have impacted the quantification results obtained with the Denovix NanoDrop™ ND-2000. The concentrated protein was analyzed on a 10% SDS-PAGE gel against two-fold serially diluted BSA standards of known concentration to determine the total quantity of each protein, as shown in **Figure 16**.

(A) αCD33(scFv)-SNAP densitometry

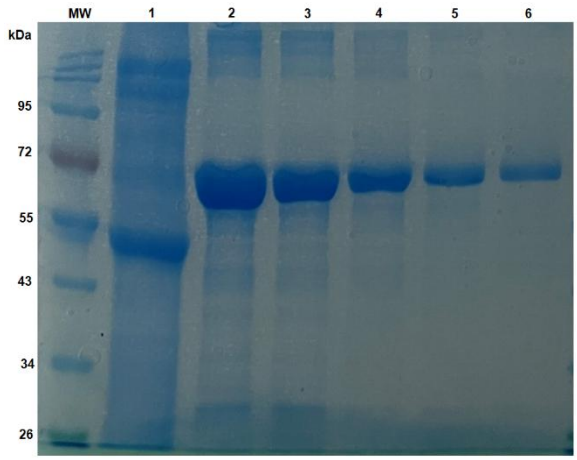


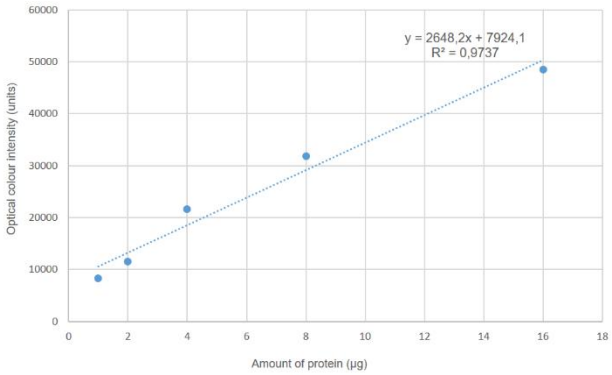


(B) αCD45(scFv)-SNAP densitometry

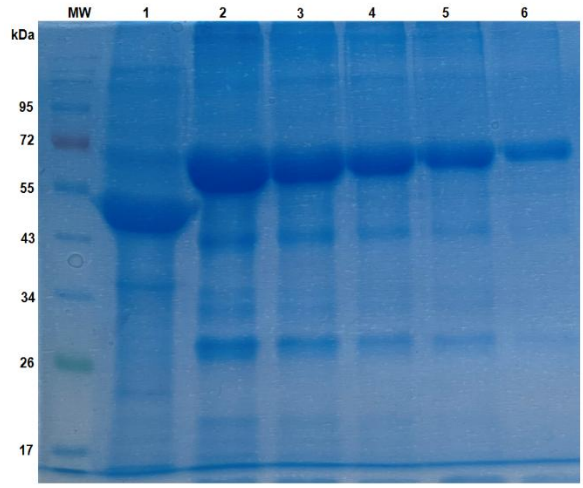


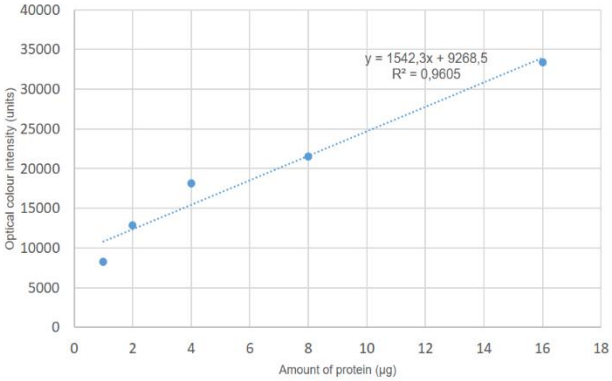

**Figure 16. SNAP FP concentration determination by densitometry.** (A) αCD33(scFv)-SNAP densitometry analysis and (B) αCD45(scFv)-SNAP densitometry analysis. (Left) 10% SDS-PAGE gels were run to determine the concentration of each SNAP FP (lane 1) against a pre-stained protein MW standard and two-fold serially diluted BSA proteins of known concentrations. BSA standards of 16 µg, 8 µg, 4 µg, 2 µg, and 1 µg were represented by lanes 2, 3, 4, 5 and 6, respectively. Standard BSA curves depicting optical colour intensity (in units) against protein amount (in µg) were created using Microsoft Office Excel after the optical colour intensity of the BSA bands was measured by ImageJ Software. The generated linear equation was used to estimate the concentration of SNAP FP only from total protein sample. The protein yield and purity (in percentage) were also determined using the linear equations.

Once electrophoresis was complete, the gel was stained and analysed on ImageJ software as described in section 2.4.2.3. The optical colour intensity measured for each BSA standard protein band aided in the creation of a BSA standard curve (see **Figure 16**), which was used to calculate the purity and total yield of the SNAP FPs provided in **Table 7.**

**Table 7.** The percentage purity and total yield of the SNAP FPs using the BSA standard curves.

| SNAP fusion protein | Densitometry concentration (µg/µL) | Nanodrop concentration (µg/µL) | Purity (%) | Total protein yield (mg/L) |
|---|---|---|---|---|
| αCD33(scFv)-SNAP | 4.1 | 8.3 | 49.4 | 6.8 |
| αCD45(scFv)-SNAP | 6.5 | 12.7 | 51.2 | 8.7 |

### 3.4.4. Confirmation of full-length SNAP FPs via functionality analysis of N- and C-terminus

#### 3.4.4.1. Western blotting analysis

Western blotting was performed to further verify the attainment of full-length recombinant SNAP FPs. In addition, this technique also assessed the presence and functionality of the N-terminus 10 X His-tag. Using an anti-polyhistidine HRP mouse monoclonal antibody, the 10 X His-tag on each protein was successfully targeted, bound, and detected following incubation with the appropriate blotting solution (see section 2.4.2.4.). The presence of full-length protein and a functional N-terminus 10 X His-tag was confirmed by a comparative assessment between stained SDS-PAGE gels and WB PVDF membranes in **Figure 17**. Protein bands were detected at the same molecular weight marker position (~52 kDa) on both the gel and PVDF membrane. Any protein bands detected below the anticipated protein molecular weight depicted minor proteolytic degradation.

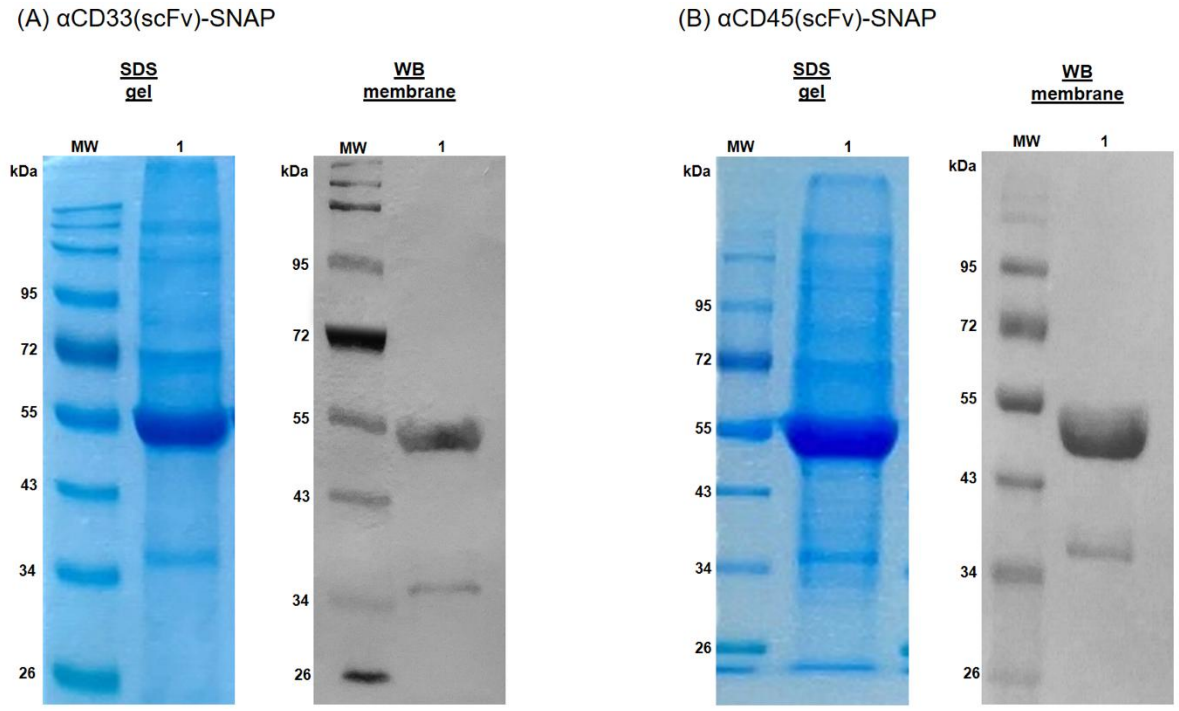


**Figure 17. Confirmation of full-length SNAP FP by detection of functional N-terminus.** (A) SDS-gel and Western Blot PVDF membrane of αCD33(scFv)-SNAP and (B) SDS-gel and Western Blot PVDF membrane of αCD45(scFv)-SNAP. In lane 1, each full-length SNAP FP was detected around the MW mark of ~ 52 kDa on the SDS gels. Similarly, the presence of full-length proteins was further confirmed on the PVDF membrane following western blotting. By using an anti-polyhistidine antibody, the N-terminus of each SNAP FP polyhidistine tag was bound and detected following staining with 1-Step Ultra TMB-Blotting Solution.

### 3.4.4.2. BG-modified substrate conjugation to the SNAP-tag

The acquisition of full-length recombinant SNAP FPs was confirmed by conjugating the proteins with a BG-modified substrate (Alexa Fluor® 488). Similar to section 3.4.4.1, the presence and functionality of the C-terminus SNAP-tag were also analyzed in this experiment. After incubating each recombinant SNAP FP with Alexa Fluor® 488, the conjugated proteins were run on a 10% SDS-PAGE gel under dark conditions (see section 2.4.3). Following electrophoresis, the gel was viewed under blue light using a Dark Reader Transilluminator. Effective conjugation of full-length recombinant SNAP FPs with a functional C-terminus SNAP-tag was validated by a fluorescent signal detected at the expected molecular weight (~52 kDa) and emitted at a wavelength of approximately 520 nm, as shown in **Figure 18**.

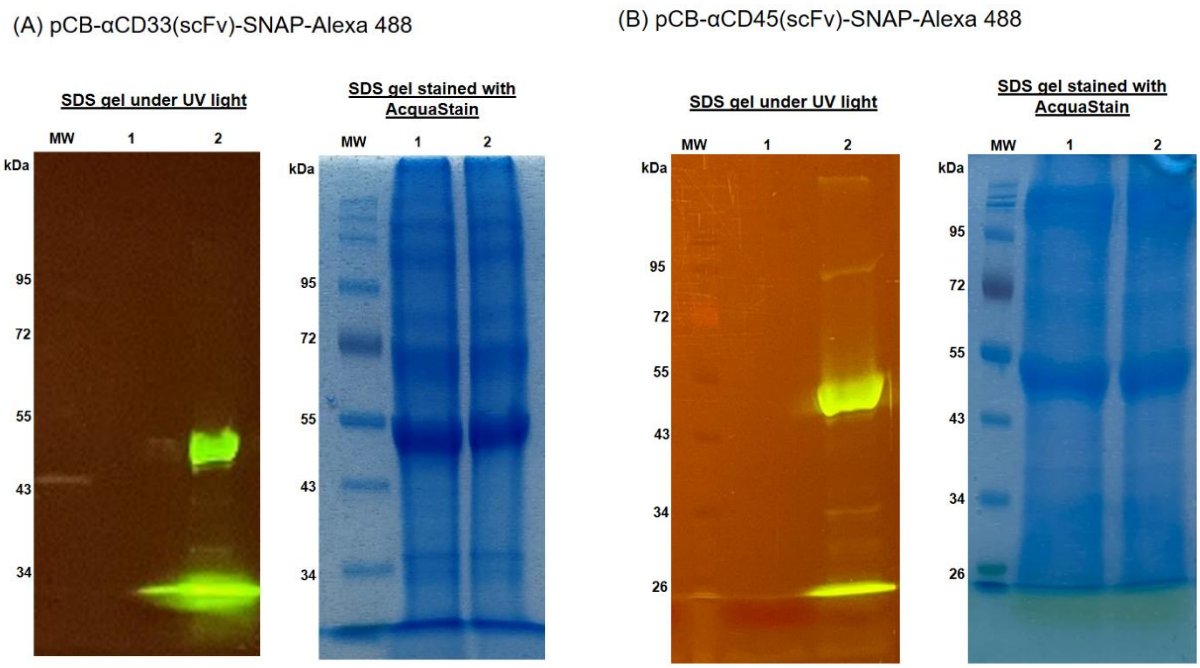


**Figure 18. Verifying functionality of the C-terminus SNAP-tag by BG-Alexa 488 conjugation**. (A) αCD33(scFv)-SNAP-Alexa 488 and (B) αCD45(scFv)-SNAP-Alexa 488. BG-Alexa 488 was used to assess functionality of the C-terminus SNAP-tag and verify the presence of full-length protein. 10% SDS gels were run with a protein molecular weight (MW) marker, unconjugated SNAP FP as a control (lane 1) and BG-Alexa 488 conjugated SNAP FP (lane 2). The green fluorescent band of each BG-Alexa 488 conjugated SNAP FP detected under UV light was indicative of a functional C-terminus SNAP-tag and full length protein. By staining each gel with AcquaStain, the presence of full-length SNAP FP, unconjugated and conjugated was verified.

## 3.5 In vitro studies

### 3.5.1. Binding analysis of the SNAP FPs against AML cells

#### 3.5.1.1. Determination of the ideal optimal concentrations for staining by titration of the SNAP FPs

Flow cytometry analysis was conducted to assess the binding activity of each SNAP FP against selected cell lines: HL60 (expressing CD33 and CD45), THP-1 (expressing CD33 and CD45), and HEK293T (non-expressing CD33 and CD45). Both αCD33(scFv)-SNAP and αCD45(scFv)-SNAP were labeled with BG-Alexa 488 fluorophore as described in section 2.4.3. Subsequently, the conjugated SNAP FPs underwent a two-fold serial titration from 250 µg/mL to 1.95 µg/mL, as outlined in section 2.5.2.1. This titration allowed for the determination of the optimal antibody concentration for staining, which yielded the strongest positive signal while minimizing unwanted background signal that could compromise the accuracy of the analysis. Due to the sensitivity of this experiment, two biological repeats and at least four technical repeats were conducted to ensure that the most accurate results were obtained. Using median fluorescence intensity values provided by FlowJo software version 10.9.0, the

signal-to-noise ratio and staining index for each titre (ranging from 250 µg/mL to 1.95 µg/mL) were calculated with the formulas found in **Table A17**. The signal-to-noise ratio measured the difference in fluorescence between negative and positive cell populations, while the staining index served as a standardized indicator of staining performance, accounting for both background noise and signal. These two metrics were employed to select the ideal SNAP FP concentration for staining each cell line. Upon completion of this selection process, the chosen staining concentrations for αCD33(scFv)-SNAP-Alexa 488 were 250 µg/mL and 125 µg/mL for HL60 and THP-1, respectively. For αCD45(scFv)-SNAP-Alexa 488, the selected staining concentration was 250 µg/mL for both HL60 and THP-1 cells. Additionally, 62.5 µg/mL of each SNAP FP conjugated to Alexa 488 was utilized to stain HEK cells, which express minimal to no CD33 and CD45 antigens.

#### 3.5.1.2. Determining target antigen distribution on AML cells by applying the gating strategy

Subsequent to obtaining suitable concentrations for staining, quantification (as a percentage) of the proportion of cells expressing the targeted antigens was conducted. In addition, this quantification was directly correlated with each SNAP FP's binding strength to the relevant antigens. As seen in **Figure 19**, a technique known as gating strategy was applied on pseudocolour plots of each cell line stained with the chosen antibody concentration and was used to determine the frequency of cells that highly expressed the target antigen using FlowJo software version 10.9.0 (see section 3.5.1.1.). The first gate was used for the inclusion of all the cells that possessed suitable granularity measured by the side scatter area (SSC-A) and size measured by forward scatter area (FSC-A). Any cellular debris which was found on the bottom of the scale was also excluded by the first gate. To avoid including doublet or aggregate cells which could cause inaccuracy in analysis, a second gate which only included single cells was applied. Next, to exclude all the dead cells which produced a positive signal for the Live-Dead marker, a third gate was applied. Finally, to differentiate between the antigen positive and antigen negative cells, a fourth gate was applied where an unstained population of cells was used as a threshold for differentiation.

(A) Positive controls: αMPO(scFv)-SNAP-Alexa 488 assessed on HL60 cells and αCD14(scFv)-SNAP-Alexa 488 assessed on THP-1 cells

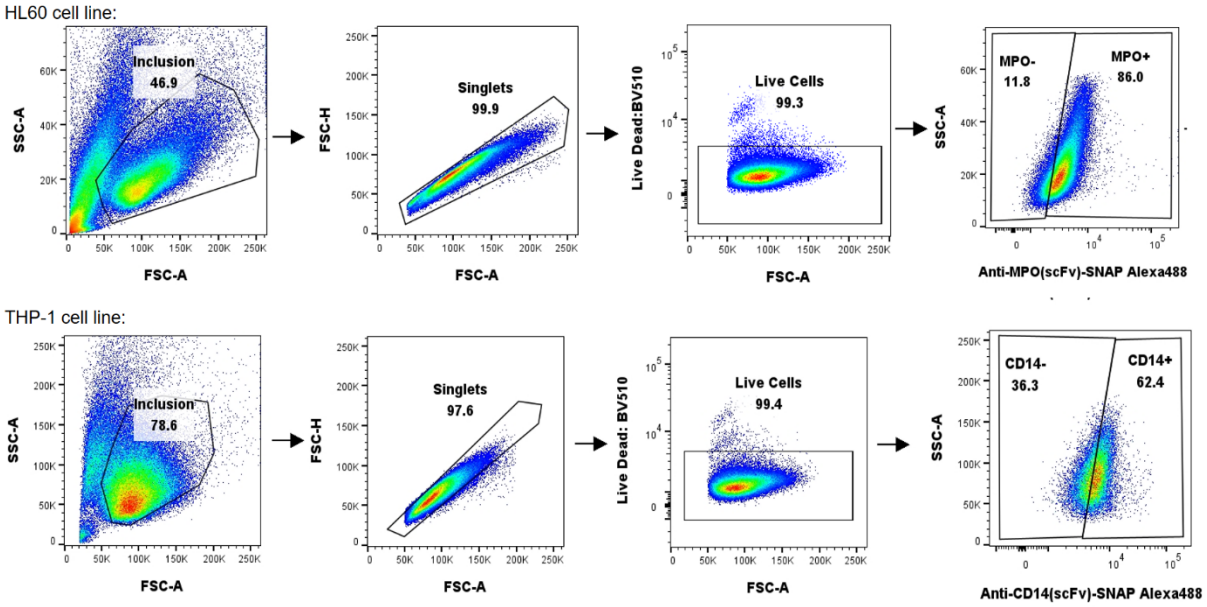


(B) Binding of αCD33(scFv)-SNAP-Alexa 488 on HL60, THP-1 and HEK293T cells

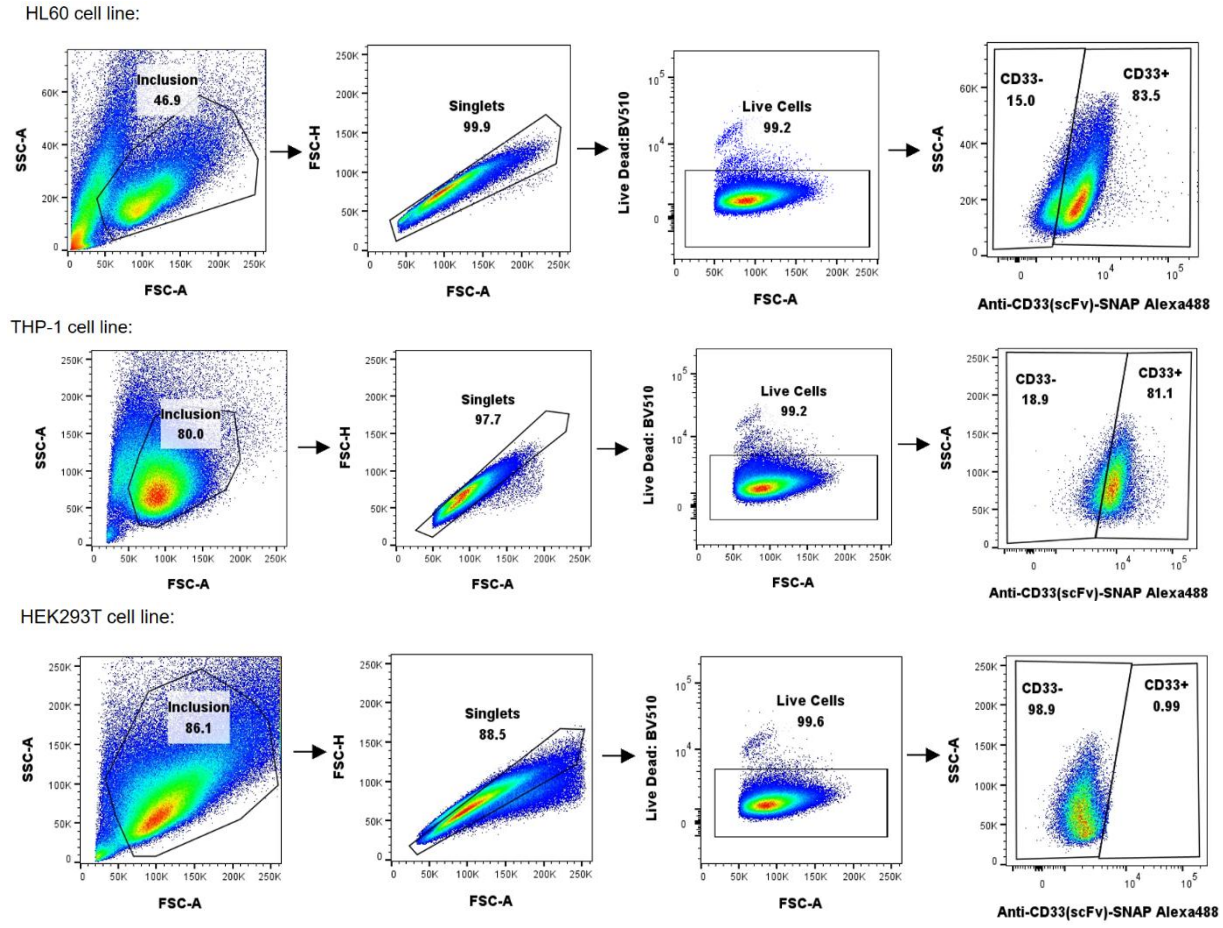

(C) Binding of αCD45(scFv)-SNAP-Alexa 488 on HL60, THP-1 and HEK293T cells

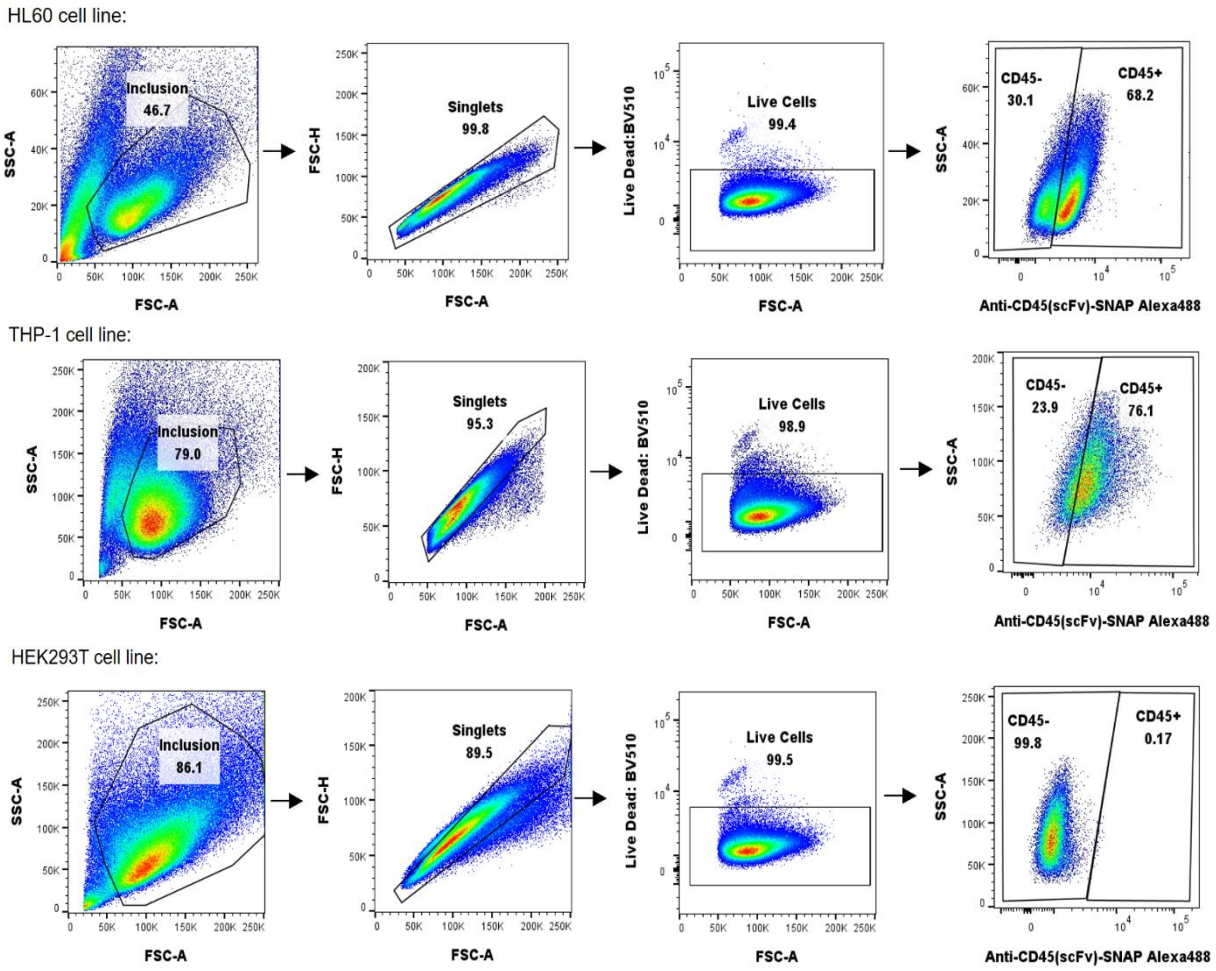


**Figure 19: Flow cytometry analysis of the SNAP FPs' binding on target antigens present on AML cell lines.** (A) 250 µg/mL of αMPO(scFv)-SNAP-Alexa 488 and 250 µg/mL αCD14(scFv)-SNAP-Alexa 488 were used as positive controls which exhibited 86.0% and 62.4% binding on HL60 and THP-1 cells, respectively. (B) At selected optimum staining concentrations of 250 µg/mL and 125 µg/mL, αCD33(scFv)-SNAP-Alexa 488 demonstrated binding to CD33 at 83.5% and 81.1% on HL60 and THP-1 cells (top and middle panel). No binding was observed on non-expressing CD33 HEK293T cells (bottom panel). (C) At selected optimum staining concentrations of 250 µg/mL and 250 µg/mL, αCD45(scFv)-SNAP-Alexa 488 demonstrated binding to CD45 at 68.2% and 76.1% on HL60 and THP-1 cells (top and middle panel). No binding was observed on non-expressing CD45 HEK293T cells (bottom panel). Two biological repeats and four technical repeats were done for this experiment.

### 3.5.2. Analysis of BG-AURIF conjugated SNAP FPs

With confirmed binding of the SNAP FPs to antigens CD33 and CD45 on HL60 and THP-1 cells (section 3.5.1.), the cytotoxic effect of these recombinant proteins was evaluated. ADCs produced through conjugation of BG-modified Auristatin F to αCD33(scFv)-SNAP and αCD45(scFv)-SNAP were assessed on the same cell lines used for binding, excluding THP-1 due to low cell count at the point this assay was performed (section 2.5.3.).

#### 3.5.2.1. Confirming effective BG-AURIF conjugation of the C-terminal SNAP-tag

Before performing the cytotoxicity assays, 10% SDS gels were run at 150 V for 90 minutes to confirm that proper conjugation had occurred and that each SNAP FP was saturated. To achieve this, BG-Alexa 488 was added to the cytotoxin-conjugated SNAP FPs (**Figure A3**). Three samples were analyzed on the gels: SNAP FP conjugated with BG-Alexa 488 only, SNAP FP conjugated with BG-AURIF only, and SNAP FP conjugated with both BG-AURIF and BG-Alexa 488. Due to full saturation and competitive conjugation of the cytotoxic substrate over the fluorophore, it was anticipated that the SNAP FP containing both BG-modified substrates would not flouresce when observed under UV light. In contrast, it was expected that the SNAP FP conjugated with BG-Alexa 488 alone would exhibit a fluorescent band at the correct MW mark, as conjugation could not be prevented by BG-AURIF which was not added. Any fluorescence detected below the anticipated MW mark indicated either proteolytic degradation or excess BG-Alexa 488.

#### 3.5.2.2. Conducting XTT assays to determine the cytotoxic effect of the SNAP FPs

Following confirmation of successful BG-AURIF conjugation to each SNAP FP, forming ADCs, HL60 and HEK293T cells were treated with increasing concentrations of these drugs as described in section 2.5.3.2. Due to the sensitivity of the XTT assay, four biological and three technical repeats were conducted to ensure the most accurate data. Additionally, each experiment included controls of ADC untreated cells that maintained approximately 100% viability and Zeocin treated cells that exhibited nearly 0% viability. After 72 hours of ADC treatment, XTT reagent was added to the cells for colorimetric analysis of the treatment's effects using an iMark™ Absorbance reader spectrophotometer. All absorbance readings from the spectrophotometer were averaged, transformed, and normalized with GraphPad Prism version 5. Following this, sigmoid curves demonstrating ADC dose-dependent cell killing were generated, as displayed in **Figure 20**. Through monitoring cell proliferation, the curve also helped in determining the half-maximal inhibitory concentration ($IC_{50}$), defined as the concentration at which cell responses or processes were inhibited. Treatment of HL60 cells with increasing concentrations (3,906 nM – 1,000 nM) of αCD33(scFv)-SNAP-AURIF and αCD45(scFv)-SNAP-AURIF was found to have $IC_{50}$ values of 4.409 nM and 11.34 nM, respectively. The HEK293T cells used as the negative control showed minor, negligible changes in cell viability.

(A) αCD33(scFv)-SNAP-AURIF cytotoxicity

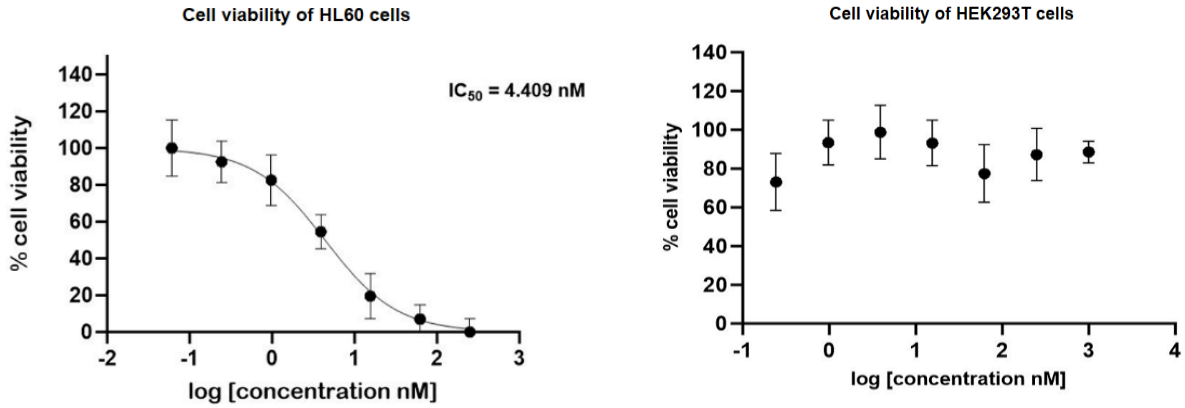


(B) αCD45(scFv)-SNAP-AURIF cytotoxicity

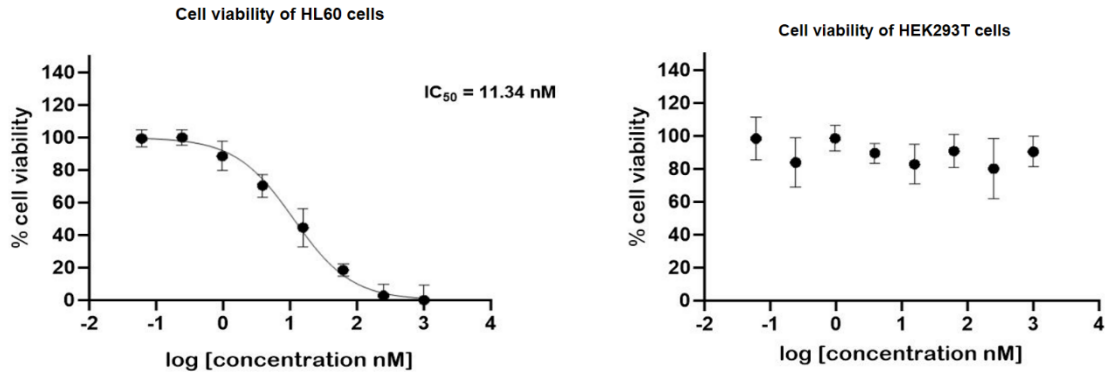


**Figure 20. Sigmoid curves illustrating BG-AURIF conjugated SNAP FPs dose-dependent killing of an AML cell line**. (A) αCD33(scFv)-SNAP-AURIF cytotoxic effect. (B) αCD45(scFv)-SNAP-AURIF cytotoxic effect. HL60 cells which express CD33 and CD45 antigens were treated with increasing concentrations (3,906 nM – 1000 nM) of appropriate ADC. 72 hours post treatment; cell viability was determined using XTT Cell Proliferation Kit II. Controls including untreated cells and antibiotic (Zeocin) treated cells were analysed together with the ADC treated cells. Following spectrophotometer reading of the XTT plates, GraphPad Prism v5. was used to analyse the data and generate sigmoid curves demonstrating dose-dependent killing of the ADCs. In addition, the $IC_{50}$ values of each ADC were computed on this software. XTT assays comprised quadruple biological replicates and triple technical replicates. Any substantial variations between replicates were represented as error bars.

# Chapter 4: Discussion

### 4.1. A precision medicine-based approach to address the unmet clinical need for AML

As the most aggressive of the four known types of leukemia, AML has been recognized as a significant global health concern that urgently requires effective preventive and treatment interventions. With an overall five-year survival rate of nearly 30% and a poor prognosis [57][193], there is an undeniable push to improve the clinical outcomes of this blood cancer and enhance the quality of life for patients diagnosed with it. Most AML cases occur in individuals over the age of 60, a stage at which studies have revealed a drastic drop in the survival rate to a dismal 5% to 15%. This crisis emphasizes the critical efforts that must be made to provide these patients with substantial attention and care.

Despite the evident impact of age on the prognosis and survival of AML, the minimal research and funding dedicated to understanding and managing this life-threatening illness in developing countries, such as those in Africa, has been found to significantly contribute to the rise in cases and fatalities [29]. Studies conducted over the past decade have consistently demonstrated how prevention, early diagnosis, and timely treatment have disproportionately benefited AML patients in developed countries compared to those in developing countries, which often lack the resources to achieve optimal outcomes for their patients [194][195][196].To begin with, the lack of a regularly updated cancer registry creates the impression that more individuals may actually be affected by AML than is believed or documented in the limited publications available. This has inevitably made it extremely challenging to track the incidence trends of AML on the African continent, further complicating the process of obtaining an accurate diagnosis and ultimately administering the most appropriate treatment to affected patients [21][25]. A suitable medical system that satisfies patients' health needs similarly to that of high-income countries has yet to be established in Africa. Delays or failures in addressing socioeconomic barriers promptly and effectively will not only impact patients in resource-constrained countries but will also validate the contribution of AML to the alarming projections of increased cases and deaths by 2040 [26].

Currently, the treatment of AML relies heavily on a non-specific chemotherapeutic approach often followed by the costly procedure of hematopoietic stem cell transplantation [68][71]. The effects of chemotherapy have thus far shown reduced signs and symptoms of AML, referred to as complete remission (CR). Recent independent studies conducted by Shireen (2022) and Mehboob (2024) assessed the CR rates following the standard '7+3' induction regimen, estimating CR rates of 54% and 61.1%, respectively [197][198]. Despite these encouraging results, nearly 50% of patients who achieve CR after receiving the '7+3' regimen experience a

relapse within three years post-treatment [199]. These findings clearly demonstrate the need to explore new treatment strategies that sustain high CR rates and minimize relapse rates.

Researchers have begun investigating ways to improve the previously mentioned parameters, namely CR, OS, and event-free survival, in order to maximize the benefits of therapy. This progress has been made possible through a deeper understanding of precision medicine and bioengineering techniques, which have subsequently facilitated the development of more tailored and targeted therapies. Vismodegib, Enasidenib, Venetoclax, and Rydapt are a few targeted therapies commonly used with or after chemotherapy to achieve the best treatment outcomes [200]. A pivotal trial indicated that Rydapt combined with ara-C and DNR, when administered simultaneously, resulted in an impressive median overall survival of 74.7 months. This was significantly higher than the median overall survival of 25.6 months observed in the placebo control group [201]. In another study examining the effectiveness of Enasidenib in patients with refractory AML, the median OS for this targeted drug was 9.3 months, while patients who achieved complete remission had a median OS of 19.7 months [202]. Similarly, GO, the leading ADC for AML treatment, has shown in numerous trials that it not only enhances OS and CR but also significantly improves event-free survival when added to induction therapy for both children and adults [203][204][205]. These treatments have undoubtedly transformed the landscape of AML therapy and significantly improved patient survival and quality of life. However, the availability, affordability, and accessibility of these targeted therapy options remain major challenges in resource-limited areas, such as Africa.

The evidence suggests that optimal treatment for AML requires a novel strategy based on precision and targeted medicine. However, as studies have consistently shown, such an approach has been largely absent in Africa for a considerable amount of time. The lack of research, resources, and funding in many countries on this continent are major contributors to this healthcare crisis, which demands urgent attention and action. Consequently, this dissertation investigates how to treat African patients with AML through the local generation of immunotherapies, specifically ADCs. Given Africa's socioeconomic challenges and the high cost of available targeted treatments, this project highlights the importance of bridging the gap between these factors and, ultimately, advocates for addressing global healthcare inequities. The recombinant ADCs developed in this project are more compact and comparatively less expensive than standard ADCs. Furthermore, the recombinant ADCs generated in this study were expected to function similarly to traditional ADCs, if not better due to their reduced size, in terms of strong binding activity and cytotoxic effects.

Several studies have investigated the use of ADCs containing full-length mAbs conjugated to effector molecules that target the biomarkers CD33 and CD45, which both play a role in the growth and survival of AML cells. Other than GO, SGN-CD33A was another ADC that was created to target CD33 for AML treatment. The humanized antibody that made up this ADC was coupled to a synthetic pyrrolobenzodiazepine dimer that cross-links DNA [206]. One noteworthy aspect of this treatment was the antibody's designed cysteine residues, which enabled the conjugation of about two drugs to the antibody, thereby increasing potency, through a linker that can be broken down by proteases. Preclinical research using SGN-CD33A against multidrug resistant AML cell lines and xenotransplanted mice showed higher killing activity via DNA damage resulting in apoptosis when compared with GO. A comparably effective CD33-targeting ADC, IMGN779, comprising a humanized antibody cross-linking a DNA-alkylating effector was later produced [207]. When employed against AML patient-derived cell lines, it was found that the ADC induced cell-cycle arrest leading to cell death. Furthermore, in AML xenograft and disseminated disease models, IMGN779 achieved a reduction in the size of tumours and longer survival times. Regarding CD45 ADCs, studies have mostly demonstrated the use of a full-length IgG antibody bound to drug payloads such as DNA-damaging, tubulin-targeting and RNA polymerase-inhibiting molecules for conditioning prior to gene therapy and HSCT [208][209]. CD45 ADC conditioning has exhibited a decrease in deaths due to specific killing, resulting in reduced off-target toxicity. Additionally, this conditioning regimen has been well-tolerated by patients hence allowing successful engraftment and reduced side effects of HSCT. Ultimately, these studies show that ADCs are a prime example of immunotherapy's potential to improve specificity, reduce toxicity and side effects, and increase patients' chances of survival.

A paradigm shift from conventional chemotherapy to specific therapies has emerged through a better understanding of cancer development and management. Several ADCs continue to pass trials for eventual approval despite the years-long challenges that scientists have faced in advancing these drugs [87][155]. The therapeutic efficiency demonstrated by ADCs continues to support clinical applications not only in AML but also for the treatment of various other cancers [141][142]. However, until now, there has been almost no research on antibody fragment-based ADCs targeting these highly overexpressed antigens in AML, which warrants the work presented in this dissertation.

### 4.2. Development of the AML immunotherapeutic agents

Due to its heterogeneous nature, AML requires a holistic and innovative approach for treatment [24]. This complex hematological malignancy, much like other cancers, thrives on evading and

suppressing the immune system. In addition to continuous proliferation and differentiation avoidance prompted by oncogenes, leukemic cells alter the phenotype and function of cells that play a role in immunity, thus allowing them to escape immune surveillance [210]. Immunotherapy has thus far served as a powerful and effective therapeutic tool that works to block immune bypassing by AML cells. To elicit an anti-AML immunity, scientists have investigated passive immunotherapy which mostly uses immune system elements or cellular proteins that are not naturally created by the body to aid in the destruction of cancer cells [82]. In a similar way, this work explored a passive immunotherapy approach through the design, production, and evaluation of recombinant antibody FPs for AML.

Improving the precision of treatments to reduce harmful side effects from toxicity has always been a top priority in cancer therapy. Protein engineering, coupled with a deeper understanding of cancer biology, has allowed for therapeutic innovation to be achieved, as various properties of proteins can be improved to bring about desired effects. One of the best examples of how this powerful biotechnological approach has made a remarkable contribution is the ability to modify antibodies and conjugate them with diverse molecules, thus providing the antibody with an additional function apart from specific targeting and binding of antigens. Primary or unconjugated antibodies have proven to be functional in hindering cellular pathways that promote the development and survival of cancer cells and thus, consequently induce cell death. Numerous tactics, such as immunostimulation, apoptosis induction, angiogenesis or growth factor receptor inhibition, and the activation of complement-dependent cytotoxicity or antibody-dependent cell-mediated cytotoxicity, have been used by these antibodies to accomplish this effect. The use of unconjugated antibodies continues to this day due to their successful targeting. However, their potency in this form remains contentious [211]. Moreover, unconjugated antibodies are frequently employed in conjunction with other medicines to achieve high therapeutic efficacy, which ultimately affects treatment costs.

The potential for conjugation to produce hybrid drugs has reignited interest in antibody-based treatments. ADCs are a class of hybrid drugs that have thus far shown promising activity for the enhancement of immunotherapy without the stringent application of secondary antibodies or additional treatments [212]. ADC pharmacokinetics and pharmacodynamics are thought to be changed by conjugation, which is believed to boost the activity of both the effector molecule and the antibody. Furthermore, conjugated antibodies have better drug distribution and effects and lowered toxicity profiles relative to unconjugated antibodies [213]. Over five conjugation reactions involving the chemical joining of two components are used in biopharmaceuticals. The first of these components is a molecule containing reactive ends to specific functional

groups present on the other component, which is normally an antibody. Common conjugation reactions include isothiocyanates, NHS esters and anhydrides which occur by the interaction of reactive groups on effector molecules with primary amines on antibodies. Amine conjugates are typically used for protein detection, sorting and microscopy with fluorophores [214]. Similarly, carbodiimide coupling is a reaction used to produce carboxylate conjugates which are often used for protein labelling or crosslinking to carboxylic acids [215]. Another form includes thiol conjugation, which relies on the reaction of free thiol groups on an antibody and malemide compounds to achieve protein detection or labelling [216]. Click chemistry is another selective and highly yielding conventional conjugation reaction used in drug discovery, radiochemistry, and labeling, involving copper to cycloaddition alkyne or alkene functional groups [217].

Conjugation has made it possible for immunoconjugates with decreased immunogenicity and recognition to disseminate steadily. Furthermore, conjugation has improved drug penetration and prolonged the half-life of immunoconjugates in comparison to unconjugated antibodies through endocytosis [213][218]. This technique has reduced systemic toxicities by delivering conjugated drugs directly to cancer cells without harming healthy cells, hence making this approach impressive and worthy of continued usage with the possibility of new drug targeting options [218]. The inventive SNAP-tag is a self-labelling protein that, through a specific, covalent and irreversible bond to BG-functionalized ligands, enables conjugation [146]. Numerous diagnostic and therapeutic uses are produced by the fusion of this human $O^6$-AGT derived single-turnover enzyme with recombinant antibodies like scFvs and further coupling to BG-substrates. For example, the 1:1 stoichiometric conjugation of either cytotoxic compounds to selectively kill cancer cells or fluorophores for in vitro, in vivo, and ex vivo studies of target antigens [148][219]. Additionally, conjugation of suitable substrates with this protein tag can be completed in approximately half an hour without the requirement for catalysts or prior activation [143][220]. Because of these and other benefits, protein tags are still regarded as one of the most cost-effective options for targeted therapy that may be used repeatedly without incurring excessive costs.

In the last decade, a number of scFv-SNAP FPs have been produced for diseases such as breast, brain and blood cancer [151][156][221][222]. Results shown in proof of concept and preclinical studies of producing and utilizing scFv-SNAP FPs have thus far shown great promise for future immunotherapeutic application. In order to accomplish similar goals, our work generated recombinant antibodies that target overexpressed CD33 and CD45 in AML.

For versatility of the produced proteins, SNAP-tag was attached to these recombinant antibodies for downstream functionality studies.

### 4.2.1. Production of mammalian SNAP-tag FPs

#### 4.2.1.1. The *in silico* design of αCD33(scFv)-SNAP and αCD45(scFv)-SNAP

The *in silico* design of mammalian expression vectors with the necessary antibody fragment sequences was essential for achieving the study's ultimate goal: producing recombinant SNAP-tag FPs for treating AML. The CD33 and CD45 targeting scFv sequences were sought and carefully analyzed using established nucleotide and protein analysis tools. To ensure efficient transcription and subsequent translation of optimally functioning recombinant FPs in high quantities, these sequences were refined by incorporating the most suitable codons for mammalian expression. The optimized scFv sequences were then successfully cloned into the backbone of the MB&I-provided mammalian (pCB) expression plasmid, which contained the multipurpose SNAP-tag (see **Figure 9).** Using SNAPGene, the sizes of the designed plasmids were estimated at 8026 bp for pCB-aCD33(scFv)-SNAP and 8047 bp for pCB-aCD45(scFv)-SNAP. Furthermore, the theoretical molecular weights of the recombinant SNAP FPs resulting from these plasmids were both estimated to be around 52 kDa, according to Expasy. Obtaining these estimates facilitated accurate identification and verification of the recombinant FPs among degrading and contaminating proteins during downstream protein characterization.

With the aim of wanting to produce innovative treatments for the management of AML, the use of *in silico* techniques in this study was the first step in achieving this. This approach was initially used by Miramontes P. in the late 1980s to describe biological experiments carried out entirely on a computer [224]. This elaborate computational process has since been used to accelerate the development of desired antibodies in a cost-effective and time-saving manner as opposed to conventional methods, which usually require the use of expensive and high-maintenance equipment [225][226].By enabling the ability to design antibody fragments with specific desired formats yielding predictive capabilities [227][228][229], and by exploiting the ability to add or remove particular residues when designing the complementarity determining regions of the scFv fragments—particularly CDR3, which exhibits the highest diversity and plays the most significant role in antigen binding [230]—high quality of various properties such as binding strength, specificity, and affinity can be achieved.

The goal of this work was to turn from producing complete monoclonal antibodies to producing small antibody fragments, such scFvs, which are less costly and quicker to generate than standard monoclonal antibodies due to their smaller size [136][139]. In line with the purpose of this study, being able to use *in silico* techniques as part of producing recombinant ADCs for

patients in resource-limited settings serves a significant beneficial impact as the goal of producing highly efficacious treatments at a lower cost would be achieved. In addition, with more research being conducted on the progression of AML, there would be possibilities to design more plasmids which would produce similar scFv proteins for recombinant ADCs targeting other highly expressed antigens.

#### 4.2.1.2. Efficacy of the molecular cloning process

Following *in silico* design of the plasmids, wet bench experiments were conducted beginning with molecular cloning. The GenScript produced pUC57-αCD45(scFv), MB&I provided pCB-SNAP plasmid backbone and previously cloned pCB-αCD33(scFv)-SNAP were prepared suitably to allow visualization and validation of the plasmid sizes using appropriate restriction endonucleases and agarose gels. As shown in **Figure 10** and **Figure 12**, the DNA band sizes seen on the simulated agarose gels on the left matched those obtained on the actual gels that were run on the right. This demonstrated that the restriction enzymes used and duration of digestion were ideal and resulted in effective separation of DNA fragments. However, there were challenges faced that resulted in minor differences observed between the simulations and gels. Firstly, it was seen that some DNA bands appeared faintly with some smearing at the bottom of the gels. These observations may be attributed to low DNA concentration, inadequate electrophoresis conditions or problems with gel or buffer preparation [231]. Moreover, factors like partial digestion, vector re-ligation, and DNA supercoiling either produced additional DNA bands or bands with a higher MW than anticipated [232]. Partial digestion occurs when DNA fragments with restriction endonuclease sites are not cleaved fully [233], while vector re-ligation occurs when the vector backbone's sticky ends join incorrectly. DNA supercoiling is the process of twisting DNA into a compact structure [232]. Such issues seem not to be uncommon in the molecular cloning process of other studies which also focused on producing similar recombinant FPs for the treatment of other cancers [163][221][223][234][235]. To overcome the challenges and optimize results, it was found that increasing the DNA concentration, lengthening the running time, and lowering the voltage of electrophoresis might improve band resolution, band thickness, and encourage uniform migration [236][237]. **Figure 10** shows that even though these factors might have impacted molecular cloning, it was still possible to effectively excise and acquire the necessary DNA bands for ligation.

Using competent DH5α *E. coli* cells, ligated DNA was effectively transformed for small plasmid propagation. In **Figure 11** the colonies carried correctly ligated plasmids, as demonstrated by the several colonies found on each experimental plate (1:1 and 1:5 ratios) while none grew on

the vector backbone control plate. In spite of the positive outcomes, the transformation efficiencies measured fell short of the typical average of > 1 x $10^6$ CFU/µg for cloning with DH5α *E. coli* cells [238]. Several factors may have been the cause of the differences in transformation efficiencies, for instance: DNA concentration, plasmid purity, incubation time and temperature [239]. Research has shown that another well-established technique which can be used to achieve amplified transformation is by electroporation, which employs high-voltage electric field pulses to induce DNA uptake into competent cells [238]. This technique allows for transformation efficiency of more than 1 x $10^{10}$ CFU/µg [240][241]. Other studies have shown that using alternative bacterial cells apart from *DH5α E. coli* cells for the uptake of recombinant plasmid DNA could help to achieve transformation efficiencies >$10^9$ [242][243][244][245]. Despite having obtained lower transformation efficiencies than the standard range, it was nevertheless possible to finalize cloning by confirming correct ligation from the few selected colonies using restriction mapping and Sanger sequencing (**Figure 12** and **Figure A1**). From the restriction mapping agarose gels, the ligated clones which had inserts encoding the relevant scFvs, displayed different fragment patterns from the backbone vector (**Figure 12**). The differential cutting patterns of the backbone vector and ligated clones using the relevant endonucleases confirmed that the ligation process had been conducted successfully. Furthermore, the plasmids' validity was proven using Sanger sequencing which enabled the alignment of the plasmids' sequences with primers designed by Inqaba. Alignment of these sequences showed close to 100% homology and provided confirmation for progression to transfection for eventual protein production.

#### 4.2.1.3. Recombinant SNAP FPs expression

The production of recombinant SNAP FPs was achieved through the efficient transfection of the ligated plasmids into HEK293T cells. According to existing research, the bacterial expression system for protein production is usually employed when producing recombinant proteins [246][247]. This is due to the fact that bacteria can be easily manipulated, are capable of producing large amounts of protein in shorter periods of time, and are less expensive than mammalian expression systems [246]. Despite the advantages, this study would not benefit most from the adoption of a bacterial expression system. HEK293T cells have remained the most dominant mammalian expression systems for the heterologous production of scFv-SNAP-tagged fusion proteins. In addition to this, the criteria for cell line selection were based on their ability to perform authentic assembly and folding of recombinant proteins, and their ability to secrete recombinant proteins into the medium. Instead, the use of a mammalian expression vector was opted for due to the goal of this study was to produce mammalian immunotherapeutic proteins intended for human use [248]. Additionally, the mammalian

expression system was used to accommodate any complex post-translational modifications which are often required by mammalian proteins, which cannot be fully achieved or replicated using bacterial expression systems [249]. Consequently, due to the high transfection efficiency and rapid growth rate of the mammalian HEK293T cell line, it was employed in this study [250]. In this investigation, transfection efficiencies exceeding 50% were recorded via flow cytometry (**Figure A2**); these values were moderately lower than the approximately 70% reported by other MB&I members who used the same reagents and methods to transfect recombinant DNA plasmids into HEK293T cells [163][223]. Several variables, including sample preparation, cell viability, and DNA concentration and purity, may explain the variations in this quantitative analysis [251][252].

Although various transfection methods exist [253], chemical-based transfection using XtremeGENE HP Transfection Reagent was chosen for this instance. For comparison, polyethylenimine (PEI) was also used for transfection to assess any potential improvements in transfection efficiencies; it was found that this reagent provided comparable transfection efficiencies and could be a suitable alternative (data not shown). Another method for transfection was electroporation. While this technique is relatively straightforward and yields efficiencies of over 90% [254], it requires specialized equipment and poses a significant risk of toxicity and cell death due to excessive heat [255]. Given the transfection efficiencies achieved, a longer duration of antibiotic selection using Zeocin was anticipated. After antibiotic selection, the transfected cells exhibited elevated eGFP signals and increased cell confluency, making it feasible to collect the protein-containing supernatant (**Figure 13**).

#### 4.2.1.4. Recombinant SNAP FPs purification

After collecting the supernatant, IMAC protein purification of the recombinant SNAP FPs was conducted. By attaching to the $Ni^{2+}$-charged purification column, the N-terminal polyhistidine tag on the recombinant SNAP FPs effectively facilitated immobilization, enabling selective purification of the proteins. A 6 x His-tag had been previously used in the design of the MB&I plasmids. The primary challenge encountered during the purification of this plasmid was the binding of other unwanted proteins with similarly sized polyhistidine tags to the column. Consequently, the plasmids were modified to address this issue by replacing the 6 x His-tag with a 10 x His-tag. Compared to the previously used tag and possible contaminating proteins, the 10 x His-tag demonstrated a stronger affinity for the $Ni^{2+}$ matrix due to the additional N-terminal histidine amino acids [256][257]. Moreover, research has shown that the length of the modified His-tag does not negatively affect the structure, function, or folding of the generated proteins [258]. To successfully extract the desired proteins from the charged column, imidazole

was employed (**Figure 14**); it was first applied at a low concentration during the wash step to prevent nonspecific binding and the removal of contaminating proteins. The recombinant SNAP FPs were then effectively eluted from the column by applying a higher concentration of imidazole, which competitively bound to the column, enhancing the elution efficiency [259].

#### 4.2.1.5. Recombinant SNAP FPs characterisation

Protein characterisation and effective recovery of full-length recombinant SNAP FPs upon elution was verified using SDS-PAGE and western blot. The SDS gels in **Figure 15** showed the presence of each full-length recombinant protein as aliquots reflected by protein bands at the anticipated MW marker (around 52 kDa). Following pooling of the aliquots using Amicon Ultra Centrifugal filters, the concentrated recombinant SNAP FPs remained observable at the correct MW marker (**Figure 17**). N-terminal activity and the presence of full-length recombinant proteins were further confirmed by employing the sensitive western blot approach, which was seen to correlate with and yield results comparable to those of the SDS gels (**Figure 17**). Despite having detected the presence of each protein accordingly, multiple challenges were faced during the process. The most prominent issue faced during protein characterisation was the presence of additional bands on the SDS gels, nearby those of the protein of interest, which were visible above the 72 kDa MW mark and between the 34 and 43 kDa MW mark (**Figures 15, 16** and **17**). Several reasons may account for these observations; for instance, proteolysis of the recombinant proteins during or after purification may have resulted in the artefact bands displayed [260]. Since these bands were also seen on the WB PVDF membrane, it was assumed that they represented partially degraded or truncated scFv segments that contained the N-terminal histidine amino acids forming the polyhistidine tag, which the anti-His antibody could also bind to [261][262]. Alternatively, the recombinant FPs fortuitously bound to other endogenous His-tag containing proteins, perhaps present in the CCSN. Thus, these proteins were co-eluted as a complex from the IMAC column during purification [263]. The artefact bands observed on the SDS gels and Western blot membranes could also potentially be explained by incomplete protein translation, which produces truncated protein products in addition to full-length recombinant SNAP FPs. It is anticipated that when affinity chromatography is used, both the full-length FPs and the truncated products bind to the resin and elute simultaneously once imidazole is added, which explains the numerous bands seen (**Figures 15, 16** and **17**). Similar outcomes have been shown in other independent investigations and by other MB&I colleagues [163][221][223][234].

Various attempts to improve protein characterization have been explored. This study utilized IMAC purification, which demonstrated moderate effectiveness in fully isolating recombinant

FPs from impurities (**Figures 15, 16,** and **17**). The results showed that achieving 90% or more protein purity [264][265], considered optimal for protein studies, could not be attained with this purification technique alone. Research indicates that His-tagged protein purity of up to 96% can be achieved by employing multiple purification methods, such as size exclusion chromatography following IMAC and subsequently ion exchange chromatography [266]. Despite its high effectiveness, this approach is relatively expensive and may not always be feasible to implement [267]. One of the simpler methods that has shown an enhancement in the quality of FPs after purification involves using multiple filters for enrichment. An MB&I colleague reported a protein purity of nearly 60% after initially removing potentially contaminating proteins above the 72 kDa mark with a large MW Amicon Ultra Centrifugal filter. By using a filter with a molecular weight cut-off similar to the size of recombinant FPs, the proteins were further enriched for downstream analysis [163]. Although the protein purity exceeded what was found in this study by 5%, it still fell short of the desired purification level. Additionally, this method did not always prevent degradation products below the 43 kDa level. To avoid the formation of bands below the MW of 43 kDa, which are usually associated with protein degradation, it is ideal to use a protease inhibitor cocktail (PIC). PICs are compounds that limit the activity of proteases while causing minimal damage, aiming to preserve protein stability [268]. Proteins supplemented with PICs in tissue culture media remain stable for about 8 months or 4 years when stored at 4°C or -20°C, respectively [269]. When possible, implementing both strategies described to prevent protein contamination and degradation is ideal. In a study like this, obtaining high-quality purified proteins is crucial, as they form the foundation for reliable outcomes of essential aspects, such as the functionality of each recombinant SNAP FP determined by in vitro studies. Furthermore, these outcomes ultimately impact the quality of the developed immunotherapeutics.

Subsequent to assessing the presence and quality of the concentrated proteins, they were subjected to quantitative analysis. The total quantity and percentage purity of αCD33(scFv)-SNAP and αCD45(scFv)-SNAP against BSA standards by densitometry were recorded as 6.8 mg/L (purity of 49.4%) and 8.7 mg/L (purity of 51.2%), respectively (**Figure 16**). Typically, the total amount of proteins is often computed between 10 - 30 mg/L [270][271]. The overall yield of proteins calculated in this study through densitometry was relatively lower than this range. The yield of proteins can vary significantly, primarily falling within or possibly exceeding the normal range, depending on a number of factors [272]. It was thought that the differences from the expected range were mainly caused by variations in the conditions of protein expression. Optimizing cell culture factors, including temperature, pH, aeration, and nutrient availability in media, can help to promote cell viability, appropriate protein folding, and secretion, all of which

can ultimately improve protein expression efficiency and overall yield [273]. Furthermore, protein yields may be greatly impacted by the choice of the protein expression system used. In addition to the widely used bacterial and mammalian systems, other alternatives for increasing protein quantity include insect, yeast, or cell-free systems [274].

Together, these findings essentially highlight the necessity of streamlining procedures from cell culture to protein characterization. However, it is crucial to consider the cost and accessibility of resources when doing so, particularly in relation to protein purification. In order to promote scientific advancement and facilitate downstream applications, it is essential to optimize protein yields in expression experiments. Even though there was potential for improvement, the results were satisfactory to perform in vitro research for this proof-of-concept study.

Once the FPs were characterized, the presence and intact state of the C-terminal SNAP-tag were assessed. Given the limited range of recommended fluorophore quantities to ensure substrate saturation [143], previous MB&I members conjugated various molar concentration ratios of FP to BG-Alexa 488 to determine the most effective conjugation reaction [221][223][234]. These studies showed that the optimal conjugation ratio was 1:1 molar concentration. By using this same ratio, the fluorescent bands observed at ~52 kDa confirmed that the SNAP-tag of each recombinant FP was intact and functioning optimally (**Figure 18**). Additionally, excess BG-Alexa 488 was detected at the bottom of each SDS gel examined under UV light. This observation further indicated that the SNAP-tag was fully saturated and that the 1:1 ratio was indeed sufficient and cost-effective for effective SNAP-tag conjugation. Although the results of the conjugation experiment were promising, there were minor issues that could have been avoided. Faintly fluorescing bands were detected both above and below each recombinant FP's 52 kDa band when viewed under UV light (**Figure 18).** The direct effects of these truncated proteins on binding and cytotoxic action remain unknown. However, through competitive binding, it was hypothesized that an accumulation of these SNAP-tag-containing segments could hinder the binding and cytotoxic activity of the intended recombinant FPs. Similar to protein characterization, a suitable strategy to prevent the formation of these artefact bands would be to optimize protein expression and purification protocols [260][263]. Nonetheless, in vitro research could be pursued, as it was adequately demonstrated that both FPs' C-terminal SNAP-tags were present and functioning as intended.

### 4.2.2. Functionality of mammalian SNAP-tag FPs

#### 4.2.2.1. Binding by flow cytometry

Once it had been confirmed that the recombinant FPs' SNAP-tags were functioning appropriately, the binding activity of both FPs was assessed against AML cell lines using flow cytometry. In preparation, the FPs were first conjugated to BG-Alexa 488. This resulted in fluorophore-conjugated FPs that, when exposed to the flow cytometer laser, allowed for the identification of directly targeted antigens of interest [275]. A key step in this protocol was to perform antibody titration, which was vital in identifying the FP concentrations that produced the best positive signal from the background, with saturation of all binding sites and minimal FP surplus [276][277][278]. A number of issues can arise when titrated antibodies are not used for flow cytometry analysis. These issues include inaccuracies in binding, the tendency for high fluorescence spillover if excess concentrated antibodies are used, and measurement variability that leads to poor data resolution [276][279]. The utilization of multiple fluorochromes in this analysis, specifically BG-Alexa 488 and the LIVE/DEAD fixable stain applied to the AML cells, only enhanced the ability to clearly distinguish between antigen-positive and antigen-negative cell populations by measuring multiple cell markers simultaneously [280][281]. MFI, which essentially correlates the measure of shift in fluorescence intensity with measure of relative antigen abundance, was another population distinguisher that was used [282]. Although it is anticipated that antigen negative cells would not be bound by the recombinant FP, these cells still have a MFI (**Figure A4**). This is due to autofluorescence, which refers to the natural fluorescence emitted by cells due to the accumulation of endogenous cellular compounds with fluorophore-like properties [283].

Following data acquisition, analysis using FlowJo was conducted. **Figure 19B** demonstrated that the targeted CD33 antigen was present in approximately 84% of HL60 cells and 81% of THP-1 cells. From these findings, it was deduced that the CD33-targeting recombinant SNAP FP had a high affinity and an effective binding ability to its target. A similar result was reported by Bvudzijena (2023), who used αCD33(scFv)-SNAP-Alexa488 as a positive control in flow cytometry studies and demonstrated 78% and 89% binding of this recombinant antibody on HL60 cells and THP-1 cells, respectively [163]. In both these studies, HEK293T cell line was used as a CD33-negative control, which demonstrated negligible binding relative to binding on antigen positive cell lines which usually express approximately 10 000 sites per cell line [284]. The MFI values were then referred to and it was found that the MFI for the three cell lines varied greatly, with HL60 and THP-1 cells having higher values than HEK293T cells (**Figure A4**). The differences observed indicated that HL60 and THP-1 cells expressed more CD33 antigens on their surface and thus further affirmed the effective binding and specificity of αCD33(scFv)-SNAP-Alexa488. Comparable binding results demonstrated 87% to 99% fluorescence of the positive M2 HL60 cells in a study by Emberson (2005), where two variants

of the CD33 targeting scFv antibody were produced for therapeutic use, further confirming the binding affinity and specificity of this recombinant antibody to CD33-positive cells [285]. Based on these flow cytometry outcomes, the produced αCD33(scFv)-SNAP-Alexa488 has shown the ability to reach similar outstanding therapeutic outcomes as GO, the primary targeted treatment for AML, which has shown binding rates above 80% in various studies [98][286].

Thereafter, the binding of αCD45(scFv)-SNAP was assessed. From **Figure 19C**, it was seen that the targeted CD45 antigen was present in 68% of HL60 cells and 76% THP-1 cells. Relative to the minimal binding of 0.17% observed on HEK293T cells, it was deduced that this recombinant FP bound to its target antigen with high affinity and specificity. The notable difference between the MFI values of the CD45-positive cell lines and the HEK293T negative control further supported this conclusion (**Figure A4**). Comparisons to previous research on the binding of αCD45(scFv)-SNAP to CD45-positive cells are relatively limited as there has not been much research based exclusively on this recombinant FP. Despite this, the high copy number of approximately 100–300,000 antigenic sites per leukemic cell [287] was expected to result in binding to the CD45-positive HL60 and THP-1 cells. However, one particular study by Green (2009) investigating the therapeutic effect of pre-targeting CD45 in non-human primates demonstrated that the αCD45 FP retained the full antigen-binding capacity of intact αCD45 full monoclonal antibody [288].

These flow cytometry results put together, and studies used for comparison further encourage the production and use of recombinant FPs for therapeutics as the structural distinctions between them and full monoclonal Abs do not substantially affect binding affinity and specificity.

#### 4.2.2.2. Cytotoxicity assays

After confirming the binding of αCD33(scFv)-SNAP and αCD45(scFv)-SNAP to AML cell lines through flow cytometry, we assessed the cytotoxic effect of each recombinant SNAP FP. To ensure the consistency of *in vitro* studies and obtain reliable results, we used the same cell lines that were assessed for binding in this cytotoxicity experiment. However, due to the low cell count calculated for THP-1 cells at the time of this experiment, we excluded this cell line.

Although generating AML-specific ADCs was the study's final objective and ultimate goal, it was crucial to initially demonstrate that each of these conjugates' separate components were not responsible for the lethal effect on the specific target cells. Thus, when the cells were first treated with unconjugated BG-AURIF, it was seen that the toxin resulted in non-specific killing of the cells in a dose-dependent manner (**Figure A5**). The cytotoxic effects of unconjugated

BG-AURIF against particular breast cancer cell lines were seen in a study assessing the effective removal of solid tumor cells by breast cancer specific SNAP FPs conjugated to BG-AURIF [156]. Similar results were shown through micrographs by Karaan (2023), who used the same protocol as outlined in this thesis to produce ADCs for the treatment of triple-negative breast cancer [234]. The images helped visualize the physical effects that unconjugated BG-AURIF had on target and surrounding cells, showing that the administration of this toxin alone caused cell shrinkage and blebbing, which ultimately resulted in apoptosis. This led to the idea that unspecific killing could be avoided by attaching an antibody moiety to the toxin, which would serve as a guiding head for tailored therapy. However, prior to this attachment, the effects of unconjugated αCD33(scFv)-SNAP and αCD45(scFv)-SNAP administration alone were also examined. Contrary to unconjugated toxin treatment, there was no discernible cellular damage following treatment with the unconjugated recombinant SNAP FPs (**Figure A5**). Similar investigations that also aimed to create recombinant SNAP FPs found no apparent fatal consequences when administering the different cancer cell lines that were being studied [221][223][234][289].Following this evaluation, each recombinant SNAP FP was then conjugated to a two-fold molar excess of BG-AURIF to prepare for XTT assays. To ensure saturation of each FP, a second conjugation with BG-Alexa 488 was performed and the analysed on 10% SDS gel (**Figure A3**).

The cytotoxic potential of the recombinant SNAP FPs linked to the microtubule inhibitor BG-AURIF was ascertained by a colorimetric cell assay using the Cell Proliferation Kit. Following treatment of the antigen-positive HL60 cells with the recombinant ADCs, $IC_{50}$ values of 4.41 nM and 11.34 nM were computed for αCD33(scFv)-SNAP-AURIF and αCD45(scFv)-SNAP-AURIF, respectively. Both sigmoidal curves displayed in **Figure 20** confirmed that each recombinant ADC effected a dose-dependent reduction in the cell viability of HL60 cells. When compared to the CD33- and CD45-negative HEK293T cells, it was seen that the recombinant ADCs had little to no toxic effect on the viability of the cells. This difference essentially showed that the recombinant antibody portions of the ADCs were highly effective at binding to their targets, as evidenced by the negative control cell line's lack of comparable dose-dependent responses. Additionally, conjugating each scFv-SNAP component to BG-AURIF only highlights the drugs' potential as effective vehicles for delivering specific toxins into AML cells.

ADCs are a crucial part of the treatment arsenal for leukemia, however their recombinant forms appear to be rather rare. Due to the limited amount of existing literature that has created such recombinant ADCs for AML treatment, particularly in a manner similar to that described in the MB&I SOP, it was difficult to compare the cytotoxic assay results reported in this thesis to those of other publications. Consequently, the results of this dissertation were compared with

those of a few MB&I Masters submissions. Despite the fact that the SOPs utilized to produce recombinant ADCs in these dissertations were identical to those in this study, comparisons were made cautiously as the cell lines and antigenic targets employed differed.

Mayuni G. (2023) effectively developed a mammalian-expressed recombinant ADC aimed at treating glioblastoma multiforme. This drug targeted overexpressed EGRF on A431, MDA-MB 468 and U87 cell lines; A2058 was used as the negative control. $IC_{50}$ values of 0.6723 nM, 1.033 nM and 100.6 nM were computed, respectively, after treating the cells with the generated αEGFR(scFv)-SNAP-AURIF [221]. Two CPSG4-targeting recombinant ADCs, one monovalent and another bivalent, were successfully developed in a different study by Karaan (2023) with the intention of treating triple negative breast cancer [234]. After treatment of the antigen overexpressing Hs578T cells with each ADC, the $IC_{50}$ values were found to be 409 nM for the monovalent form and 277 nM for the bivalent form. Even though these two ADCs' $IC_{50}$ values were greater than those of the previous study and this thesis, it was intriguing to observe how increasing valency favourably impacted antibody avidity, which in turn led to the lower $IC_{50}$ value observed when the Hs578T cells were treated with the bivalent ADC.

In a different study that is more closely related to this thesis, Fajemisin (2023), a colleague from the MB&I Research Unit, successfully produced αH22(scFv)-SNAP-AURIF. This ADC aimed to treat monocytic leukemia and atopic dermatitis [235]. Since CD64 overexpression is characteristic of these disorders, the cell lines U937 and HL60 were employed as they generally contain more of this antigen than other cancer cell lines. In contrast to the other aforementioned studies, this ADC's cytotoxic effect was evaluated on both IFN-y stimulated and unstimulated cells. After treatment, the $IC_{50}$ values for stimulated and unstimulated U937 cells were 14.58 nM and 617.0 nM, respectively. The $IC_{50}$ values for the stimulated and unstimulated HL60 cells were recorded at 125.0 nM and 255.2 nM, respectively. An intriguing finding of this study was that the $IC_{50}$ values of IFN-y simulated cells were lower. This was attributed to the simulation-induced increase in antigen expression, which resulted in an elevated number of antigen target sites and, in turn, reduced the amount of ADC needed for therapy.

Based on the fact that the $IC_{50}$ values acquired in this dissertation tend to be lower than those previously published in the MB&I Unit, it is essentially reasonable to interpret these comparisons as indications of improved cytotoxicity. Despite this, these $IC_{50}$ values could potentially be lowered even further. The particular factor that causes cytotoxicity of an ADC is its payload. The AURIF toxin used in the ADCs generated by the MB&I Unit has been modified to contain an inert PEG3-NH2 spacer. The distance created by this spacer enhances water

solubility and conjugation efficiency, thus rendering BG-AURIF a suitable toxin for these studies [290]. Additionally, existing literature has shown that payloads are required to be highly cytotoxic, providing $IC_{50}$ values at low nanomolar or picomolar levels [291]. Since the same toxin was incorporated in the ADCs generated in this study and those in the previous MB&I MSc submissions, it is evident that the efficiency of cytotoxicity is not always solely influenced by the payload. The effectiveness of cytotoxicity is also significantly influenced by the quality of the guiding antibody [292]. The variations seen between $IC_{50}$ values could be explained by the purity of the fusion proteins [293]. As understood thus far, low purity of proteins negatively affects the quality of ADCs. Therefore, this underscores the need to employ multiple protein purification techniques which can help in retrieving proteins with fewer competing degradation products that may impede cytotoxicity. Another possible explanation could be the difference in expression levels of the target antigen. In cases where antigen expression is low, a similar approach as Fajemisin (2023) could be taken whereby cells are appropriately stimulated to induce higher levels of antigen expression [235].

Demonstration that each recombinant ADC could produce desired targeted cell killing, despite the variations in cytotoxic effects across the experiments, bodes well for the success of future immunotherapeutics once there is sufficient funding and resources for the aforementioned advancements to be implemented.

# Chapter 5: Broader impacts and future work

Given our current understanding that multiple factors influence the development and outcome of leukemia, it is imperative that appropriate and effective medical interventions for early diagnosis and timely treatment are always available for those who rely on them. In the context of Africa, the limited funds and resources have made it extremely difficult for many years to provide AML patients with access to treatments as soon as they become necessary. Consequently, a large number of patients in this resource-limited region often succumb before receiving the necessary assistance. The number of AML cases and fatalities in Africa has thus faced a markedly detrimental impact.

This proof-of-concept study illustrates that it is feasible to develop novel treatments aimed at assisting patients in environments where insufficient funding and resources hinder their access to currently available treatments. This situation raises questions about the likelihood of patients receiving high-quality care and an improved quality of life. Given that less generic and non-specific treatments also affect healthy cells and often lead to severe side effects due to cytotoxicity, our study deliberately avoided creating such drugs. Instead, this study employed protein engineering to develop immunotherapeutics that selectively target therapeutically relevant cell surface markers significantly elevated in AML.

By carefully carrying out the SOPs described in chapter 2, this study was able to successfully demonstrate efficacious functionality of the generated AML-specific ADCs (αCD33(scFv)-SNAP and αCD45(scFv)-SNAP). Additionally, because it allowed for the simultaneous study of several factors including binding and cytotoxicity, the adaptable SNAP-tag turned out to be a valuable incorporation. Although this investigation yielded informative results that give optimism for the future application of these ADCs as immunotherapeutics in the treatment of AML, as is the case with many studies, some obstacles prevented the acquisition of even more precise and meaningful outcomes. The most notable drawbacks were: (1) at times the absence of certain consumables and reagents when needed, particularly for tissue culture, which made it challenging to maintain positively transfected cells, thus affecting the fluorescence and essentially the production of the necessary recombinant proteins. (2) As size exclusion and ion exchange could not be carried out following IMAC, not all bulk impurities could be removed, thus making it difficult to reach the desired purity of 95%. (3) Extensive assessment of the recombinant SNAP FP's functionality was restricted due to the lack of access to other viable AML cell lines. (4) Protein quality was impacted by the lack of protein cocktails to prevent or even delay degradation. Achieving accurate and high-quality findings is crucial since it has

been demonstrated that when all a study's objectives have been thoroughly and extensively addressed without financial or resource constraints, more informed conclusions and decisions on how to progress can be made.

Given the opportunity to expand on this work in an ideal scenario where funds and access to cutting-edge equipment are not constraints, a few adjustments or additions could be made to help enhance or gather more substantial data from this investigation. While the MB&I Unit's SOPs have clearly demonstrated their effectiveness in achieving the intended results, the process of producing recombinant proteins is typically carried out through trial and error, with various expression variables examined separately. Therefore, it would be interesting to research the techniques that can optimize the mammalian expression vector, as this is the first and fundamental structure that significantly impacts protein yields. Additionally, investigating other existing expression vectors that may offer better translation efficiency and stability could help improve protein production. Furthermore, to enhance the purity of the generated proteins by employing multiple purification techniques would be fascinating. It would also be intriguing to evaluate how these recombinant SNAP FPs perform across a broader range of models. This would provide a more comprehensive understanding of how factors like antibody specificity, avidity, solubility, sensitivity, and affinity for their targets could be affected in different environments. Nevertheless, demonstrating effectiveness in additional antigen-positive AML cell lines, peripheral blood mononuclear cells (PBMCs), and leukemic cells in serially transplanted mouse models would pave the way for highly sought-after clinical trials.

Concerns about the decrease in size from a full monoclonal antibody to a small scFv antibody fragment regarding the functionality and targeting ability of an antibody were also addressed. Flow cytometry and XTT analysis showed that the binding and cytotoxicity capabilities were not significantly reduced or completely lost when compared to a full monoclonal antibody. Despite this, there are still modifications that can improve the function of such antibody fragments. One feasible and previously conducted modification is the creation of bivalent antibodies, which link two scFv antibody fragments using a flexible linker [231]. By increasing the valency of these antibody fragments, the number of antigen-binding sites can also be elevated, thereby greatly enhancing the affinity, avidity, and potency of the recombinant antibodies.

Having understood the purpose of this study, it can be understood that the broader impact it has is to place a higher priority on improving the health of all AML patients, particularly in Africa. Secondly, the cost-effective production and distribution of these locally produced recombinant

immunotherapeutics would encourage affordability for all patients, underscoring the importance of exercising the fundamental right to optimal health for all individuals. Moreover, the benefit of having these treatments locally sourced would have a beneficial effect on economic growth and minimize sole reliance on imported treatments. Although further research and application of these recombinant SNAP-tag based antibody fusion proteins is still required to show their utility and possibly even further development, they have thus far proven to be a promising tool in cancer therapy.

## Conclusion

Access to cutting-edge diagnostic tools and therapies could significantly improve the predicted challenges of the expected rise in AML cases and fatalities in Africa. This situation requires immediate development of sustainable solutions to either delay or even prevent it. However, in the African context, where the primary barriers are a lack of funds and resources, patients often experience delays in receiving, much less benefiting from, available medical interventions. Thus, considering these circumstances, developing therapies for AML patients in Africa that are accessible, affordable in production and procurement, and highly effective seems more beneficial. Additionally, having locally produced treatments that aim to enhance patients' outcomes to match those that have been successful for patients in non-African regions, where individuals can afford and obtain access to current treatments, would also help promote equity and reduce existing disparities in global healthcare.

This study achieved its overall goal through the successful design of mammalian protein expression plasmids that incorporate AML-targeting antibody fragments fused to SNAP-tag. By transfecting these plasmids into suitable cells, recombinant SNAP FPs were produced, and the functionality of the generated FPs was subsequently demonstrated. Despite encountering several challenges throughout the experimental process, both αCD33(scFv)-SNAP and αCD45(scFv)-SNAP displayed the necessary binding and potency, with $IC_{50}$ values in the nanomolar range. Given the encouraging preliminary *in vitro* results from this study, it can be inferred that these recombinant ADCs show significant potential for the development of innovative immunotherapeutics for AML.

While there were instances when financial and resource limitations were a major issue, it was nonetheless a remarkable accomplishment to be able to get such perceptive insights and positive outcomes from our proof-of-concept study at the university level. This work raises curiosity and instills a sense of excitement about the efficiency of recombinant SNAP FPs when produced under conditions where limitations are reduced, as this would allow other approaches that can introduce enhancements to these potential immunotherapeutics to be implemented. In addition, continuing to conduct studies such as this can help to increase the depth of knowledge on the requirements for the production of suitable treatments based on the etiology and developments of the disease under study. Successful outcomes from this study and future studies alike can lay the groundwork for efforts to eventually transition from small-

scale laboratory production of ADCs to large-scale local industrial production of these biopharmaceuticals. Reaching this level of potential ADC production locally, given the context and purpose of this study, could lead to the integral shift in the way AML is treated and managed in Africa, which would enhance the overall health of patients with this disease.

## References


[1]: Rappaport, Noa, *et al.* "MalaCards: an amalgamated human disease compendium with diverse clinical and genetic annotation and structured search." *Nucleic acids research* 45.D1 (2017): D877-D887.

[2]: Witsch, Esther, Michael Sela, and Yosef Yarden. "Roles for growth factors in cancer progression." *Physiology* 25.2 (2010): 85-101.

[3]: Mathur, Garima, Sumitra Nain, and Pramod Kumar Sharma. "Cancer: an overview." *Acad. J. Cancer Res* 8.1 (2015): 01-09.

[4]: Weinberg, Robert A. "How cancer arises." *Scientific American* 275.3 (1996): 62-70.

[5]: Cooper GM. The Cell: A Molecular Approach. 2nd edition. Sunderland (MA): Sinauer Associates; 2000. The Development and Causes of Cancer. Available from: https://www.ncbi.nlm.nih.gov/books/NBK9963/

[6]: Meacham, Corbin E., and Sean J. Morrison. "Tumour heterogeneity and cancer cell plasticity." *Nature* 501.7467 (2013): 328-337.

[7]: Fisher, Rosie, Lazos Pusztai, and C. Swanton. "Cancer heterogeneity: implications for targeted therapeutics." *British journal of cancer* 108.3 (2013): 479-485.

[8]: Sung, Hyuna, *et al.* "Global cancer statistics 2020: GLOBOCAN estimates of incidence and mortality worldwide for 36 cancers in 185 countries." *CA: a cancer journal for clinicians* 71.3 (2021): 209-249.

[9]: Pan American Health Organisation [Internet]. Available from: https://www.paho.org/en/campaigns/world-cancer-day-2023-close-care-gap#. (Accessed: 12 Mar 2023 )

[10]: Roser, Max, and Hannah Ritchie. "Cancer. Our World in Data (2015)." Available from: https://ourworldindata.org/cancer. (Accessed: 12 Mar 2023 )

[11]: World Health Organization. "CureAll framework: WHO global initiative for childhood cancer: increasing access, advancing quality, saving lives." (2021).

[12]: Atun, Rifat, *et al.* "Sustainable care for children with cancer: a Lancet Oncology Commission." *The Lancet Oncology* 21.4 (2020): e185-e224.

[13]: National Cancer Institute. (2021). What is cancer? National Cancer Institute [Internet]. Available from: https://www.cancer.gov/about-cancer/understanding/what-is-cancer#. (Accessed: 12 Mar 2023 )

[14]: Stein, C. J., and G. A. Colditz. "Modifiable risk factors for cancer." *British journal of cancer* 90.2 (2004): 299-303.

[15]: Vogelstein, Bert, *et al.* "Cancer genome landscapes." *science* 339.6127 (2013): 1546-1558.

[16]: Benz Jr, Edward J. "The Jeremiah Metzger lecture cancer in the twenty-first century: an inside view from an outsider." *Transactions of the American Clinical and Climatological Association* 128 (2017): 275.

[17]: Hanahan, Douglas, and Robert A. Weinberg. "The hallmarks of cancer." *cell* 100.1 (2000): 57-70.

[18]: Hanahan, Douglas, and Robert A. Weinberg. "Hallmarks of cancer: the next generation." *cell* 144.5 (2011): 646-674.

[19]: Hendricks, Marc, *et al.* "Socioeconomic status significantly impacts childhood cancer survival in South Africa." *Pediatric Blood & Cancer* 70.12 (2023): e30669.

[20]: Azubuike, Samuel Onyinyechukwu, *et al.* "Socio-economic status and the risk of breast cancer among Nigerian women: a case control study." *Pan African Medical Journal* 41.1 (2022).

[21]: Hamdi, Yosr, *et al.* "Cancer in Africa: the untold story." *Frontiers in oncology* 11 (2021): 650117.

[22]: Stringhini, Silvia, *et al.* "Association of socioeconomic status with overall and cause specific mortality in the Republic of Seychelles: results from a cohort study in the African region." *PloS one* 9.7 (2014): e102858.

[23]: McCormack, Valerie, and Robert Newton. "Research priorities for social inequalities in cancer in sub-Saharan Africa." *Reducing social inequalities in cancer: evidence and priorities for research* (2019): 195-204.

[24]: Omotoso, Olabode, *et al.* "Addressing cancer care inequities in sub-Saharan Africa: current challenges and proposed solutions." *International Journal for Equity in Health* 22.1 (2023): 189.

[25]: Coughlin, Steven S. "Social determinants of breast cancer risk, stage, and survival." *Breast cancer research and treatment* 177 (2019): 537-548.

[26]: Sharma, Rajesh, *et al.* "Mapping cancer in Africa: a comprehensive and comparable characterization of 34 cancer types using estimates from GLOBOCAN 2020." *Frontiers in public health* 10 (2022): 839835.

[27]: Wale-Oshinowo, Bamidele A., *et al.* “Least Developed Countries in Africa.” *The Palgrave Encyclopedia of Global Security Studies* (2020): pp. 1–16.

[28]: Kayamba, Violet, *et al.* "Systematic review of cancer research output from Africa, with Zambia as an example." *JCO global oncology* 7 (2021): 802-810.

[29]: Ngoma, Twalib, and Mamsau Ngoma. “Cancer Control in Africa: Is Cancer Research a Luxury or Necessity?” *Ecancermedicalscience*, vol. 13, 25 July (2019).

[30]: Rubagumya, Fidel, *et al.* "An analysis of the African cancer research ecosystem: tackling disparities." *BMJ Global Health* 8.2 (2023): e011338.

[31]: Boutayeb, A. "The impact of infectious diseases on the development of Africa." *Handbook of disease burdens and quality of life measures* (2010): 1171 - 1188.

[32]: Bigna, Jean Joel, and Jean Jacques Noubiap. "The rising burden of non-communicable diseases in sub-Saharan Africa." *The Lancet Global Health* 7.10 (2019): e1295-e1296.

[33]: Mboera, Leonard EG, *et al.* "The changing landscape of public health in sub-Saharan Africa: control and prevention of communicable diseases needs rethinking: proceedings." *Onderstepoort Journal of Veterinary Research* 81.2 (2014): 1-6.

[34]: National Cancer Institute. “Cancer Types.” *National Cancer Institute*, Cancer.gov, 2019 [Internet]. Available from: www.cancer.gov/types. (Accessed: 13 Mar 2023 )

[35]: Global Cancer Observatory. “Cancer Today.” *Gco.iarc.who.int* [Internet]. Available from: https://gco.iarc.fr/today/en. (Accessed13 Mar 2023: )

[36]: Kassahun, Woldeteklehaymanot, *et al.* "Prevalence of Leukemia and Associated Factors among Patients with Abnormal Hematological Parameters in Jimma Medical Center, Southwest Ethiopia: A Cross-Sectional Study." *Advances in Hematology* 2020.1 (2020): 2014152.

[37]: Hodkinson, Katherine E., Nikki Bouwer, and Jenifer Vaughan. "South African study of blast phase chronic myeloid leukaemia: A poor prognostic outlook." *African Journal of Laboratory Medicine* 11.1 (2022): 1-7.

[38]: Nell, Erica-Mari, *et al.* "Epidemiology of Adult T-Cell Leukaemia/Lymphoma in South Africa over a 10-Year Period." *Journal of Cancer Epidemiology* 2022.1 (2022): 2058280.

[39]: Whiteley, Andrew E., *et al.* "Leukaemia: a model metastatic disease." *Nature Reviews Cancer* 21.7 (2021): 461-475.

[40]: Jagannathan-Bogdan, Madhumita, and Leonard I. Zon. "Hematopoiesis." *Development* 140.12 (2013): 2463-2467.

[41]: Smith, B R. “Regulation of hematopoiesis.” *The Yale journal of biology and medicine* vol. 63,5 (1990): 371-80.

[42]: Orkin, Stuart H., and Leonard I. Zon. "Hematopoiesis: an evolving paradigm for stem cell biology." *Cell* 132.4 (2008): 631-644.

[43]: Mahalingaiah, Prathap Kumar, Tammy Palenski, and Terry R. Van Vleet. "An In Vitro Model of Hematotoxicity: Differentiation of Bone Marrow–Derived Stem/Progenitor Cells into

Hematopoietic Lineages and Evaluation of Lineage-Specific Hematotoxicity." *Current protocols in toxicology* 76.1 (2018): e45.

[44]: Fiedler, Katja, and Cornelia Brunner. "Mechanisms controlling hematopoiesis." *Hematology-Science and Practice* (2012): 3-28.

[45]: Chennamadhavuni, A., V. Lyengar, and A. LeuNemia ShimanovsNy. "Updated 2021 Nov 21." *StatPearl, Treasure Island (FL): StatPearls Publishing* (2022) [Internet]. Available from: https://www.ncbi.nlm.nih.gov/books/NBK560490/. (Accessed: 16 Mar 2023 )

[46]: Gilliland, D. Gary, Craig T. Jordan, and Carolyn A. Felix. "The molecular basis of leukemia." *ASH Education Program Book* 2004.1 (2004): 80-97.

[47]: Tigner, Alyssa, *et al.* “Histology, White Blood Cell.” *PubMed*, StatPearls Publishing (2022) [Internet]. Available from: www.ncbi.nlm.nih.gov/books/NBK563148/. (Accessed: 17 Mar 2023 )

[48]: American Cancer Society. Acute Myeloid Leukemia (AML) Subtypes and Prognostic Factors.” (2018) [Internet]. Available from: www.cancer.org/cancer/types/acute-myeloid-leukemia/detection-diagnosis-staging/how-classified.html#. (Accessed: 17 Mar 2023 )

[49]: Ladines-Castro, W., *et al.* "Morphology of leukaemias." *Revista Médica del Hospital General de México* 79.2 (2016): 107-113.

[50]: Schiffer CA, Stone RM. “Morphologic Classification and Clinical and Laboratory Correlates”. *Holland-Frei Cancer Medicine, 6th Edition* (2003).

[51]: Porwit, Anna, and Marie C. Béné. "Acute leukemias of ambiguous origin." *American journal of clinical pathology* 144.3 (2015): 361-376.

[52]: Vardiman, James W., Nancy Lee Harris, and Richard D. Brunning. "The World Health Organization (WHO) classification of the myeloid neoplasms." *Blood, The Journal of the American Society of Hematology* 100.7 (2002): 2292-2302.

[53]: Khoury, Joseph D *et al.* “The 5th edition of the World Health Organization Classification of Haematolymphoid Tumours: Myeloid and Histiocytic/Dendritic Neoplasms.” *Leukemia* vol. 36,7 (2022): 1703-1719

[54]: Park, Hee Sue. "What is new in acute myeloid leukemia classification?" *Blood Research* 59.1 (2024): 15.

[55]: Worldwide cancer data | World Cancer Research Fund International, WCRF International. [Internet]. Available from: https://www.wcrf.org/cancer-trends/worldwide-cancer-data. (Accessed: 21 Mar 2023 )

[56]: Du, Mengbao, *et al.* "The global burden of leukemia and its attributable factors in 204 countries and territories: findings from the global burden of disease 2019 study and projections to 2030." *Journal of oncology* 2022.1 (2022): 1612702.

[57]: Deschler, Barbara, and Michael Lübbert. "Acute myeloid leukemia: epidemiology and etiology." *Cancer: Interdisciplinary International Journal of the American Cancer Society* 107.9 (2006): 2099-2107.

[58]: Creutzig, Ursula, *et al.* "Acute myelogenous leukemia in adolescents and young adults." *Pediatric blood & cancer* 65.9 (2018): e27089.

[59]: Vakiti, A. & Mewawalla, P. “Acute myeloid leukemia”. *In: StatPearls* [Internet]. Treasure Island (FL): StatPearls Publishing; 2020 Jan. 2020 Nov 21. Available from: https://www.ncbi.nlm.nih.gov/books/NBK507875/ (Accessed: 27 Mar 2023 )

[60]: Li, Ming, *et al.* "Treatment and Survival in Acute Leukemia: A New South Wales Study Comparing Adolescents and Young Adults with Children and Adults." *European Journal of Cancer Care* 2023.1 (2023): 8600327.

[61]: Chaudhury, Shahzya, *et al.* "Age-specific biological and molecular profiling distinguishes paediatric from adult acute myeloid leukaemias." *Nature communications* 9.1 (2018): 5280.

[62]: Mayo Clinic. “Acute myelogenous leukemia - Symptoms and causes” [Internet]. Available from: https://www.mayoclinic.org/diseases-conditions/acute-myelogenous-leukemia/symptoms-causes/syc-20369109 (Accessed: 4 Apr 2023 )

[63]: University of Iowa Hospitals & Clincs. "Acute Myeloid Leukemia." (2021) [Internet]. Available from: https://uihc.org/health-topics/acute-myeloid-leukemia-aml (Accessed: 4 Apr 2023 )

[64]: American Cancer Society.” Tests for Acute Myeloid Leukemia (AML),” (2024) [Internet]. Available from: https://www.cancer.org/cancer/types/acute-myeloid-leukemia/detection-diagnosis-staging/how-diagnosed.html (Accessed: 5 Apr 2023 )

[65]: Nygren, Peter. "What is cancer chemotherapy?." *Acta Oncologica* 40.2-3 (2001): 166-174.

[66]: Bosch, Fèlix, and Laia Rosich. "The contributions of Paul Ehrlich to pharmacology: a tribute on the occasion of the centenary of his Nobel Prize." *Pharmacology* 82.3 (2008): 171-179.

[67]: Farber, Sidney, *et al.* "Temporary remissions in acute leukemia in children produced by folic acid antagonist, 4-aminopteroyl-glutamic acid (aminopterin)." *New England Journal of Medicine* 238.23 (1948): 787-793.

[68]: Yates, J. W., *et al.* "Cytosine arabinoside (NSC-63878) and daunorubicin (NSC-83142) therapy in acute nonlymphocytic leukemia." *Cancer chemotherapy reports* 57.4 (1973): 485-488.

[69]: American Cancer Society. "Typical Treatment of Acute Myeloid Leukemia (Except APL)" (2023) [Internet]. Available from: https://www.cancer.org/cancer/types/acute-myeloid-leukemia/treating/typical-treatment-of-aml.html (Accessed: 16 Apr 2023)

[70]: Crossnohere, Norah L., *et al.* "Side effects from acute myeloid leukemia treatment: results from a national survey." *Current medical research and opinion* 35.11 (2019): 1965-1970.

[71]: National Cancer Institute. “NCI Dictionary of Cancer Terms.” (2023) [Internet] Available from: https://www.cancer.gov/publications/dictionaries/cancer-terms (Accessed: 16 Apr 2023)

[72]: Hill, Geoffrey R., *et al.* "Current concepts and advances in graft-versus-host disease immunology." *Annual review of immunology* 39.1 (2021): 19-49.

[73]: Erwin, Hailey. "Medical Advantages of Allogeneic vs Autologous Stem Cell Transplants as Treatment in Blood Related Cancer Patients." (2018).

[74]: Younan, Patrick, John Kowalski, and Hans-Peter Kiem. "Genetic modification of hematopoietic stem cells as a therapy for HIV/AIDS." *Viruses* 5.12 (2013): 2946-2962.

[75]: National Cancer Institute. "Targeted Therapy to Treat Cancer." (2022) [Internet]. Available from: https://www.cancer.gov/about-cancer/treatment/types/targeted-therapies (Accessed: 30 Apr 2023)

[76]: Meisel, Jane Lowe, *et al.* "Evolution of targeted therapy in breast cancer: where precision medicine began." *American Society of Clinical Oncology Educational Book* 38 (2018): 78-86.

[77]: Totiger, Tulasigeri M., *et al.* "Targeted Therapy Development in Acute Myeloid Leukemia." *Biomedicines* 11.2 (2023): 641.

[78]: Couzin-Frankel, Jennifer. “Cancer Immunotherapy.” *Science*, vol. 342, no. 6165, 19 Dec. (2013) pp. 1432–1433.

[79]: McCarthy, Edward F. "The toxins of William B. Coley and the treatment of bone and soft-tissue sarcomas." *The Iowa orthopaedic journal* 26 (2006): 154.

[80]: Starnes, Charlie O. "Coley's toxins in perspective." *Nature* 357.6373 (1992): 11-12.

[81]: Mathé, Georges, *et al.* "Active immunotherapy for acute lymphoblastic leukaemia." *The Lancet* 293.7597 (1969): 697-699.

[82]: Nagasawa, Daniel T., *et al.* "Passive immunotherapeutic strategies for the treatment of malignant gliomas." *Neurosurgery Clinics* 23.3 (2012): 481-495.

[83]: Noh, Ji-Yoon, *et al.* "Immunotherapy in hematologic malignancies: emerging therapies and novel approaches." *International journal of molecular sciences* 21.21 (2020): 8000.

[84]: Ma, Jiabing, *et al.* "Bispecific antibodies: from research to clinical application." *Frontiers in immunology* 12 (2021): 626616.

[85]: Fan, Gaowei, *et al.* "Bispecific antibodies and their applications." *Journal of hematology & oncology* 8 (2015): 1-14.

[86]: Selby, Chris, Lisa R. Yacko, and Ashley E. Glode. "Gemtuzumab ozogamicin: back again." *Journal of the Advanced Practitioner in Oncology* 10.1 (2019): 68 - 82.

[87]: American Society of Hematology. "FDA Approves Gemtuzumab Ozogamicin for AML" (2017) [Internet] Available from: https://ashpublications.org/ashclinicalnews/news/3386/FDA-Approves-Gemtuzumab-Ozogamicin-for-AML (Accessed: 11 May 2023 )

[88]: Mohammed, Shamayel, *et al.* "Cancer vaccines: past, present, and future." *Advances in anatomic pathology* 23.3 (2016): 180-191.

[89]: Zhao, Yue, *et al.* "Cancer Vaccines: Antigen Selection Strategy." *Vaccines*, vol. 9, no. 2, 25 Jan. (2021): p. 85.

[90]: Wu, Mo, *et al.* "Learn from antibody–drug conjugates: consideration in the future construction of peptide-drug conjugates for cancer therapy." *Experimental Hematology & Oncology* 11.1 (2022): 93.

[91]: Hinrichs, Christian S., and Nicholas P. Restifo. "Reassessing target antigens for adoptive T-cell therapy." *Nature biotechnology* 31.11 (2013): 999-1008.

[92]: Okarvi, Subhani M., and Ibrahim AlJammaz. "Development of the tumor-specific antigen-derived synthetic peptides as potential candidates for targeting breast and other possible human carcinomas." *Molecules* 24.17 (2019): 3142.

[93]: Hofmann, Susanne, *et al.* "Chimeric antigen receptor (CAR) T cell therapy in acute myeloid leukemia (AML)." *Journal of clinical medicine* 8.2 (2019): 200.

[94]: Schorr, Christopher, and Fabiana Perna. "Targets for chimeric antigen receptor T-cell therapy of acute myeloid leukemia." *Frontiers in Immunology* 13 (2022): 1085978.

[95]: Takei, Y., *et al.* "Molecular cloning of a novel gene similar to myeloid antigen CD33 and its specific expression in placenta." *Cytogenetic and Genome Research* 78.3-4 (1997): 295-300.

[96]: Amadori, Sergio, and Roberto Stasi. "Monoclonal antibodies and immunoconjugates in acute myeloid leukemia." *Best Practice & Research Clinical Haematology* 19.4 (2006): 715-736.

[97]: Walter, Roland B., *et al.* "CD33 expression and P-glycoprotein–mediated drug efflux inversely correlate and predict clinical outcome in patients with acute myeloid leukemia treated with gemtuzumab ozogamicin monotherapy." *Blood* 109.10 (2007): 4168-4170.

[98]: Laszlo, George S., Elihu H. Estey, and Roland B. Walter. "The past and future of CD33 as therapeutic target in acute myeloid leukemia." *Blood reviews* 28.4 (2014): 143-153.

[99]: Hernández-Caselles, Trinidad, *et al.* "A study of CD33 (SIGLEC-3) antigen expression and function on activated human T and NK cells: two isoforms of CD33 are generated by alternative splicing." Journal of leukocyte biology 79.1 (2006): 46-58.

[100]: National Cancer Institute. “NCI Dictionaries: CD33 positive” (2024). Available from: https://www.cancer.gov/publications/dictionaries/cancer-terms/def/cd33-positive# (Accessed: 26 May 2023 )

[101]: Macauley, Matthew S., Paul R. Crocker, and James C. Paulson. "Siglec-mediated regulation of immune cell function in disease." *Nature Reviews Immunology* 14.10 (2014): 653-666.

[102]: Jilani, Iman, *et al.* "Differences in CD33 intensity between various myeloid neoplasms." *American journal of clinical pathology* 118.4 (2002): 560-566.

[103]: Guglielmi, Cesare, *et al.* "Immunophenotype of adult and childhood acute promyelocytic leukaemia: correlation with morphology, type of PML gene breakpoint and clinical outcome. A cooperative Italian study on 196 cases." *British journal of haematology* 102.4 (1998): 1035-10412.

[104]: Nakano, Akinobu, *et al.* "Expression of leukocyte common antigen (CD45) on various human leukemia/lymphoma cell lines." *Acta Patholigica Japonica* 40.2 (1990): 107-115.

[105]: Williams, A. F. "Glycoprotein antigens of the lymphocyte surface and their purification by antibody affinity chromatography." *Handbook of experimental immunology* 22 (1986).

[106]: Harfmann, Maraike, *et al.* "CD45-Directed CAR-T Cells with CD45 Knockout Efficiently Kill Myeloid Leukemia and Lymphoma Cells In Vitro Even after Extended Culture." *Cancers* 16.2 (2024): 334.

[107]: Ralph, Stephen J., *et al.* "Structural variants of human T200 glycoprotein (leukocyte-common antigen)." *The EMBO journal* 6.5 (1987): 1251-1257.

[108]: Desai, Dev M., *et al.* "The catalytic activity of the CD45 membrane-proximal phosphatase domain is required for TCR signaling and regulation." *The EMBO journal* 13.17 (1994): 4002-4010.

[109]: Streuli, M., *et al.* "Differential usage of three exons generates at least five different mRNAs encoding human leukocyte common antigens." *The Journal of experimental medicine* 166.5 (1987): 1548-1566.

[110]: Chui, D., *et al.* "Specific CD45 isoforms differentially regulate T cell receptor signaling." *The EMBO journal* 13.4 (1994): 798-807.

[111]: Johnson, Kenneth G., *et al.* "A supramolecular basis for CD45 tyrosine phosphatase regulation in sustained T cell activation." *Proceedings of the National Academy of Sciences* 97.18 (2000): 10138-10143.

[112]: National Cancer Institute. NCI Dictionary of Cancer Terms [Internet]. Available from: https://www.cancer.gov/publications/dictionaries/cancer-terms/def/antigen. (Accessed: 07 Jun 2023).

[113]: Alberts B, Johnson A, Lewis J, *et al.* Molecular Biology of the Cell. 4th edition. New York: Garland Science (2002). Chapter 24, The Adaptive Immune System. Available from: https://www.ncbi.nlm.nih.gov/books/NBK21070/ (Accessed: 07 Jun 2023)

[114]: Alberts, Bruce. “B Cells and Antibodies.” Molecular Biology of the Cell. 4th Edition., U.S. National Library of Medicine, 1 Jan. (1970). Available from: www.ncbi.nlm.nih.gov/books/NBK26884/ (Accessed: 07 Jun 2023)

[115]: Lanzavecchia, Antonio, and Federica Sallusto. "Human B cell memory." *Current opinion in immunology* 21.3 (2009): 298-304.

[116]: Janeway CA Jr, Travers P, Walport M, *et al.* Immunobiology: The Immune System in Health and Disease. 5th edition. New York: Garland Science; 2001. Part V, The Immune System in Health and Disease. Available from: https://www.ncbi.nlm.nih.gov/books/NBK10775/

[117]: Creative Biolabs Antibody. "Antibody Structure & Isotypes." (2024) [Internet]. Available from: https://www.antibody-creativebiolabs.com/antibody-structure-isotypes.htm (Accessed: 28 Jun 2023 )

[118]: Schroeder Jr, Harry W., and Lisa Cavacini. "Structure and function of immunoglobulins." *Journal of allergy and clinical immunology* 125.2 (2010): S41-S52.

[119]: Damelang, Timon, *et al.* "Impact of structural modifications of IgG antibodies on effector functions." *Frontiers in immunology* 14 (2024): 1304365.

[120]: Franchin, Giovanni, Yong-Rui Zou, and Betty Diamond. "The structure and derivation of antibodies and autoantibodies." *Dubois' Lupus Erythematosus and Related Syndromes*. WB Saunders, 2013. 76-95.

[121]: iRepertoire. "Diversity and differentiation in the adaptive immune system" (2024) [Internet]. Available from: https://irepertoire.com/diversity-and-differentiation-in-the-adaptive-immune-system/ (Accessed: 3 Jul 2023)

[122]: Rees, Anthony R. "Understanding the human antibody repertoire." *MAbs*. Vol. 12. No. 1. Taylor & Francis, 2020.

[123]: Askonas, BoA, A. R. Williamson, and B. E. G. Wright. "Selection of a single antibody-forming cell clone and its propagation in syngeneic mice." *Proceedings of the National Academy of Sciences* 67.3 (1970): 1398-1403.

[124]: Köhler, G, and C Milstein. “Continuous cultures of fused cells secreting antibody of predefined specificity.” *Nature* vol. 256,5517 (1975): 495-7

[125]: Mitra, Sanchita, and Pushpa Chaudhary Tomar. "Hybridoma technology; advancements, clinical significance, and future aspects." *Journal of Genetic Engineering and Biotechnology* 19 (2021): 1-12.

[126]: Khazaeli, M. B., Robert M. Conry, and Albert F. LoBuglio. "Human immune response to monoclonal antibodies." *Journal of immunotherapy* 15.1 (1994): 42-52.

[127]: Lu, Ruei-Min, *et al.* "Development of therapeutic antibodies for the treatment of diseases." *Journal of biomedical science* 27 (2020): 1-30.

[128]: Kaluza, Brigitte, *et al.* "A general method for chimerization of monoclonal antibodies by inverse polymerase chain reaction which conserves authentic N-terminal sequences." *Gene* 122.2 (1992): 321-328.

[129]: Chen, Hsiao-Chun, *et al.* "Monoclonal Antibodies as a Therapeutic Strategy against Multidrug-Resistant Bacterial Infections in a Post-COVID-19 Era." *Life* 14.2 (2024): 246.

[130]: Grillo-Lopez, A. J., *et al.* "Rituximab the first monoclonal antibody approved for the treatment of lymphoma." *Current pharmaceutical biotechnology* 1.1 (2000): 1-9.

[131]: Yang, Benjamin. "Drug Profile: Erbitux." *Discovery Medicine* 4.20 (2009): 22-23.

[132]: Bell, Jenny, and Jean Colaneri. "Basiliximab (Simulect [R]): Simplifying Induction Therapy." *Nephrology Nursing Journal* 27.2 (2000): 243-243.

[133]: Wang, Zeng, *et al.* "Development of therapeutic antibodies for the treatment of diseases." *Molecular biomedicine* 3.1 (2022): 35.

[134]: Jones, Peter T., *et al.* "Replacing the complementarity-determining regions in a human antibody with those from a mouse." *Nature* 321.6069 (1986): 522-525.

[135]: Davis, C. Geoffrey, Michael L. Gallo, and Jose RF Corvalan. "Transgenic mice as a source of fully human antibodies for the treatment of cancer." *Cancer and Metastasis Reviews* 18 (1999): 421-425.

[136]: Pirkalkhoran, Sama, *et al.* "Bioengineering of antibody fragments: challenges and opportunities." *Bioengineering* 10.2 (2023): 122.

[137]: Zeng, Xiangqun, Zhihong Shen, and Ray Mernaugh. "Recombinant antibodies and their use in biosensors." *Analytical and bioanalytical chemistry* 402 (2012): 3027-3038.

[138]: Kumar, Gautam, *et al.* "Biologicals to direct nanotherapeutics towards HER2-positive breast cancers." *Nanomedicine: Nanotechnology, Biology and Medicine* 27 (2020): 102197.

[139]: Manoutcharian, Karen, and Goar Gevorkian. "Shark VNAR phage display libraries: An alternative source for therapeutic and diagnostic recombinant antibody fragments." *Fish & Shellfish Immunology* 138 (2023): 108808.

[140]: Arbabi-Ghahroudi, Mehdi. "Camelid single-domain antibodies: promises and challenges as lifesaving treatments." *International journal of molecular sciences* 23.9 (2022): 5009.

[141]: Tong, Juliana TW, *et al.* "An insight into FDA approved antibody-drug conjugates for cancer therapy." *Molecules* 26.19 (2021): 5847.

[142]: Teicher, Beverly A., and Ravi VJ Chari. "Antibody conjugate therapeutics: challenges and potential." *Clinical cancer research* 17.20 (2011): 6389-6397.

[143]: Hussain, Ahmad Fawzi, *et al.* "One-step site-specific antibody fragment auto-conjugation using SNAP-tag technology." *Nature Protocols* 14.11 (2019): 3101-3125.

[144]: Beck, Alain, *et al.* "Strategies and challenges for the next generation of antibody–drug conjugates." *Nature reviews Drug discovery* 16.5 (2017): 315-337.

[145]: Hamblett, Kevin J., *et al.* "Effects of drug loading on the antitumor activity of a monoclonal antibody drug conjugate." *Clinical cancer research* 10.20 (2004): 7063-7070.

[146]: Fawzi Hussain, Ahmad, Manal Amoury, and Stefan Barth. "SNAP-tag technology: a powerful tool for site specific conjugation of therapeutic and imaging agents." *Current pharmaceutical design* 19.30 (2013): 5437-5442.

[147]: Cole, Nelson B. "Site-specific protein labeling with SNAP-tags." *Current protocols in protein science* 73.1 (2013): 30-1.

[148]: Gronemeyer, Thomas, Guillaume Godin, and Kai Johnsson. "Adding value to fusion proteins through covalent labelling." *Current opinion in biotechnology* 16.4 (2005): 453-458.

[149]: Dreyer, Rudolf, *et al.* "The evolution of SNAP-Tag labels." *Biomacromolecules* 24.2 (2023): 517-530.

[150]: Keppler, Antje, *et al.* "Labeling of fusion proteins of O6-alkylguanine-DNA alkyltransferase with small molecules in vivo and in vitro." *Methods* 32.4 (2004): 437-444.

[151]: Amoury, Manal, *et al.* "SNAP-tag based agents for preclinical in vitro imaging in malignant diseases." *Current pharmaceutical design* 19.30 (2013): 5429-5436.

[152]: Otani, Masashi, *et al.* "TZT-1027, an antimicrotubule agent, attacks tumor vasculature and induces tumor cell death." *Japanese journal of cancer research* 91.8 (2000): 837-844.

[153]: Gao, Gang, *et al.* "Marine antitumor peptide dolastatin 10: Biological activity, structural modification and synthetic chemistry." *Marine Drugs* 19.7 (2021): 363.

[154]: Jerjian, Taleen V., *et al.* "Antibody-drug conjugates: a clinical pharmacy perspective on an emerging cancer therapy." *Pharmacotherapy: The Journal of Human Pharmacology and Drug Therapy* 36.1 (2016): 99-116.

[155]: Fu, Zhiwen, *et al.* "Antibody drug conjugate: the “biological missile” for targeted cancer therapy." *Signal transduction and targeted therapy* 7.1 (2022): 93.

[156]: Woitok, Mira, *et al.* "The efficient elimination of solid tumor cells by EGFR-specific and HER2-specific scFv-SNAP fusion proteins conjugated to benzylguanine-modified auristatin F." *Cancer letters* 381.2 (2016): 323-330.

[157]: Arlotta, Keith J., and Shawn C. Owen. "Antibody and antibody derivatives as cancer therapeutics." *Wiley Interdisciplinary Reviews: Nanomedicine and Nanobiotechnology* 11.5 (2019): e1556.

[158]: Murphy, Kenneth P. "Janeway's Immunobiology*". Garland Science*. Taylor & Francis Group, LLC New York, (2011).

[159]: Kaksonen, Marko, and Aurélien Roux. "Mechanisms of clathrin-mediated endocytosis." *Nature reviews Molecular cell biology* 19.5 (2018): 313-326.

[160]: Cullen, Peter J., and Florian Steinberg. "To degrade or not to degrade: mechanisms and significance of endocytic recycling." *Nature reviews Molecular cell biology* 19.11 (2018): 679-696.

[161]: Ritchie, Michael, Lioudmila Tchistiakova, and Nathan Scott. "Implications of receptor-mediated endocytosis and intracellular trafficking dynamics in the development of antibody drug conjugates." *MAbs*. Vol. 5. No. 1. Taylor & Francis, (2013): 13-21.

[162]: Marei, Hany E., Carlo Cenciarelli, and Anwarul Hasan. "Potential of antibody–drug conjugates (ADCs) for cancer therapy." *Cancer Cell International* 22.1 (2022): 255.

[163]: Bvudzijena TL. "Developing novel SNAP tag-based antibody fusion proteins directionally conjugated to fluorophores for immunophenotyping of acute myeloid leukemia." *University of Cape Town* (2023).

[164]: Fu, Hongguang, et al. "Codon optimization with deep learning to enhance protein expression." *Scientific reports* 10.1 (2020): 17617.

[165]: Nguyen, Phuoc Vinh, et al. "Targeted nanomedicine with anti-EGFR scFv for siRNA delivery into triple negative breast cancer cells." *European Journal of Pharmaceutics and Biopharmaceutics* 157 (2020): 74-84.

[166]: Arafat, W et al. "Antineoplastic effect of anti-erbB-2 intrabody is not correlated with scFv affinity for its target." Cancer gene therapy vol. 7,9 (2000): 1250-6.

[167]: Conrad, Thomas, et al. "Maximizing transcription of nucleic acids with efficient T7 promoters." Communications Biology 3.1 (2020): 439.

[168]: Mohanty, Arun K, and Michael C Wiener. "Membrane protein expression and production: effects of polyhistidine tag length and position." Protein expression and purification vol. 33,2 (2004): 311-25.

[169]: Volkmann, Gerrit, Verena Volkmann, and Xiang-Qin Liu. "Site-specific protein cleavage in vivo by an intein-derived protease." FEBS letters 586.1 (2012): 79-84.

[170]: Ahmad, Zuhaida Asra et al. “scFv antibody: principles and clinical application.” Clinical & developmental immunology vol. 2012 (2012): 980250.

[171]: Sun, Xiaoli et al. “Development of SNAP-tag fluorogenic probes for wash-free fluorescence imaging.” Chembiochem: a European journal of chemical biology vol. 12,14 (2011): 2217-26.

[172]: Hermening, Stephan et al. “Increased protein expression from adenoviral shuttle plasmids and vectors by insertion of a small chimeric intron sequence.” Journal of virological methods vol. 122,1 (2004): 73-7.

[173]: Renaud-Gabardos, Edith, et al. "Internal ribosome entry site-based vectors for combined gene therapy." World journal of experimental medicine 5.1 (2015): 11.

[174]: Dai, Chao, et al. "Improved fusion protein expression of EGFP via the mutation of both Kozak and the initial ATG codon." Cellular and Molecular Biology Letters 12.3 (2007): 362-369.

[175]: Batt, David B., Ying Luo, and Gordon G. Carmichael. "Polyadenylation and transcription termination in gene constructs containing multiple tandem polyadenylation signals." Nucleic acids research 22.14 (1994): 2811-2816.

[176]: Johnson, Síle A., et al. "Increasing the bactofection capacity of a mammalian expression vector by removal of the f1 ori." Cancer gene therapy 26.7 (2019): 183-194.

[177]: Prasad, Tekkatte Krishnamurthy, and Nalam Madhusudhana Rao. "The role of plasmid constructs containing the SV40 DNA nuclear-targeting sequence in cationic lipid-mediated DNA delivery." Cell Mol Biol Lett 10.2 (2005): 203-15.

[178]: Clark, D. P., and N. J. Pazdernik. "Chapter 7. Cloning Genes for Analysis." Molecular Biology, 2nd ed.; Academic Cell Update Edition; Elsevier Inc.: Waltham, MA, USA (2013): 194-226.

[179]: Dortet, Laurent, et al. "Characterization of BRPMBL, the bleomycin resistance protein associated with the Carbapenemase NDM." Antimicrobial agents and chemotherapy 61.3 (2017): 10-1128.

[180]: Roberts, Thomas C., Robert Langer, and Matthew JA Wood. "Advances in oligonucleotide drug delivery." Nature reviews Drug discovery 19.10 (2020): 673-694.

[181]: Czarniecki, D., Richard J. Noel Jr, and William S. Reznikoff. "The-45 region of the Escherichia coli lac promoter: CAP-dependent and CAP-independent transcription." Journal of bacteriology 179.2 (1997): 423-429.

[182]: Lewis, Mitchell. "The lac repressor." Comptes rendus biologies 328.6 (2005): 521-548.

[183]: Choi, Kyoung-Hee, et al. "Genetic tools for select-agent-compliant manipulation of Burkholderia pseudomallei." Applied and environmental microbiology 74.4 (2008): 1064-1075.

[184]: Poirel, Laurent, et al. "Antimicrobial resistance in Escherichia coli." Microbiology spectrum 6.4 (2018): 10-1128.

[185]: Johari, Yusuf B., et al. "Engineering of the CMV promoter for controlled expression of recombinant genes in HEK293 cells." Biotechnology Journal 17.8 (2022): 2200062

[186]: Takara Bio. “Plasmid DNA purification.” [Internet] https://www.takarabio.com/documents/User%20Manual/NucleoBond%20Xtra%20Plasmid%20DNA%20Purification%20User%20Manual_Rev_15.pdf (Accessed: 26 Nov 2023).

[187]: Gautam, Akash. "Phenol-chloroform DNA isolation method." DNA and RNA Isolation Techniques for Non-Experts. Cham: Springer International Publishing, 2022. 33-39.

[188]: Thermofisher. “Fixation Strategies and Formulations Used in IHC Staining” [Internet]: https://www.thermofisher.com/za/en/home/life-science/protein-biology/protein-biology-learning-center/protein-biology-resource-library/pierce-protein-methods/fixation-strategies-formulations.html. (Accessed:.24 Feb 2024)

[189]: Sousa, Fani, Duarte MF Prazeres, and João A. Queiroz. "Affinity chromatography approaches to overcome the challenges of purifying plasmid DNA." Trends in biotechnology 26.9 (2008): 518-525.

[190]: Hulspas, Ruud, et al. "Considerations for the control of background fluorescence in clinical flow cytometry." Cytometry part b: Clinical cytometry: The journal of the international society for analytical cytology 76.6 (2009): 355-364.

[191]: Monroe K., et al. “Anti - CD33 Antibodies and Methods of Use Thereof.” (2016) [Internet] Available from: https://patents.google.com/patent/US11136390B2/. (Accessed: 02 Mar 2024)

[192]: Ivrine DJ, Zheng Y, and Tang L. “Cell Surface Coupling of Nanoparticles.” (2016) [Internet] Available from: https://patents.google.com/patent/US11034752B2/. (Accessed: 02 Mar 2024)

[193]: Rowe, Jacob M. "Perspectives on current survival and new developments in AML." Best Practice & Research Clinical Haematology 34.1 (2021): 101248.

[194]: Meillon-Garcia, Luis Antonio, and Roberta Demichelis-Gomez. "Access to therapy for acute myeloid leukemia in the developing world: barriers and solutions." Current Oncology Reports 22 (2020): 1-11.

[195]: van Weelderen, Romy E., et al. "Outcomes of pediatric acute myeloid leukemia treatment in Western Kenya." Cancer reports 5.10 (2022): e1576.

[196]: Okello, Clement D., et al. "Haematological malignancies in sub-Saharan Africa: east Africa as an example for improving care." The Lancet Haematology 8.10 (2021): e756-e769.

[197]: Shireen, Iram et al. “Frequency of complete remission after standard 3+7 induction therapy in patients with acute myeloid leukemia.” Pakistan journal of medical sciences vol. 38,5 (2022): 1138-1142.

[198]: Mehboob, Nazish, et al. "Assessment of Complete Remission Rate in Patients with Acute Myeloid Leukemia Undergoing 7+ 3 Induction Chemotherapy: Remission Rates in Acute Myeloid Leukemia Patients." Pakistan Journal of Health Sciences (2024): 79-83.

[199]: Leukemia Care. "A Guide for Patients: Relapse in AcutecMyeloid Leukemia" (2021). [Internet]. https://www.google.com/url?sa=t&source=web&rct=j&opi=89978449&url=https://media.leukaemiacare.org.uk/wp-content/uploads/Relapse-in-Acute-Myeloid-Leukaemia-AML-Web Version.pdf&ved=2ahUKEwje342G4OGJAxVmg_0HHYAYPawQFnoECBoQBg&usg=AOvVaw0sSNcR1hEhwueTmxDORypd. (Accessed: 11 Apr 2024)

[200]: Tzogani, Kyriaki, et al. "European Medicines Agency review of midostaurin (Rydapt) for the treatment of adult patients with acute myeloid leukaemia and systemic mastocytosis." ESMO open 4.6 (2019): e000606.

[201]: Stone, Richard M., et al. "Midostaurin plus chemotherapy for acute myeloid leukemia with a FLT3 mutation." New England Journal of Medicine 377.5 (2017): 454-464.

[202]: Stein, Eytan M., et al. "Enasidenib in mutant IDH2 relapsed or refractory acute myeloid leukemia." Blood, The Journal of the American Society of Hematology 130.6 (2017): 722-731.

[203]: Gamis, Alan S., et al. "Gemtuzumab ozogamicin in children and adolescents with de novo acute myeloid leukemia improves event-free survival by reducing relapse risk: results from the randomized phase III Children's Oncology Group trial AAML0531." Journal of Clinical Oncology 32.27 (2014): 3021-3032..

[204]: Castaigne, Sylvie, et al. "Effect of gemtuzumab ozogamicin on survival of adult patients with de-novo acute myeloid leukaemia (ALFA-0701): a randomised, open-label, phase 3 study." The Lancet 379.9825 (2012): 1508-1516.

[205]: Jen, Emily Y., et al. "FDA approval: gemtuzumab ozogamicin for the treatment of adults with newly diagnosed CD33-positive acute myeloid leukemia." Clinical cancer research 24.14 (2018): 3242-3246.

[206]: Kung Sutherland, May S., et al. "SGN-CD33A: a novel CD33-targeting antibody–drug conjugate using a pyrrolobenzodiazepine dimer is active in models of drug-resistant AML." Blood, The Journal of the American Society of Hematology122.8 (2013): 1455-1463.

[207]: Kovtun, Yelena, et al. "IMGN779, a novel CD33-targeting antibody–drug conjugate with DNA-alkylating activity, exhibits potent antitumor activity in models of AML." Molecular cancer therapeutics 17.6 (2018): 1271-1279.

[208]: Saha, Asim, et al. "A CD45-targeted antibody-drug conjugate successfully conditions for allogeneic hematopoietic stem cell transplantation in mice." Blood, The Journal of the American Society of Hematology 139.11 (2022): 1743-1759.

[209]: Yeung, Jenny, et al. "Anti-CD45 PBD-based antibody-drug conjugates are effective targeted conditioning agents for gene therapy and stem cell transplant." Molecular Therapy (2024).

[210]: Pastorczak, Agata, et al. "Mechanisms of immune evasion in acute lymphoblastic leukemia." Cancers 13.07 (2021): 1536.

[211]: Modjtahedi, Helmout, Sumaira Ali, and Sharadah Essapen. "Therapeutic application of monoclonal antibodies in cancer: advances and challenges." British medical bulletin 104.1 (2012): 41-59.

[212]: Sharkey, Robert M., and David M. Goldenberg. "Use of antibodies and immunoconjugates for the therapy of more accessible cancers." Advanced drug delivery reviews 60.12 (2008): 1407-1420.

[213]: Janthur, Wolf-Dieter, Nathan Cantoni, and Christoph Mamot. "Drug conjugates such as Antibody Drug Conjugates (ADCs), immunotoxins and immunoliposomes challenge daily clinical practice." International journal of molecular sciences 13.12 (2012): 16020-16045.

[214]: Hermanson, Greg T. Bioconjugate techniques. Academic press (2013).

[215]: Nakajima, Naoki, and Yoshito Ikada. "Mechanism of amide formation by carbodiimide for bioconjugation in aqueous media." Bioconjugate chemistry 6.1 (1995): 123-130.

[216]: Renault, Kévin, et al. "Covalent modification of biomolecules through maleimide-based labeling strategies." Bioconjugate Chemistry 29.8 (2018): 2497-2513.

[217]: Pellico, Juan, Peter J. Gawne, and Rafael TM de Rosales. "Radiolabelling of nanomaterials for medical imaging and therapy." Chemical Society Reviews 50.5 (2021): 3355-3423.

[218]: Veronese, F. M., and Margherita Morpurgo. "Bioconjugation in pharmaceutical chemistry." Il Farmaco 54.8 (1999): 497-516.

[219]: Choudhary, Swati, Stefan Barth, and Rama S. Verma. "SNAP-Tag technology: a promising tool for ex vivo immunophenotyping." Molecular Diagnosis & Therapy 21 (2017): 315-326.

[220]: Kolberg, Katharina, et al. "SNAP-tag technology: a general introduction." Curr. Pharm. Des 19.30 (2013): 5406-5413

[221]: Mayuni, Grace. "Generation of Glioblastoma specific SNAP based antibody fusion proteins for future radiolabelling application." (2023). (Accessed: https://open.uct.ac.za/home)

[222]: Tai, Siew, et al. "1369 CD64-directed scFv fusion protein exhibits cytotoxicity and is a tool for site-specific diagnosis of acute myeloid leukemia." (2022).

[223]: Mungra, Neelakshi. "Development of SNAP-tag based fusion proteins as novel auristatin F-containing immunoconjugates and photoimmunotheranostics in the detection and treatment of triple-negative breast cancer." (2022). (Accessed: https://open.uct.ac.za/home)

[224]: Miramontes, P. "Un modelo de autómata celular para la evolución de los ácidos nucleicos [A cellular automaton model for the evolution of nucleic acids]." *UNAM* (1992).

[225]: Benjin, Xu, and Liu Ling. "Developments, applications, and prospects of cryo-electron microscopy." *Protein Science* 29.4 (2020): 872-882.

[226]: Brito, José A., and Margarida Archer. "Structural biology techniques: X-ray crystallography, cryo-electron microscopy, and small-angle X-ray scattering." *Practical approaches to biological inorganic chemistry*. Elsevier, 2020. 375-416.

[227]: Subramaniam, Tasshitra, et al. "Unlocking the Potential of in silico Approach in Designing Antibodies Against SARS-CoV-2." *Frontiers in Bioinformatics* 5: 1533983.

[228]: Wolf Pérez, Adriana-Michelle, et al. "Assessment of therapeutic antibody developability by combinations of in vitro and in silico methods." *Therapeutic Antibodies: Methods and Protocols* (2022): 57-113.

[229]: Roney, Miah, and Mohd Fadhlizil Fasihi Mohd Aluwi. "The importance of in-silico studies in drug discovery." *Intelligent Pharmacy* (2024).

[230]: Xu, John L., and Mark M. Davis. "Diversity in the CDR3 region of VH is sufficient for most antibody specificities." *Immunity* 13.1 (2000): 37-45.

[231]: ThermoFisher. "Eight Tips on How to Improve Gel Electrophoresis Results." [Internet] Available from: https://www.thermofisher.com/za/en/home/brands/thermo-scientific/molecular-biology/molecular-biology-learning-center/molecular-biology-resource-library/spotlight-articles/8-DNA-ladder-tips.html. (Accessed: 02 May 2024)

[232]: Gibson, Elizabeth G., Alexandria A. Oviatt, and Neil Osheroff. "Two-dimensional gel electrophoresis to resolve DNA topoisomers." *DNA Electrophoresis: Methods and Protocols* (2020): 15-24.

[233]: New England Biolabs. “FAQ: Why do I see additional DNA bands on my gel after a restriction digest?” [Internet]. Available from: https://www.neb.com/en/faqs/2016/04/07/why-do-i-see-additional-dna-bands-on-my-gel-after-a-restriction-digest?srsltid=AfmBOorwKxb8p68Mt7um_2eZ33aKHhF-6ZbkwVm6LlAhcK1AnQ4-aMMI. (Accessed: 13 May 2024)

[234]: Karaan, Maryam. "Antibody engineering to evaluate binding, internalisation, and intracellular routing of tumour-targeting fusion proteins." (2023). (Accessed: https://open.uct.ac.za/home)

[235]: Fajemisin, Emmanuel A. "Generation and therapeutic evaluation of CD64-targeting immunotherapeutics on CD64+ cell lines and ex vivo differentiated human macrophages." (2023). (Accessed: https://open.uct.ac.za/home)

[236]: ThermoFisher. “Troubleshooting Common Issues with Restriction Digestion Reactions: How to Avoid or Solve Problems.” [Internet] Available from: https://www.thermofisher.com/za/en/home/brands/thermo-scientific/molecular-biology/molecular-biology-learning-center/molecular-biology-resource-library/spotlight-articles/7-common-issues-with-restriction-digestion-reactions-and-how-to-avoid-them.html (Accessed: 27 Aug 2024)

[237]: SigmaAldrich. “Sample Preparation & Gel Electrophoresis Troubleshooting. [Internet] Available from: https://www.sigmaaldrich.com/ZA/en/technical-documents/technical-article/protein-biology/gel-electrophoresis/sample-preparation-gel-electrophoresis (Accessed: 27 Aug 2024)

[238]: Yoshida, Naoto, and Misa Sato. "Plasmid uptake by bacteria: a comparison of methods and efficiencies." Applied microbiology and biotechnology 83 (2009): 791-798.

[239]: Hanahan, Douglas. "Studies on transformation of Escherichia coli with plasmids." Journal of molecular biology 166.4 (1983): 557-580.

[240]: Dower, William J., Jeff F. Miller, and Charles W. Ragsdale. "High efficiency transformation of E. coli by high voltage electroporation." (1988): 6127-6145.

[241]: Hanahan, Douglas, Joel Jessee, and Fredric R. Bloom. "[4] Plasmid transformation of Escherichia coli and other bacteria." *Methods in enzymology* 204 (1991): 63-113.

[242]: McCormac, A. C., M. C. Elliott, and D. F. Chen. "A simple method for the production of highly competent cells of Agrobacterium for transformation via electroporation." *Molecular biotechnology* 9 (1998): 155-159.

[243]: Okamoto, Akiko, et al. "High efficiency transformation of Bacillus brevis by electroporation." *Bioscience, biotechnology, and biochemistry* 61.1 (1997): 202-203.

[244]: Yi, Yanglei, and Oscar P. Kuipers. "Development of an efficient electroporation method for rhizobacterial Bacillus mycoides strains." *Journal of microbiological methods* 133 (2017): 82-86.

[245]: Luo, Jianmei, et al. "Optimization of electroporation." *Adv Appl Biotechnol* 393 (2018).

[246]: Khow, Orawan, and Sunutcha Suntrarachun. "Strategies for production of active eukaryotic proteins in bacterial expression system." *Asian Pacific journal of tropical biomedicine* 2.2 (2012): 159-162.

[247]: Verma, R., E. Boleti, and A. J. T. George. "Antibody engineering: comparison of bacterial, yeast, insect and mammalian expression systems." *Journal of immunological methods* 216.1-2 (1998): 165-181.

[248]: ThermoFisher. “Overview of Protein Expression Systems.” [Internet] Available from: https://www.thermofisher.com/za/en/home/life-science/protein-biology/protein-biology-learning-center/protein-biology-resource-library/pierce-protein-methods/overview-protein-expression-systems.html#:~:text=The%20choice%20of%20an%20optimal,better%20expressed%20in%20mammalian%20systems. (Accessed: 03 Sep 2024)

[249]: Schütz, Anja, et al. "A concise guide to choosing suitable gene expression systems for recombinant protein production." *STAR protocols* 4.4 (2023): 102572.

[250]: Tan, Evan, et al. "HEK293 cell line as a platform to produce recombinant proteins and viral vectors." Frontiers in bioengineering and biotechnology 9 (2021): 796991.

[251]: Nikcevic, Gordana, Natasa Kovacevic-Grujicic, and Milena Stevanovic. "Improved transfection efficiency of cultured human cells." *Cell biology international* 27.9 (2003): 735-737.

[252]: Promega Corporate. “Overview of Transfection Methods” [Internet] Available from: https://worldwide.promega.com/resources/guides/cell-biology/transfection/ (Accessed: 15 Sep 2024)

[253]: Jamour, Parisa, et al. "Comparing chemical transfection, electroporation, and lentiviral vector transduction to achieve optimal transfection conditions in the Vero cell line." *BMC Molecular and Cell Biology* 25.1 (2024): 15.

[254]: Andreason, Grai L., and Glen A. Evans. "Optimization of electroporation for transfection of mammalian cell lines." *Analytical biochemistry* 180.2 (1989): 269-275.

[255]: ThermoFisher. “Electroporation” [Internet] Available from: https://www.thermofisher.com/za/en/home/references/gibco-cell-culture-basics/transfection-basics/methods/electroporation.html (Accessed: 16 Sep 2024)

[256]: Grisshammer, Reinhard, and Julie Tucker. "Quantitative evaluation of neurotensin receptor purification by immobilized metal affinity chromatography." *Protein expression and purification* 11.1 (1997): 53-60.

[257]: Young, Carissa L., Zachary T. Britton, and Anne S. Robinson. "Recombinant protein expression and purification: a comprehensive review of affinity tags and microbial applications." *Biotechnology journal* 7.5 (2012): 620-634.

[258]: Mohanty, Arun K., and Michael C. Wiener. "Membrane protein expression and production: effects of polyhistidine tag length and position." Protein expression and purification 33.2 (2004): 311-325.

[259]: Völzke, Jule L., et al. "Efficient Purification of Polyhistidine-Tagged Recombinant Proteins Using Functionalized Corundum Particles." *BioTech* 12.2 (2023): 31.

[260]: Wu, Chenyi, et al. "Proteolysis of native proteins: trapping of a reaction intermediate." *Journal of Biological Chemistry* 274.2 (1999): 1108-1115.

[261]: SigmaAldrich. “Western Blotting: Why Are Observed and Calculated Molecular Weights Different?” [Internet] Available from: https://www.sigmaaldrich.com/ZA/en/technical-documents/technical-article/protein-biology/western-blotting/observed-vs-calculated-molecular-weight (Accessed: 29 Sep 2024)

[262]: ThermoFisher. “Western Blot Troubleshooting” [Internet] Available from: https://www.thermofisher.com/za/en/home/life-science/protein-biology/protein-biology-learning-center/protein-gel-electrophoresis-information/western-blot-troubleshooting.html

[263]: Spriestersbach, Anne, et al. "Purification of his-tagged proteins." Methods in enzymology. Vol. 559. Academic Press, 2015. 1-15.

[264]: Gencefe.” What are the differences in protein purity requirements for different experiments?” [Internet] Available from: https://www.gencefebio.com/Blog/337.html (Accessed: 01 Oct 2024)

[265]: Adhikari, Sanjay, et al. "A unified method for purification of basic proteins." *Analytical biochemistry* 400.2 (2010): 203-206.

[266]: Elkerdany, Eman D., et al. "In vitro effect of a novel protease inhibitor cocktail on Toxoplasma gondii tachyzoites." Experimental Parasitology 219 (2020): 108010.

[267]: Freitag, Ruth, and Csaba Horváth. "Chromatography in the downstream processing of biotechnological products." *Downstream Processing Biosurfactants Carotenoids* (2006): 17-59.

[268]: Sigma-Aldrich. "Protease Inhibitor Cocktail." [Internet] Available on: https://www.google.com/url?sa=t&source=web&rct=j&opi=89978449&url=https://www.sigmaaldrich.com/deepweb/assets/sigmaaldrich/product/documents/128/288/p1860dat-mk.pdf%3Fsrsltid%3DAfmBOorDqCsZjfMiJFDhneZxPoBBYJp0IMjEnd-zAlm-04WaMZ8L3N1q&ved=2ahUKEwjrmOjhi4eLAxX8QkEAHY4OK8AQFnoECDkQAQ&usg=AOvVaw2PCFL0T0aOKwDM3AT5YueM (Accessed: 07 Oct 2024)

[269]: Gibert, Stephanie, Norbert Bakalara, and Xavier Santarelli. "Three-step chromatographic purification procedure for the production of a His-tag recombinant kinesin overexpressed in E. coli." Journal of Chromatography B: Biomedical Sciences and Applications 737.1-2 (2000): 143-150.

[270]: Woitok, Mira, et al. "Using the SNAP-Tag technology to easily measure and demonstrate apoptotic changes in cancer and blood cells with different dyes." Plos one 15.12 (2020): e0243286.

[271]: Hussain, Ahmad Fawzi, et al. "SNAP-tag technology mediates site specific conjugation of antibody fragments with a photosensitizer and improves target specific phototoxicity in tumor cells." Bioconjugate chemistry 22.12 (2011): 2487-2495.

[272]: Li, Zheng-Mei, et al. "Factors affecting the expression of recombinant protein and improvement strategies in Chinese hamster ovary cells." Frontiers in Bioengineering and Biotechnology 10 (2022): 880155.

[273] LenioBio. “Maximize Protein Expression: Overcoming Challenges and Boosting Yields” [Internet] Available from: https://www.leniobio.com/maximize-protein-expression-overcoming-challenges-and-boosting-yields/#:~:text=Factors%20such%20as%20temperature%2C%20pH,can%20ultimately%20enhance%20expression%20efficiency. (Accessed: 21 Oct 2024)

[274]: Nettleship, Joanne E., et al. "Recent advances in the production of proteins in insect and mammalian cells for structural biology." Journal of structural biology 172.1 (2010): 55-65.

[275]: McKinnon, Katherine M. "Flow cytometry: an overview." *Current protocols in immunology* 120.1 (2018): 5-1.

[276]: Bonilla, Diana L., et al. "The Power of Reagent Titration in Flow Cytometry." Cells 13.20 (2024): 1677.

[277]: BioRad. “Antibody Titration in Flow Cytometry.” [Internet] Available from: https://www.bio-rad-antibodies.com/flow-antibody-titration.html#:~:text=Why%20Is%20Antibody%20Titration%20Important,bind%20to%20low%20affinity%20targets. (Accessed: 30 Oct 2024)

[278]: Holmes, Kevin, et al. "Preparation of cells and reagents for flow cytometry." *Current protocols in immunology* 44.1 (2001): 5-3.

[279]: Bio-techne. “Flow Cytometry Troubleshooting Guide” [Internet] Available from: https://www.bio-techne.com/applications/flow-cytometry/flow-cytometry-troubleshooting-guide (Accessed: 05 Nov 2024)

[280]: Veal, D. A., et al. "Fluorescence staining and flow cytometry for monitoring microbial cells." *Journal of immunological methods* 243.1-2 (2000): 191-210.

[281]: Flores-Montero, Juan, et al. "Fluorochrome choices for multi-color flow cytometry." *Journal of immunological methods* 475 (2019): 112618.

[282]: Shapiro, Howard M. *Practical flow cytometry*. John Wiley & Sons, 2005.

[283]: Kharraz, Yacine, et al. "Full spectrum cytometry improves the resolution of highly autofluorescent biological samples: Identification of myeloid cells in regenerating skeletal muscles." *Cytometry Part A* 101.10 (2022): 862-876.

[284]: Tanimoto, M., et al. “Restricted expression of an early myeloid and monocytic cell surface antigen defined by monoclonal antibody M195.” *Leukemia* 3.5 (1989): 339-348.

[285]: Emberson, Louise M., et al. "Expression of an anti-CD33 single-chain antibody by Pichia pastoris." Journal of immunological methods 305.2 (2005): 135-151.

[286]: van der Velden, Vincent HJ, et al. "Targeting of the CD33-calicheamicin immunoconjugate Mylotarg (CMA-676) in acute myeloid leukemia: in vivo and in vitro saturation and internalization by leukemic and normal myeloid cells." *Blood, The Journal of the American Society of Hematology* 97.10 (2001): 3197-3204.

[287]: Press, Oliver W., et al. "Endocytosis and degradation of monoclonal antibodies targeting human B-cell malignancies." *Cancer research* 49.17 (1989): 4906-4912.

[288]: Green, Damian J., et al. "Pretargeting CD45 enhances the selective delivery of radiation to hematolymphoid tissues in nonhuman primates." *Blood, The Journal of the American Society of Hematology* 114.6 (2009): 1226-1235.

[289]: Mungra, Neelakshi, et al. "CSPG4 as a target for the specific killing of triple-negative breast cancer cells by a recombinant SNAP-tag-based antibody-auristatin F drug conjugate." *Journal of Cancer Research and Clinical Oncology* 149.13 (2023): 12203-12225.

[290]: Woitok, Mira, et al. "Comparison of a mouse and a novel human scFv-SNAP-auristatin F drug conjugate with potent activity against EGFR-overexpressing human solid tumor cells." *OncoTargets and therapy* (2017): 3313-3327.

[291]: Huysamen, Allan M., et al. "Click Chemistry-Generated Auristatin F–Linker–Benzylguanine for a SNAP-Tag-Based Recombinant Antibody–Drug Conjugate Demonstrating Selective Cytotoxicity toward EGFR-Overexpressing Tumor Cells." *ACS omega* 8.4 (2023): 4026-4037.

[292]: Samantasinghar, Anupama, et al. "A comprehensive review of key factors affecting the efficacy of antibody drug conjugate." *Biomedicine & Pharmacotherapy* 161 (2023): 114408.

[293]: El-Naggar, Noura El-Ahmady, et al. "Purification, characterization, cytotoxicity and anticancer activities of L-asparaginase, anti-colon cancer protein, from the newly isolated alkaliphilic Streptomyces fradiae NEAE-82." *Scientific reports* 6.1 (2016): 32926.

# Appendix

**Table A1.** Phenol-chloroform extraction buffer reagents

| | |
|---|---|
| **Solution I** | **Reagents:**<br>• 10 mL of 0.5 M Glucose (final concentration 50 mM)<br>• 2.5 mL of 1 M Tris-HCL (pH 8) (final concentration 25 mM)<br>• 2 mL of 0.5 M EDTA (pH 8) (final concentration 10 mM)<br>• 85.5 mL sterile distilled water |
| **Solution II** | **Reagents:**<br>• 20 mL of 10% SDS (final concentration 1%)<br>• 4 mL of 10 M NaOH (final concentration 0.2 M)<br>• 176 mL sterile distilled water |
| **Solution III** | **Reagents:**<br>• 60 mL of 5 M $C_2H_3KO_2$ (final concentration 3 M)<br>• 11.5 mL $CH_3COOH$<br>• 28.5 sterile distilled water |
| **RNase A** | • 10 mg/mL in distilled water |
| **Phenol: Chloroform Solution** | • 1:1 (v/v) |
| **Chloroform: Isoamyl alcohol** | • 24:1 (v/v) |

**Table A2.** Each component, and corresponding quantity, required for restriction digestion reactions.

| Components | Undigested parental plasmid | Single digest parental plasmid | Double digest parental plasmid | Double digest experimental plasmid | Double digest experimental plasmid |
|---|---|---|---|---|---|
| **Nuclease-free water** | 44 µL | 43 µL | 42 µL | 42 µL | 42 µL |
| **rCutSmart enzyme** | 5 µL | 5 µL | 5 µL | 5 µL | 5 µL |
| **DNA** | 1 µg | 1 µg | 1 µg | 1 µg | 1 µg |
| **SfiI** | 0 µL | 1 µL | 1 µL | 1 µL | 1 µL |
| **NotI** | 0 µL | 0 µL | 1 µL | 1 µL | 1 µL |

**Table A3.** TAE buffer reagents required for agarose gel electrophoresis

| TAE buffer reagents | Quantity required |
|---|---|
| Distilled water | 600 mL |
| Trizma base | 48.4 g |
| 0.5 M EDTA (pH 8.0) | 20 mL |
| Glacial acetic acid | 11.44 mL |
| Distilled water | Fill up to 1000 mL |

**Table A4.** Constituents of T4 DNA ligation reactions

| Ligation product | Quantity |
|---|---|
| Mass of backbone (pCB-SNAP) | 50 ng |
| Mass of insert (scFv)<br>(For 1:**1** or 1:**5** ratio) | Dependent on the molecular weight and ratio of insert to be used (determined on: https://nebiocalculator.neb.com/) |
| T4 DNA ligase buffer | 2 µL |
| T4 DNA ligase | 1 µL |
| Nuclease free water | Adjust to final volume of 20 µL |
| (**Note**: The ligation control used did not contain a scFv insert) | |

**Table A5.** Transformation efficiencies of ligated DNA in *E. coli* competent cells

| Transformation efficiency formula = $\frac{\text{Number of colonies}}{\text{Mass of plasmid DNA}}$ x Dilution factor | | |
|---|---|---|
| pCB-αCD33(scFv)-SNAP | 1:1 | $4.0 \times 10^1$ |
| | 1:5 | $1.06 \times 10^2$ |
| pCB-αCD45(scFv)-SNAP | 1:1 | $8.0 \times 10^1$ |
| | 1:5 | $1.0 \times 10^1$ |
| pCB-SNAP backbone control | 1:0 | 0 |

**Table A6.** Each component, and corresponding quantity, required for restriction mapping reactions.

| **Components** | **Undigested parental plasmid** | **Single digest parental plasmid** | **Double digest parental plasmid** | **Double digest experimental plasmid** | **Double digest experimental plasmid** |
|---|---|---|---|---|---|
| **Nuclease-free water** | 44 µL | 43 µL | 42 µL | 42 µL | 42 µL |
| **rCutSmart enzyme** | 5 µL | 5 µL | 5 µL | 5 µL | 5 µL |
| **DNA** | 1 µg | 1 µg | 1 µg | 1 µg | 1 µg |
| **BamHI** | 0 µL | 1 µL | 1 µL | 1 µL | 1 µL |
| **SpeI** | 0 µL | 0 µL | 1 µL | 1 µL | 1 µL |

**Table A7.** Reagents required to make Phosphate buffered saline (PBS).

| **PBS reagents** |
|---|
| • 137 mM NaCl<br>• 8.8 mM $Na_2HPO_4$<br>• 2.7 mM KCl<br>• 1.75 mM $KH_2PO_4$<br>• Fill to a final volume of 1L and autoclave |

**Table A8.** Buffers, recommended flow rate and volume for the IMAC purification of the mammalian CCSN SNAP fusion protein.

| | **Buffer** | **Reagents** | **Flow rate** | **Volume** |
|---|---|---|---|---|
| **1** | Equilibration buffer | • 50 mM $NaH_2PO_4$<br>• 300 mM NaCl | 5 ml/min | 5 cv |
| **2** | Loading buffer | • x mL CCSN + $\frac{1}{3}$ incubation buffer<br>• Incubation buffer (200 mM $NaH_2PO_4$, 1.2 M NaCl, 40 mM $C_3N_2H_4$) | 1 ml/min | Dependent on CCSN to be purified |
| **3** | Wash buffer | • 500 mM $NaH_2PO_4$<br>• 300 mM NaCl<br>• 40 mM $C_3N_2H_4$ | 1 ml/min | 20 cv |
| **4** | Elution buffer | • 50 mM $Na_2H_2PO_4$<br>• 300 mM NaCl<br>• 250 mM $C_3N_2H_4$ | 1 ml/min | 15 cv |
| **5** | Equilibration buffer | • 50 mM $NaH_2PO_4$<br>• 300 mM NaCl | 5 ml/min | 5 cv |

**Table A9.** Reagents of solutions and buffers required to cast and run a 10% SDS-PAGE gel.

| **Solution/ buffer** | **Constituent and Quantity (in g)** |
|---|---|
| 10 X Running Buffer | • Trizma base – 30.3 g<br>• Glycine – 144.4 g<br>• SDS – 10.0 g<br>• Adjust pH to 8.3 with HCl, then make up to a final volume of 1L with distilled water |
| 10% w/v SDS solution<br>(**Cat#:** L3771, Sigma-Aldrich) | • SDS – 50.0 g<br>• Dissolve to a final volume of 500 mL with distilled water |
| 10% w/v APS solution<br>(**Cat#:** 248614, Sigma-Aldrich) | • APS – 5.0 g<br>• Dissolve to a final volume of 50 mL with distilled water |
| Tris-HCl buffer<br>(1.5 M, pH 8.8) | • Trizma base – 90.86 g<br>• Distilled water – 300 mL<br>• Adjust pH to 8.8 with HCl, then make up to a final volume of 500 mL with distilled water |
| Tris-HCl buffer<br>(0.5 M, pH 6.8) | • Trizma base – 30.3 g<br>• Distilled water – 300 mL<br>• Adjust pH to 6.8 with HCl, then make up to a final volume of 500 mL with distilled water |

**Table A10.** Quantities of SNAP fusion protein and BSA standard (in µg) for densitometry quantities.

| **Sample** | **Volume** | **1 X PBS** | **4 X loading dye** | **Total volume** |
|---|---|---|---|---|
| Protein Standard | 2.5 µL | 0 µL | 0 µL | 2.5 µL |
| SNAP FP | 10 µL | 10 µL | 5 µL | 25 µL |
| 16 µg BSA | 16 µL | 4 µL | 5 µL | 25 µL |
| 8 µg BSA | 8 µL | 12 µL | 5 µL | 25 µL |
| 4 µg BSA | 4 µL | 16 µL | 5 µL | 25 µL |
| 2 µg BSA | 2 µL | 23 µL | 5 µL | 25 µL |
| 1 µg BSA | 1 µL | 24 µL | 5 µL | 25 µL |

**Table A11.** Reagents of solutions and buffers required for Western Blot analysis.

| Solution/ buffer | Constituent and Quantity (in g) |
|---|---|
| 10 X Transfer buffer | • Trizma base – 30.3 g<br>• Glycine – 114.2 g<br>• SDS – 10.0 g<br>• Add distilled water to make up to a final volume of 1L |
| 1 X Transfer buffer | • 10 X Transfer buffer – 100 mL<br>• Methanol (20%) – 200 mL<br>• Add distilled to make up to a final volume of 1L |
| 10 X Tris-buffered saline | • Trizma base – 24.0 g<br>• NaCl – 88.0 g<br>• Distilled water – 900 mL<br>• Adjust pH to 8.8 with HCl, then make up to a final volume of 1L with distilled water |
| TBS/Tween 20 | • 10X TBS – 100 mL<br>• Tween 20 – 1 mL<br>• Add distilled water to make up to a final volume of 1L |

**Table A12.** Conjugation reaction comprised of an equimolar mixture of SNAP FP: BG-Alexa 488 (1:1).

| | Component | [Initial] | [Final] | Volume (µL) |
|---|---|---|---|---|
| **1** | PBS (make up to a final volume) | 1X | | Determine |
| **2** | DTT | 10 mM | 1 mM | 1.5 |
| **3** | BG-Alexa 488 | 25 µM | 5 µM | 3.0 |
| **4** | SNAP FP | Determine | 5 µM | Determine |
| **5** | Total | | | 15 |

**Table A13.** Two-fold titration of SNAP FP for binding analysis by flow cytometry.

| Sample | Concentration | Cells |
|---|---|---|
| Tube 1 | 250 µg/mL | $5 \times 10^5$ |
| Tube 2 | 125µg/mL | $5 \times 10^5$ |
| Tube 3 | 62.5 µg/mL | $5 \times 10^5$ |
| Tube 4 | 31.25 µg/mL | $5 \times 10^5$ |
| Tube 5 | 15.6 µg/mL | $5 \times 10^5$ |
| Tube 6 | 7.8 µg/mL | $5 \times 10^5$ |
| Tube 7 | 3.9 µg/mL | $5 \times 10^5$ |
| Tube 8 | 1.95 µg/mL | $5 \times 10^5$ |

**Table A14.** Reagents for flow cytometry FACS buffer.

| FACS buffer reagents |
|---|
| • 2 mL of Fetal Bovine Serum (FBS)<br>• 1 mL of Sodium azide<br>• Fill up to 100 mL with 1 X PBS |

**Table A15.** Conjugation reaction mixture of SNAP FP: BG-AURIF (1:2) for cytotoxicity studies.

| | Component | [Initial] | [Final] | Volume (µL) |
|---|---|---|---|---|
| **1** | PBS | 1 X | | Fill up to 500 µL |
| **2** | DTT | 50 mM | 1 µM | 10 |
| **3** | BG-AURIF | 5 mM | 20 µM | 2 |
| **4** | SNAP FP | Use online calculator | 10 µM | Determine |
| **5** | Final | | | 500 |

**Table A16.** Quantification of the concentration and purity of the isolated plasmids following transformation**.**

| **Construct** | **Nuclease -Free water** | **[Initial]** | **[Final]** | **260/280** | **260/230** |
|---|---|---|---|---|---|
| pCB-αCD33(scFv)-SNAP | 0 µL | Used glycerol stock | 3967.4 ng/µL | 1.97 | 2.23 |
| pUC57-αCD45(scFv) | 40 µL | 198.5 ng/µL | 2584.7 ng/µL | 1.89 | 2.24 |
| (**Note:** Initial quantification of pUC57-αCD33(scFv) following bacterial isolation was conducted previously by B. Mirianga (PhD). For the purpose of confirming successful molecular cloning, the process was repeated using pCB-αCD33(scFv)-SNAP.) | | | | | |

(A)

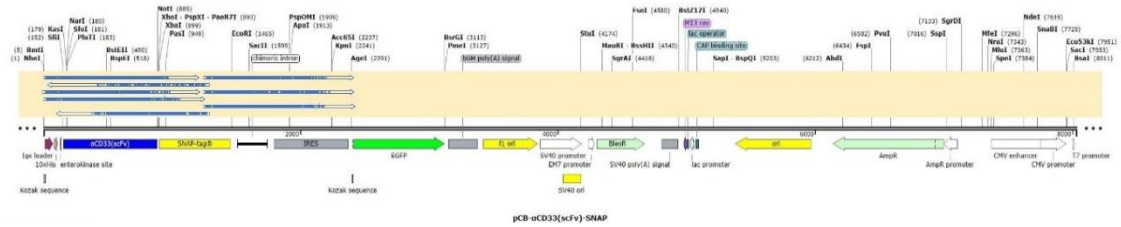

(B)

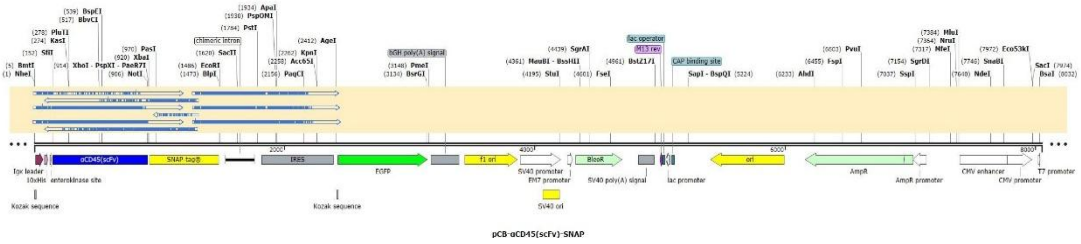

**Figure A1**. **Sanger sequencing of the recombinant plasmids.** (A) Plasmid map depicting sequence alignment of pCB-αCD33(scFv)-SNAP. (B) Plasmid map depicting sequence alignment of pCB-αCD45(scFv)-SNAP. The acquirement of positive clones following *E. coli* transformation and restriction mapping was confirmed using Sanger Sequencing conducted by Inqaba Biotechnical Industries. Several primers including: universal SNAP reverse primer, universal T7 promoter and universal SNAP internal forward primers were used in this sequencing analysis. The clones were almost 100% homologous to their *in silico* ORF sequences, as shown by the SnapGene-generated plasmid maps, indicating that the ligation procedure had been carried out appropriately.

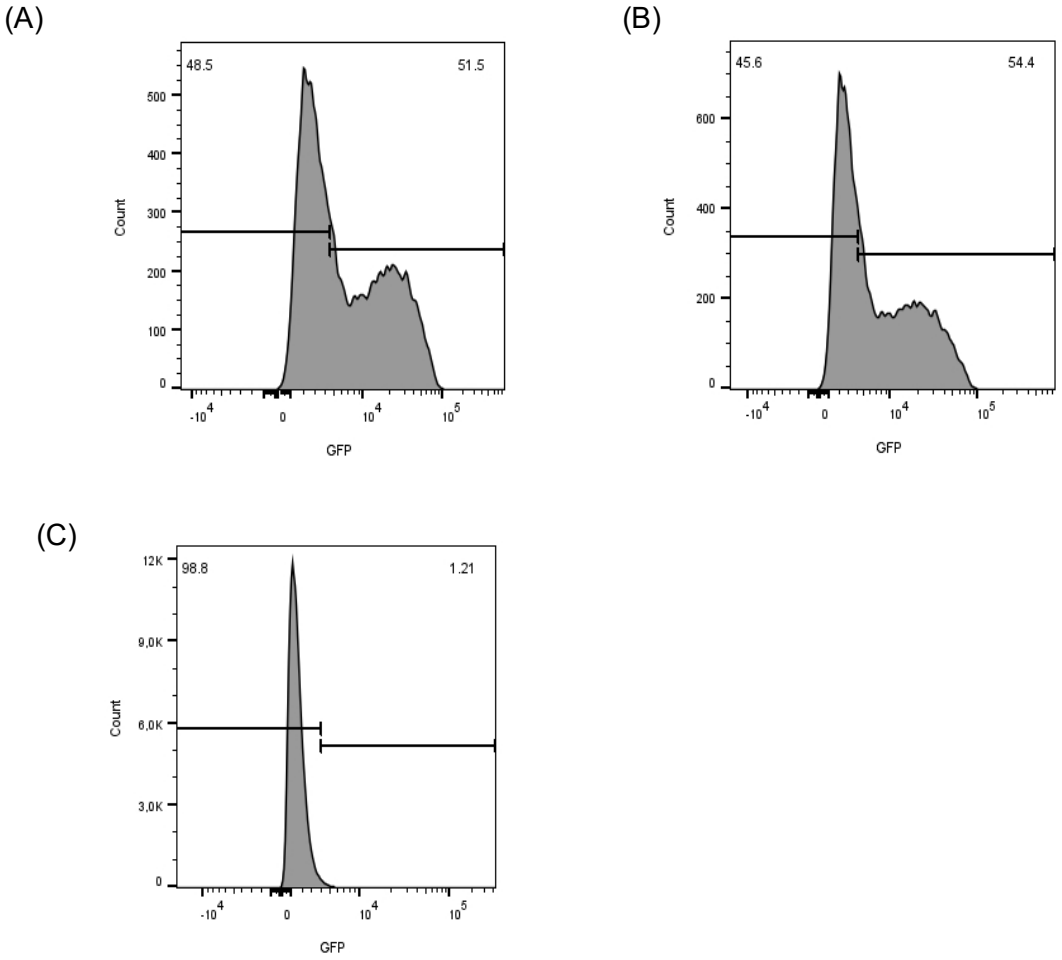


**Figure A2. Transfection efficiency of the recombinant plasmid DNA determined by flow cytometry.** The effectiveness of recombinant plasmid DNA transfection into HEK293T protein-producing cells was assessed using flow cytometry. Each FlowJo Software-generated flow cytometry plot showed the successfully transfected cells' eGFP profile. (A) A 51.5% frequency of eGFP positive cells transfected with pCB-αCD33(scFv)-SNAP was observed. (B) A 54.4 % frequency of eGFP positive cells transfected with pCB-αCD45(scFv)-SNAP was observed. (C) A low eGFP expression profile of 1.21% was detected for the non-transfected control cells.

**Table A17.** Formulas used to determine signal-to-noise ratio and staining index

| **Signal-to-noise ratio** | **Staining index** |
|---|---|
| Formula = MFI (positive population)/ MFI (negative population) | Formula = MFI (positive population) – MFI (negative population) / 2 x Robust standard deviation (negative population) |

(A) Conjugation analysis of αCD33(scFv)-SNAP with BG-AURIF

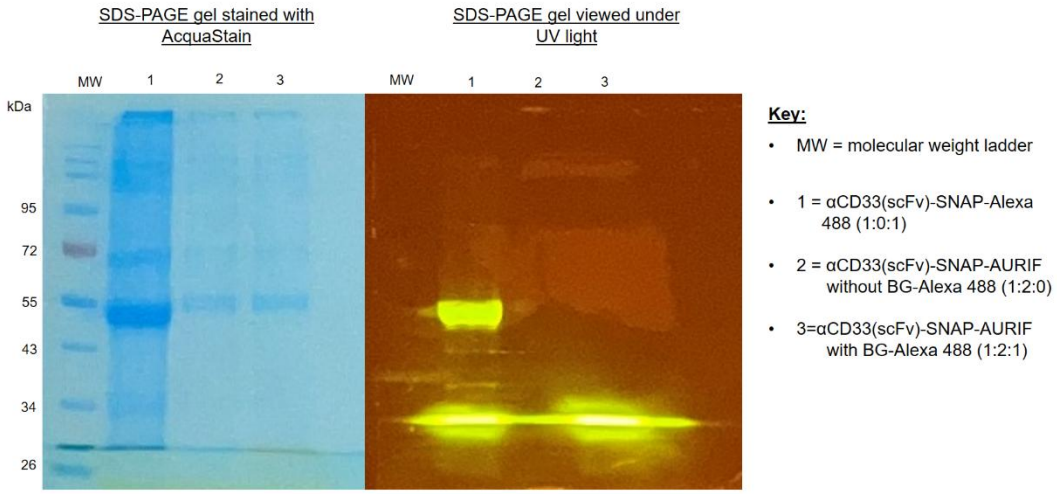


(B) Conjugation analysis of αCD45(scFv)-SNAP with BG-AURIF

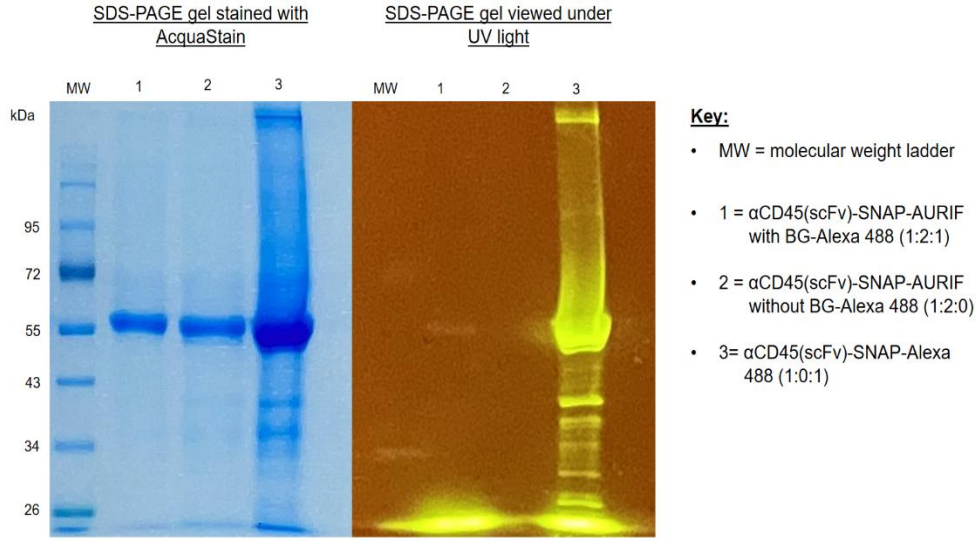


**Figure A3. Conjugation analysis of each recombinant SNAP FP to BG-AURIF.**
Successful conjugation of each recombinant SNAP FP to BG-AURIF was assessed using SDS-PAGE. To ensure saturation of each SNAP-tag active site by the BG-AURIF, an additional conjugation with BG-Alexa 488 was performed to assess to a means of competitive conjugation. The key (on right) of each figure provides the samples loaded into their corresponding lanes. Any excess or unconjugated BG-Alexa 488 was observed at the bottom of each gel. (A) Conjugation analysis of αCD33(scFv)-SNAP with BG-AURIF (B) Conjugation analysis of αCD45scFv)-SNAP with BG-AURIF.

(A) Expression profile of the CD33 antigen of HL60 and THP-1 cells

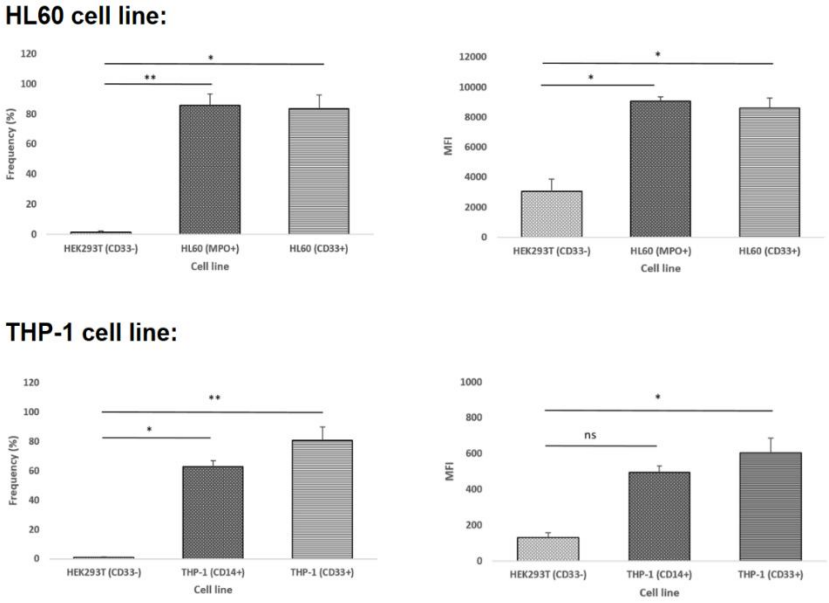


(B) Expression profile of the CD45 antigen of HL60 and THP-1 cells

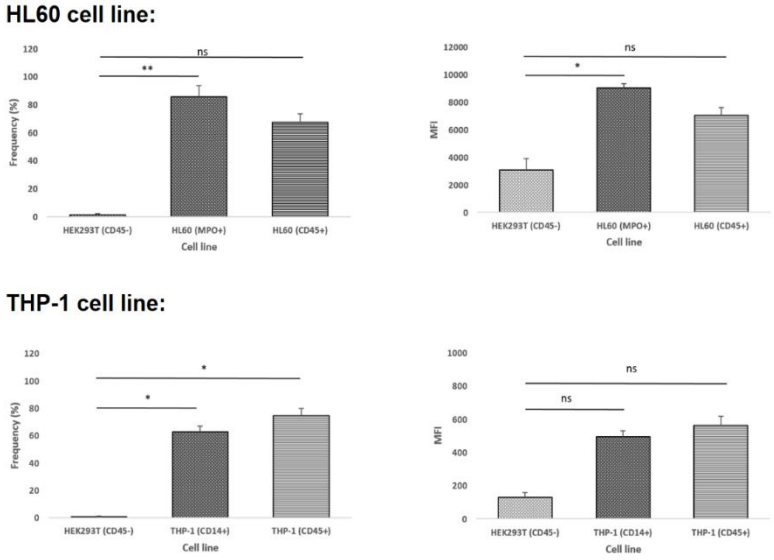


**Figure A4. Expression profiles of the target antigens on AML antigen positive cell lines.** (A) αCD33(scFv)-SNAP-Alexa 488 expression on AML cells versus HEK293T control. (B) αCD45(scFv)-SNAP-Alexa 488 expression on AML cells versus HEK293T control. Using FlowJo software, the frequency and MFI values of cells incubated with each BG-Alexa 488 conjugated recombinant SNAP FP was computed. These values were extracted and depicted using bar graphs. Data shown are representative of three biological repeat experiments. Statistical comparisons relative to the antigen-negative HEK293T cell line were calculated using Student's *t*-tests (*$p < 0.05$, **$p < 0.01$, ***$p < 0.001$, ns (not significant)).

(A) Unconjugated BG-AURIF cytotoxicity

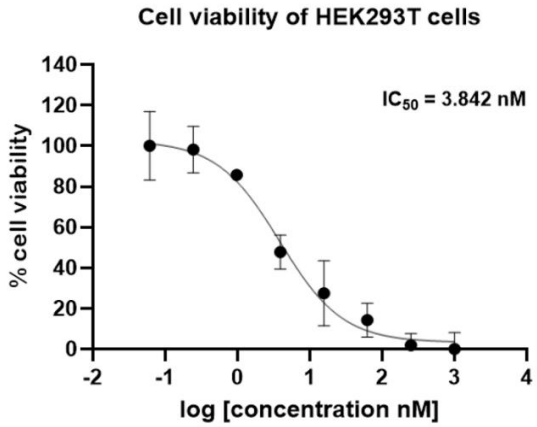


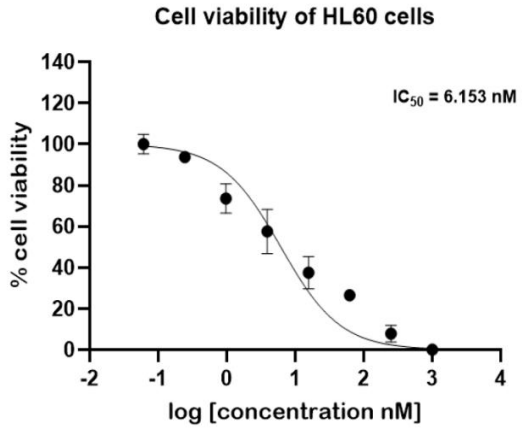


(B) Unconjugated αCD33(scFv)-SNAP cytotoxicity

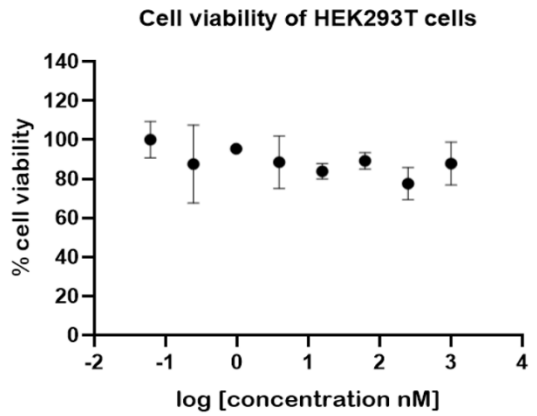


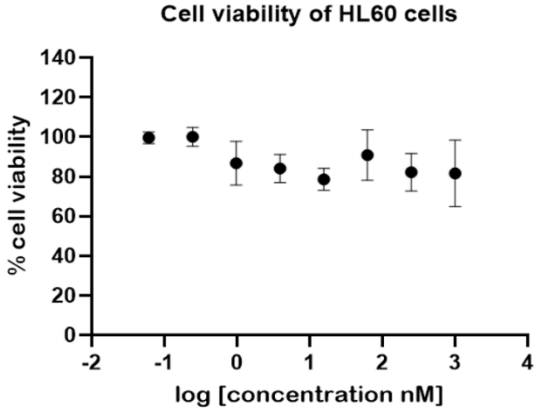


(C) Unconjugated αCD45(scFv)-SNAP cytotoxicity

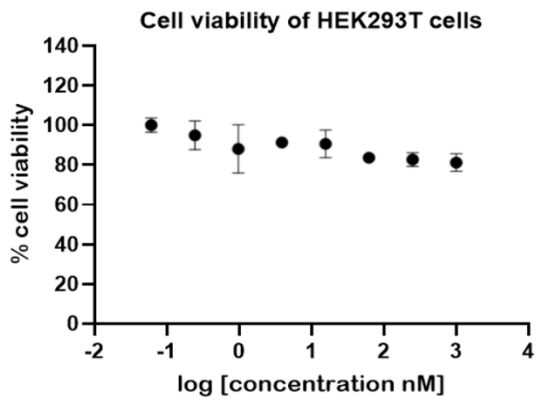


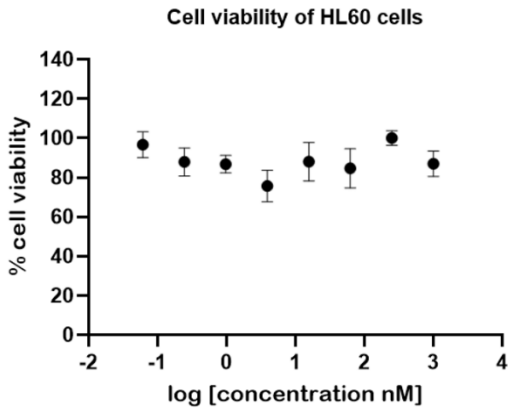

**Figure A5. Conjugation analysis of the separate components of each recombinant ADC.** GraphPad Prism v5. generated plots demonstrating the outcomes of XTT assays which were used to assess the cytotoxic effect of the recombinant ADC individual components on the cell viability of HEK293T and HL60 cells. (A) $IC_{50}$ values of 3.84 nM and 5.55 nM were computed for the administration of unconjugated BG-AURIF alone on HEK293T and HL60 cells, respectively. Negligible cytotoxicity was observed for (B) Unconjugated αCD33(scFv)-SNAP alone and (C) Unconjugated αCD45(scFv)-SNAP alone. Any substantial variations between replicates were represented as error bars.